Title

Nanomolar Electrochemical Dopamine Detection and Directed Evolution for Next Generation Electroenzymatic Gamma-Aminobutyric Acid Sensors

Author

Ruckodanov, Dmitriy Alexander

Publication Date

2024

Peer reviewed|Thesis/dissertation

UNIVERSITY OF CALIFORNIA

Los Angeles

Nanomolar Electrochemical Dopamine Detection and Directed Evolution for Next Generation Electroenzymatic Gamma-Aminobutyric Acid Sensors

A dissertation submitted in partial satisfaction of the

requirements for the degree Doctor of Philosophy

in Chemical Engineering

by

Dmitriy Alexander Ruckodanov

2024

ABSTRACT OF THE DISSERTATION

Nanomolar Electrochemical Dopamine Detection and Directed Evolution for Next Generation Electroenzymatic Gamma-Aminobutyric Acid Sensors

by

Dmitriy Alexander Ruckodanov
Doctor of Philosophy in Chemical Engineering
University of California, Los Angeles, 2024
Professor Harold G. Monbouquette, Chair

The development of highly sensitive and selective neurochemical sensors is crucial for advancing our understanding of neurotransmitter dynamics and their roles in neurological disorders. This dissertation focuses on the creation of next-generation electrochemical sensors for dopamine (DA) and γ-aminobutyric acid (GABA), employing innovative surface chemistry, nanostructured materials, and directed evolution techniques.

Dopamine is a critical neurotransmitter involved in the regulation of motivation, cognition, and motor behavior. Dysregulation of DA transmission is linked to various central nervous system (CNS) disorders, including Parkinson's disease, schizophrenia, and substance abuse. This research enhances DA sensing by integrating an on-probe iridium oxide (IrOx) reference electrode onto an implantable microelectrode array (MEA) microprobe. The inclusion of IrOx REs on-probe

provides potentially significant advantages over traditional, independent Ag/AgCl REs, such as improved stability, reduced inflammatory responses, and lower baseline noise. This post-fabrication electrochemical deposition of IrOx onto targeted microelectrodes enabled high sensitivity DA sensing with an ultralow limit of detection and high selectivity against common electroactive interferents. Comparative studies demonstrated that the integrated three-electrode configuration exhibited a five-fold lower limit of detection (~9 nM) due to an 82% reduction in baseline noise compared to sensors with separate Ag/AgCl REs. These advancements made these DA sensing microprobes highly attractive for *in vivo* applications, facilitating the study of nervous system disorders through improved DA monitoring.

To address the public health crisis of opioid abuse, a partnership was formed with several research labs to develop a high-throughput, multi-organ microphysiological system (MPS) using human induced pluripotent stem cell (iPSC)-derived, midbrain-fated dopamine (DA) and GABA neurons. These MPSs or "brain-on-a-chip" systems, incorporating microglia, a mock blood-brain barrier (BBB), and liver metabolism components, recapitulate the neurobiology of addiction. The aforementioned dopamine sensors with integrated IrOx reference electrodes were successfully integrated into the MPS design to monitor DA release in cultured neurons. However, challenges with media selection—stemming from the differing requirements of liver cells and neurons—and the lack of a reliable protocol for maintaining neuronal viability and sterility within the chips initially limited the system's overall functionality. These limitations highlighted the need for continued optimization of the MPS platform, which remains a promising avenue for future studies aimed at comprehensive drug screening and investigating the mechanisms underlying opioid-induced changes in DA response.

γ-Aminobutyric acid (GABA) is the most important inhibitory neurotransmitter in the mammalian brain, playing a vital role in maintaining the excitatory/inhibitory (E/I) balance. Dysregulation of this balance is associated with a range of neurological conditions, including seizures, autism, and traumatic brain injury, which affect millions of people in the US. Despite its importance, high-performance methods to monitor GABA signaling at the cellular level and in near-real-time have been slow to emerge, especially for deep brain regions. Our project aimed to engineer a GABA oxidase suitable for creating a high-performance, implantable, electroenzymatic GABA microsensor. The absence of a commercially available GABA oxidase necessitated the use of directed protein evolution to develop an enzyme with high activity and selectivity for GABA. Our approach involved cloning and expressing a naturally occurring enzyme with native oxidase activity for methyl-GABA, which showed modest activity with GABA. Through advanced ultrahigh throughput techniques, an enzyme was evolved for enhanced utility in GABA biosensors. The enzyme-catalyzed oxidation of GABA produced H_2O_2, which was subsequently electrooxidized at the underlying electrode, providing a current signal correlated to GABA concentration. Promising prototype biosensors demonstrated modest sensing capabilities, and further development and testing for *in vivo* models is ongoing.

This dissertation contributes significantly to the field of neurochemical sensing by addressing the critical needs for low noise, low detection limits, and high selectivity in neurotransmitter biosensors. The integration of innovative materials and techniques will facilitate the development of practical, high-performance sensors for both dopamine and GABA, with potential applications in neuroscience research and clinical diagnostics. These advancements promise to enhance our understanding of complex brain systems and improve the study and treatment of various neurological disorders.

The dissertation of Dmitriy Alexander Ruckodanov is approved.

Yi Tang

Nigel T. Maidment

Samanvaya Srivastava

Harold G. Monbouquette, Committee Chair

University of California, Los Angeles

2024

TABLE OF CONTENTS

LIST OF FIGURES

LIST OF TABLES

ACKNOWLEDGEMENTS

The work described in this dissertation was supported by the National Institute of Health (NIH) grants UH3TR003148 and R21NS139078.

This dissertation represents the culmination of years of effort, growth, and collaboration, made possible by the guidance, inspiration, and encouragement of countless individuals. As I reflect on this journey, I am struck by the profound impact of the people who have shaped and supported me along the way.

My journey into research began during my undergraduate studies, and I am deeply grateful to the mentors who guided me in those early years. Through the Aresty Summer Science Program at Rutgers, I had my first opportunity to delve into scientific research. Prof. Neimark welcomed me into his lab, and Dr. John Landers, a postdoc at the time, took me under his wing, patiently introducing me to lab techniques and sparking a curiosity that continues to drive me. That summer experience was transformative, solidifying my interest in research and setting the stage for all that followed.

Building on that foundation, I was fortunate to join the UCLA Amgen Scholars Program, an opportunity that profoundly shaped my career trajectory. My deepest thanks to Dr. Tama Hasson for her dedication to fostering young researchers and to Prof. Monbouquette, whose mentorship during that summer inspired me to pursue graduate studies. It was during those months at UCLA that research transformed from an interest into a passion. That experience instilled a sense of purpose and direction, thus guiding me to where I am today.

First and foremost, I want to express my deepest gratitude to Prof. Monbouquette, who has been an exceptional mentor throughout this journey. I would not have returned to your lab for graduate school if I had not been so confident that it was the perfect environment for both my

academic ambitions and personal growth, offering exactly the guidance and opportunities I needed to thrive. Your ability to balance challenge with encouragement has been invaluable, helping me navigate even the most difficult parts of this process. Thank you for believing in me, for your patience, and for always guiding me back on track when I felt lost. I would also like to thank my committee members, Prof. Tang, Prof. Maidment, and Prof. Srivastava, for their thoughtful feedback, scientific insights, and unwavering support. Your diverse perspectives have enriched this work immeasurably.

To my labmates and collaborators: this work would not have been possible without your collective expertise, camaraderie, and support. Dr. Brenda Huang, Dr. Yan Cao, and Dr. Zhenrong Zheng, thank you for introducing me to the intricacies of electrochemical sensing and for your patience in teaching me countless protocols. I am also deeply grateful to Prof. Tang for his generosity in providing lab space and resources critical to my research.

Friendship and mentorship often intersect, and for that, I am especially thankful to Josh Misa. Your guidance in molecular biology was instrumental to so much of my work, and your friendship has been a constant source of support, humor, and sanity. Whether we were rehearsing with GME, playing through Halo, or walking around Westwood during PokémonGo community days, you were always there to lift my spirits. Similarly, our trivia team, Josh and the Jersey Boys, was a cherished escape during graduate school. Josh, Ikechukwu Okorafor, and I created so many memories during those weekly trivia nights, where we bonded over shared victories (and occasional losses—curse you, baseball questions!). I am grateful for both of you and the grounding presence you brought to my life during this journey.

I want to express my heartfelt gratitude to my dear friend, Shiva Murali, whose steadfast support and camaraderie have been a cornerstone of my journey. Shiva and I share a bond that has

grown through nearly every pivotal stage of our lives—from our days at Montgomery High School, through studying chemical engineering together at Rutgers, and even joining the same fraternity, Sigma Phi Delta. While our paths diverged in graduate school, with Shiva pursuing his PhD at Pacific Northwest National Laboratories, being on the west coast at the same time has been a unique and grounding experience. Alternating visits between cities, countless late-night calls, and shared marathons of Call of Duty or beloved TV shows like Frasier, 30 Rock, and Burn Notice were not just escapes—they were lifelines. These moments reminded me of the importance of laughter, connection, and the balance between work and life. Shiva, your friendship has been a constant source of strength and joy, and I truly cannot imagine having navigated this chapter without you. I am endlessly grateful for your unwavering presence and look forward to seeing how our shared journey continues to evolve.

To my tabletop gaming friends—Nicholas Mazzotta, William Schwab, Shiva Murali, Eric Kraut, and Jocelyn Shillingford—thank you for the endless laughter, camaraderie, and occasional chaos we've shared. What began as in-person tabletop gaming evolved into a long-distance tradition, providing a much-needed escape during the height of graduate school. Whether it was embarking on epic Dungeons and Dragons campaigns as Pro Bono Slayinus or navigating the hilariously cutthroat world of Munchkin, these moments were a source of pure joy amidst the intensity of research. Our spirited debates over card interpretations, often as heated as a courtroom drama, became stories we'd laugh about long after the games were over. Thank you for being part of this journey and for bringing light, humor, and a sense of connection when I needed it most.

To my family, the foundation of everything I am, I owe my deepest gratitude. Mom and Dad, your unwavering love, sacrifices, and belief in me have been my greatest strength. Your support has given me the privilege to pursue my education without hesitation, and your

encouragement has kept me grounded. Whether through calls, visits, or the countless trips across 2,500 miles, you've always reminded me that home is never far. I also want to thank Robert and Susan Keithler, who have been more than neighbors, but often akin to a second set of parents. Your kindness, guidance, and steadfast support over the years have made an indelible impact on my life.

Finally, I want to express my gratitude to my California family, whose presence has been a source of joy and connection throughout this chapter of my life. To Justin Urbanski, your brilliance, humility, and unwavering support have inspired me every day. You challenge me to be better, simply by being yourself, and your encouragement has carried me through some of the most difficult moments of this journey. I also want to thank your grandparents, Barbara and Dr. Theodore Urbanski, whose warmth and kindness have made me feel so welcome. To Tristan Stern, a friend whose connection spans so many stages of my life, thank you for the shared memories, board games, barcades, and everything in between. Danielle Lee, your presence in the inner circle and our shared love of Normal Gossip has been a bright spot, and I'm grateful to have both you and Tristan in my life.

Finally, to everyone who has touched this journey, whether through fleeting moments of encouragement or years of steadfast support, thank you. This dissertation is not just a culmination of data, experiments, and writing—it is a testament to the power of community, connection, and resilience. It reflects the love, wisdom, and kindness of everyone who has walked this path with me. From the depths of my heart, thank you. This journey would not have been possible without you, and I will continue to carry your support and love into everything I do.

VITA

2010-2014	Montgomery High School Skillman, NJ
2015-2017	*Aresty Research Fellowship* Rutgers University, New Brunswick New Brunswick, NJ
2016-2017	*NASA NJ Space Grant Research Consortium Fellowship* Rutgers University, New Brunswick New Brunswick, NJ
2017	*UCLA Amgen Scholars Program* University of California, Los Angeles Los Angeles, CA
2014-2018	*B.S., Chemical and Biochemical Engineering, Minor: Mathematics* Rutgers University, New Brunswick New Brunswick, NJ
2018-2023	*Teaching Assistant, Dept. of Chemical and Biomolecular Engineering* University of California, Los Angeles Los Angeles, CA
2020-2024	*University Fellowship, Division of Graduate Education* University of California, Los Angeles Los Angeles, CA

PUBLICATIONS

Dmitriy A. Ruckodanov, Nigel T. Maidment, and Harold G. Monbouquette, "Electrochemical Sensing of Dopamine by an Implantable Microelectrode Array Microprobe with an On-Probe Iridium Oxide Reference Electrode," *In Revision.*

Dmitriy A. Ruckodanov, Joshua R. Misa, Yi Tang, and Harold G. Monbouquette, "Ultra-High Throughput Functional Enrichment of Large γ-Aminobutyric Acid Oxidase Libraries by Fluorescence Activated Cell Sorting," *In Preparation.*

Dmitriy A. Ruckodanov and Harold G. Monbouquette, "Direct Electroenzymatic Sensing of γ-Aminobutyric Acid on a Multi-Electrode Array Microprobe," *In Preparation.*

PRESENTATIONS

Dmitriy A. Ruckodanov. (2016, November 13-18). *(184e) Wearable Sensor Comprised of Nafion-Single-Walled Carbon Nanotubes-Metal Oxide Nanoparticles for the Detection of the Chemical Warfare Agent Simulant DMMP.* 2016 AIChE Annual Meeting. San Francisco, CA, United States.

John Landers, Joel Baptist, **Dmitriy A. Ruckodanov**, Kenneth Zong, and Alexander V. Neimark. (2016, November 13-18). *(305e) Wearable Sensor Comprised of Nafion-Single-Walled Carbon Nanotubes-Metal Oxide Nanoparticles for the Detection of the Chemical Warfare Agent Simulant DMMP.* 2016 AIChE Annual Meeting. San Francisco, CA, United States.

Jonathan Colon, **Dmitriy A. Ruckodanov**, John Landers, and Alexander V. Neimark. (2018, October 28 – November 2). *(639c) Facile Induction of Mesoporosity within Crystalline Metal-Oxides by Hydrogen Peroxide Treatment.* 2018 AIChE Annual Meeting. Pittsburgh, PA, United States.

Dmitriy A. Ruckodanov. (2022, May 6). *Engineering a Monoamine Oxidase for Electroenzymatic γ -Aminobutyric Acid Sensing.* UCLA Chemical and Biomolecular Engineering Fourth Year Symposium. Los Angeles, CA, United States.

Dmitriy A. Ruckodanov, Nigel T. Maidment, and Harold G. Monbouquette. (2023, November 5-10). *(360e) Electrochemical Dopamine Sensing for Blood-Brain-Barrier Microphysiological System Drug Screening Applications.* 2023 AIChE Annual Meeting. Orlando, FL, United States.

Dmitriy A. Ruckodanov and Harold G. Monbouquette. (2024, October 27-31). *(640b) Engineered GABA Oxidase for GABA Sensing in vivo.* 2024 AIChE Annual Meeting. San Diego, CA, United States.

Chapter 1 : Introduction

1.1 Electrochemical Detection of Neurotransmitters

1.1.1 Motivation

A deep understanding of information processing in the brain is critical for neuroscience studies and the rational development of effective treatments for complex neurological disorders, including Huntington's disease, Alzheimer's disease, Parkinson's disease, ALS, and Jakob-Creutzfeldt disease [1-5]. Although brain signaling is highly complex, it can be classified into electrical and chemical signals. Electrical signals are generated by the firing of action potentials, propagating electrical signals along neurons. Neurotransmitters serve as chemical messengers to deliver signals across the synapse, from one neuron to the next [6-8]. While numerous successful research studies have focused on electrical signaling monitored through electrophysiological recordings [9-11], the study of chemical signaling, which plays a crucial role in mood and behavior, is less developed. Consequently, scientists still have limited data about the specific relationships between neurotransmitters and human neurological states [12-16].

Dopamine (DA) is a critical neurotransmitter involved in the regulation of motivation, cognition, and motor behavior [17-19]. Dysregulation of DA transmission is linked to various CNS disorders, including Parkinson's disease [20-22], schizophrenia [23-25], and substance abuse [26-28]. Monitoring DA signaling *in vivo* is essential for modeling these disorders and developing effective treatments [29]. Advances in electrochemical sensor technology, including the incorporation of on-probe iridium oxide (IrOx) reference electrodes [30], have enabled the creation

of highly sensitive DA sensors with ultralow detection limits and high selectivity against common electroactive interferents [31]. These DA sensors have been integrated into microphysiological systems that emulate the biochemistry of the blood-brain barrier [32], utilizing lab-on-a-chip devices [33]. These systems potentially facilitate the screening of drug effects on neurons with different biochemical profiles, allowing researchers to observe how hypothetical drugs impact patients with varying conditions [34], such as opioid addiction versus non-addiction. This innovative approach offers new insights into the mechanisms underlying neurological disorders and aids in the development of personalized treatments.

γ-Aminobutyric acid (GABA) is the most important inhibitory neurotransmitter in the mammalian brain, playing a vital role in maintaining the excitatory/inhibitory (E/I) balance [35-37]. Dysregulation of this balance is associated with a range of neurological conditions, including seizures [38], autism [39], and traumatic brain injury [40], which affect millions of people in the US. Despite its importance, high-performance methods to monitor GABA signaling at the cellular level and in near-real-time have been slow to emerge [41-43], especially for deep brain regions. The development of electroenzymatic sensors for GABA involves engineering a suitable GABA oxidase enzyme through directed evolution and optimizing sensor fabrication techniques to achieve high sensitivity, selectivity, and fast response times. These advancements are crucial for understanding GABA dynamics and their implications in various neurological disorders, ultimately contributing to better diagnostic and therapeutic strategies.

1.1.3 Current Sensing Mechanisms for Neurotransmitter Detection

Currently, sensors focus on detecting the neurotransmitter that leaks into the extracellular space after release into the synapse during chemical signaling. Microdialysis with high

performance liquid chromatography (HPLC) is one of the most popular traditional detection schemes [44-46]. It generally has very high sensitivity and can detect a broad range of species. However, long analysis times and relatively large probe sizes (>100 μm in width) result in limited temporal and spatial resolution [47-49]. Fluorescence imaging with high sensitivity and high temporal and spatial resolution also exhibits good potential [50-55]. However, limited light penetration in the brain [56], the need for genetic encoding [57], the requirement for expensive two-photon microscopy to achieve super-high single-neuron resolution [58], and slow dissociation times that can obscure rapid signaling dynamics [59] are significant limitations.

Electrochemical sensing of neurotransmitters has emerged as a viable and rapid way to monitor neurotransmitters with high temporal and spatial resolution [60-62]. Fast scan cyclic voltammetry (FSCV) is one of the proven successful electrochemical detection methods, offering high sensitivity, high temporal and spatial resolution, and being label-free [63-65]. However, FSCV is limited to a small number of electroactive species [66] and has difficulty in multiplexing [67]. Constant potential amperometry (CPA) is a promising method where the electrode is held at a constant potential, and the oxidation of electro-oxidizable molecules is measured by current change. CPA has advantages including high spatial and temporal resolution [61, 68-70], being label-free, and providing a real-time view of species detection [71-73]. The major limitation of CPA is the inability to differentiate between different electrooxidizable species, which can be addressed by coating permselective polymers and enzymes on the electrode surfaces [62, 71, 74]. Field-effect-transistors (FETs) conjugated with aptamers also display great potential for integrated neural activity recordings at high spatiotemporal resolution and are not limited to electroactive species [75-77].

Microelectrode arrays (MEAs) have gained popularity for their ability to monitor multiple neurotransmitters simultaneously with high spatial resolution [78-81]. These devices can be integrated with microfluidic platforms, creating lab-on-a-chip systems that mimic the complex environment of the brain, facilitating the study of neurotransmitter dynamics in more physiologically relevant conditions [82-84]. Recent advances in nanomaterials, such as carbon nanotubes [85] and graphene [70], have further enhanced the performance of electrochemical sensors by increasing their sensitivity and lowering detection limits. These materials offer high surface area, excellent conductivity, and biocompatibility [86], making them ideal for neurotransmitter detection.

1.1.2 Directed Evolution for Biosensing Applications

The field of neurotransmitter detection has advanced significantly with the adoption of fast-scan cyclic voltammetry (FSCV) and constant potential amperometry (CPA). FSCV provides excellent temporal resolution, making it well-suited for capturing rapid changes in neurotransmitter concentrations. However, its applicability is limited to electroactive species, and achieving multiplexing is often challenging due to overlapping oxidation potentials [87]. CPA, on the other hand, offers a versatile platform for detecting both electroactive and non-electroactive neurotransmitters through the integration of oxidase enzymes and electrode coatings. These sensors typically rely on electrode coatings that are permselective for H_2O_2, allowing selective detection of the enzymatic byproduct while excluding interfering species. Alternatively, coatings that are permselective for the electroactive analyte itself can be employed to ensure specificity in the detection process. In both cases, the immobilization of selective enzyme layers, such as oxidases, plays a critical role in generating steady-state currents corresponding to the concentration

of the target analyte [88]. While CPA supports multiplexing and real-time monitoring, its success is contingent upon the optimization of these permselective layers to minimize interference from electroactive compounds in the extracellular environment.

The revolutionary technique of directed evolution has paved the way for new advancements in biosensing technologies, particularly in the realm of CPA. The invention of directed evolution, which recently resulted in the award of a Nobel Prize in Chemistry to Frances Arnold, emulates natural selection to evolve proteins or nucleic acids toward specific, user-defined goals [89]. This process involves iterative rounds of mutagenesis and selection to create enzymes with desired characteristics. It has proven to be a powerful tool for engineering enzymes with improved activity, stability, and selectivity for targeted substrates [90].

Applying directed evolution to biosensing technologies holds immense potential, enabling the creation of bespoke enzymes tailored for novel substrates [91, 92] and expanding the capabilities of CPA-based sensors. For example, while GABA is not inherently electroactive, directed evolution allows for the development of a GABA oxidase enzyme that can effectively catalyze GABA oxidation, producing electroactive hydrogen peroxide as a byproduct. Broadly, this technique creates a framework through which CPA-based biosensors can be fitted with novel enzymes to detect non-electroactive substrates, like GABA, with high selectivity and sensitivity. The implications of this are profound, as directed evolution allows researchers to design and implement CPA sensors for a broad range of substrates, enhancing the versatility and application scope of electroenzymatic sensors [93]. This ability to tailor enzymes for specific needs can significantly improve the monitoring of neurotransmitters and other biochemical compounds, facilitating a deeper understanding of their roles in neurological processes and diseases. As a result, directed evolution stands as a transformative approach in the advancement of biosensing

technologies, enabling precise and reliable detection of a wide array of analytes that were previously challenging to monitor.

1.2 References

[1] M. van Spronsen and C. C. Hoogenraad, "Synapse Pathology in Psychiatric and Neurologic Disease," *Current Neurology and Neuroscience Reports,* vol. 10, no. 3, pp. 207-214, 2010/05/01 2010, doi: 10.1007/s11910-010-0104-8.

[2] N. Pathak, S. K. Vimal, I. Tandon, L. Agrawal, C. Hongyi, and S. Bhattacharyya, "Neurodegenerative Disorders of Alzheimer, Parkinsonism, Amyotrophic Lateral Sclerosis and Multiple Sclerosis: An Early Diagnostic Approach for Precision Treatment," *Metabolic Brain Disease,* vol. 37, no. 1, pp. 67-104, 2022/01/01 2022, doi: 10.1007/s11011-021-00800-w.

[3] A. V. Ciurea *et al.*, "Unraveling Molecular and Genetic Insights into Neurodegenerative Diseases: Advances in Understanding Alzheimer's, Parkinson's, and Huntington's Diseases and Amyotrophic Lateral Sclerosis," *International Journal of Molecular Sciences,* vol. 24, no. 13, p. 10809, 2023. [Online]. Available: https://www.mdpi.com/1422-0067/24/13/10809.

[4] S. Majd, J. H. Power, and H. J. M. Grantham, "Neuronal response in Alzheimer's and Parkinson's disease: the effect of toxic proteins on intracellular pathways," *BMC Neuroscience,* vol. 16, no. 1, p. 69, 2015/10/23 2015, doi: 10.1186/s12868-015-0211-1.

[5] S. E. Davis, A. B. Cirincione, A. C. Jimenez-Torres, and J. Zhu, "The Impact of Neurotransmitters on the Neurobiology of Neurodegenerative Diseases," *International Journal of Molecular Sciences,* vol. 24, no. 20, p. 15340, 2023. [Online]. Available: https://www.mdpi.com/1422-0067/24/20/15340.

[6] D. O. Borroto-Escuela *et al.*, "Understanding electrical and chemical transmission in the brain," (in English), *Frontiers in Cellular Neuroscience,* Review vol. 18, 2024-June-26 2024, doi: 10.3389/fncel.2024.1398862.

[7] S. Curti, F. Davoine, and A. Dapino, "Function and Plasticity of Electrical Synapses in the Mammalian Brain: Role of Non-Junctional Mechanisms," *Biology,* vol. 11, no. 1, p. 81, 2022. [Online]. Available: https://www.mdpi.com/2079-7737/11/1/81.

[8] R. I. Teleanu, A.-G. Niculescu, E. Roza, O. Vladâcenco, A. M. Grumezescu, and D. M. Teleanu, "Neurotransmitters—Key Factors in Neurological and Neurodegenerative Disorders of the Central Nervous System," *International Journal of Molecular Sciences,* vol. 23, no. 11, p. 5954, 2022. [Online]. Available: https://www.mdpi.com/1422-0067/23/11/5954.

[9] W. L. Coleman and R. M. Burger, "53Extracellular Single-Unit Recording and Neuropharmacological Methods," in *Basic Electrophysiological Methods*, E. Covey and M. Carter Eds.: Oxford University Press, 2015, sec. Oxford Academic, p. 0.

[10] N. Graziane and Y. Dong, "Extracellular Recordings," in *Electrophysiological Analysis of Synaptic Transmission*, N. Graziane and Y. Dong Eds. New York, NY: Springer US, 2022, pp. 253-261.

[11] F. Jiang, S. T. Bello, Q. Gao, Y. Lai, X. Li, and L. He, "Advances in the Electrophysiological Recordings of Long-Term Potentiation," *International Journal of Molecular Sciences,* vol. 24, no. 8, p. 7134, 2023. [Online]. Available: https://www.mdpi.com/1422-0067/24/8/7134.

[12] S. Harilal, R. Kumar, G. E. Mathew, J. Jose, M. S. Uddin, and B. Mathew, "Neurochemicals in Nervous System and Exploring the Chemical Make-Up of Human Brain," in *Principles of Neurochemistry: Fundamentals and Applications*, B. Mathew and D. G. Thomas Parambi Eds. Singapore: Springer Singapore, 2020, pp. 19-39.

[13] L. Hampel and T. Lau, "Neurobiological Principles: Neurotransmitters," in *NeuroPsychopharmacotherapy*, P. Riederer, G. Laux, B. Mulsant, W. Le, and T. Nagatsu Eds. Cham: Springer International Publishing, 2020, pp. 1-21.

[14] S. D. Niyonambaza *et al.*, "A Review of Neurotransmitters Sensing Methods for Neuro-Engineering Research," *Applied Sciences,* vol. 9, no. 21, p. 4719, 2019. [Online]. Available: https://www.mdpi.com/2076-3417/9/21/4719.

[15] P. Kumar, S. N. Abed, Y. A. Bataineh, and M. S. Salem, "Neurotransmitters and Their Receptors—State of the Art," in *Frontiers in Pharmacology of Neurotransmitters*, P. Kumar and P. K. Deb Eds. Singapore: Springer Singapore, 2020, pp. 1-29.

[16] W. R. Clark, M. Grunstein, W. R. Clark, and M. Grunstein, "137The Role of Neurotransmitters in Human Behavior," in *Are We Hardwired?: The Role of Genes in Human Behavior*: Oxford University Press, 2004, sec. Oxford Academic, p. 0.

[17] L. Speranza, U. di Porzio, D. Viggiano, A. de Donato, and F. Volpicelli, "Dopamine: The Neuromodulator of Long-Term Synaptic Plasticity, Reward and Movement Control," *Cells,* vol. 10, no. 4, p. 735, 2021. [Online]. Available: https://www.mdpi.com/2073-4409/10/4/735.

[18] E. Aarts, M. van Holstein, and R. Cools, "Striatal Dopamine and the Interface between Motivation and Cognition," (in English), *Frontiers in Psychology,* Review vol. 2, 2011-July-14 2011, doi: 10.3389/fpsyg.2011.00163.

[19] G. P. Brinder P., Sidakbir S., "Dopamine: "The Neurotransmitter of Desire, Movement and More"," *Clinical Neuroscience & Neurological Research International Journal,* vol. 5, no. 1, 2024.

[20] M. Banwinkler *et al.*, "Putaminal dopamine modulates movement motivation in Parkinson's disease," *Brain,* vol. 147, no. 10, pp. 3352-3357, 2024, doi: 10.1093/brain/awae214.

[21] K. M. L. Cramb, D. Beccano-Kelly, S. J. Cragg, and R. Wade-Martins, "Impaired dopamine release in Parkinson's disease," *Brain,* vol. 146, no. 8, pp. 3117-3132, 2023, doi: 10.1093/brain/awad064.

[22] X. Flores-Ponce and I. Velasco, "Dopaminergic neuron metabolism: relevance for understanding Parkinson's disease," *Metabolomics,* vol. 20, no. 6, p. 116, 2024/10/13 2024, doi: 10.1007/s11306-024-02181-4.

[23] A. Heinz and F. Schlagenhauf, "Dopaminergic Dysfunction in Schizophrenia: Salience Attribution Revisited," *Schizophrenia Bulletin,* vol. 36, no. 3, pp. 472-485, 2010, doi: 10.1093/schbul/sbq031.

[24] G. J. Lyon, A. Abi-Dargham, H. Moore, J. A. Lieberman, J. A. Javitch, and D. Sulzer, "Presynaptic Regulation of Dopamine Transmission in Schizophrenia," *Schizophrenia Bulletin,* vol. 37, no. 1, pp. 108-117, 2009, doi: 10.1093/schbul/sbp010.

[25] A. A. Grace and F. V. Gomes, "The Circuitry of Dopamine System Regulation and its Disruption in Schizophrenia: Insights Into Treatment and Prevention," *Schizophrenia Bulletin,* vol. 45, no. 1, pp. 148-157, 2018, doi: 10.1093/schbul/sbx199.

[26] M. Diana, "The Dopamine Hypothesis of Drug Addiction and Its Potential Therapeutic Value," (in English), *Frontiers in Psychiatry,* Hypothesis and Theory vol. 2, 2011-November-29 2011, doi: 10.3389/fpsyt.2011.00064.

[27] N. D. Volkow, J. S. Fowler, G.-J. Wang, J. M. Swanson, and F. Telang, "Dopamine in Drug Abuse and Addiction: Results of Imaging Studies and Treatment Implications," *Archives of Neurology,* vol. 64, no. 11, pp. 1575-1579, 2007, doi: 10.1001/archneur.64.11.1575.

[28] A. Hayes, K. Herlinger, L. Paterson, and A. Lingford-Hughes, "The neurobiology of substance use and addiction: evidence from neuroimaging and relevance to treatment," *BJPsych Advances,* vol. 26, no. 6, pp. 367-378, 2020, doi: 10.1192/bja.2020.68.

[29] L. Miguel Telega, D. Ashouri Vajari, T. Stieglitz, V. A. Coenen, and M. D. Döbrössy, "New Insights into In Vivo Dopamine Physiology and Neurostimulation: A Fiber Photometry Study Highlighting the Impact of Medial Forebrain Bundle Deep Brain Stimulation on the Nucleus Accumbens," *Brain Sciences,* vol. 12, no. 8, p. 1105, 2022. [Online]. Available: https://www.mdpi.com/2076-3425/12/8/1105.

[30] V. M. Tolosa, K. M. Wassum, N. T. Maidment, and H. G. Monbouquette, "Electrochemically deposited iridium oxide reference electrode integrated with an electroenzymatic glutamate sensor on a multi-electrode array microprobe," (in eng), *Biosens Bioelectron,* vol. 42, pp. 256-60, Apr 15 2013, doi: 10.1016/j.bios.2012.10.061.

[31] B. T. Seaton and M. L. Heien, "Biocompatible reference electrodes to enhance chronic electrochemical signal fidelity in vivo," *Analytical and Bioanalytical Chemistry,* vol. 413, no. 27, pp. 6689-6701, 2021/11/01 2021, doi: 10.1007/s00216-021-03640-w.

[32] C. S. Lee and K. W. Leong, "Advances in microphysiological blood-brain barrier (BBB) models towards drug delivery," (in eng), *Curr Opin Biotechnol,* vol. 66, pp. 78-87, Dec 2020, doi: 10.1016/j.copbio.2020.06.009.

[33] R. O. Rodrigues, S.-R. Shin, and M. Bañobre-López, "Brain-on-a-chip: an emerging platform for studying the nanotechnology-biology interface for neurodegenerative disorders," *Journal of Nanobiotechnology,* vol. 22, no. 1, p. 573, 2024/09/18 2024, doi: 10.1186/s12951-024-02720-0.

[34] Y. Fan *et al.*, "Understanding drug nanocarrier and blood–brain barrier interaction based on a microfluidic microphysiological model," *Lab on a Chip,* 10.1039/D2LC01077A vol. 23, no. 7, pp. 1935-1944, 2023, doi: 10.1039/D2LC01077A.

[35] C. R. Gamlin, W.-Q. Yu, R. O. L. Wong, and M. Hoon, "Assembly and maintenance of GABAergic and Glycinergic circuits in the mammalian nervous system," *Neural Development,* vol. 13, no. 1, p. 12, 2018/06/07 2018, doi: 10.1186/s13064-018-0109-6.

[36] S. Almutairi, A. Sivadas, and A. Kwakowsky, "The Effect of Oral GABA on the Nervous System: Potential for Therapeutic Intervention," *Nutraceuticals,* vol. 4, no. 2, pp. 241-259, 2024. [Online]. Available: https://www.mdpi.com/1661-3821/4/2/15.

[37] C. J. McArdle, A. A. Arnone, C. F. Heaney, and K. F. Raab-Graham, "A paradoxical switch: the implications of excitatory GABAergic signaling in neurological disorders," (in English), *Frontiers in Psychiatry,* Review vol. 14, 2024-January-10 2024, doi: 10.3389/fpsyt.2023.1296527.

[38] V. S. Sohal and J. L. R. Rubenstein, "Excitation-inhibition balance as a framework for investigating mechanisms in neuropsychiatric disorders," *Molecular Psychiatry,* vol. 24, no. 9, pp. 1248-1257, 2019/09/01 2019, doi: 10.1038/s41380-019-0426-0.

[39] L. Culotta and P. Penzes, "Exploring the mechanisms underlying excitation/inhibition imbalance in human iPSC-derived models of ASD," *Molecular Autism,* vol. 11, no. 1, p. 32, 2020/05/11 2020, doi: 10.1186/s13229-020-00339-0.

[40] Y. Kang *et al.*, "Longitudinal alterations in gamma-aminobutyric acid (GABAA) receptor availability over ∼ 1 year following traumatic brain injury," *Brain Communications,* vol. 4, no. 4, 2022, doi: 10.1093/braincomms/fcac159.

[41] I. Hossain *et al.*, "A Novel Microbiosensor Microarray for Continuous ex Vivo Monitoring of Gamma-Aminobutyric Acid in Real-Time," (in English), *Frontiers in Neuroscience,* Original Research vol. 12, 2018-August-07 2018, doi: 10.3389/fnins.2018.00500.

[42] X. Qian, Y. Chen, B. Ma, H. Hao, and L. Li, "Chronically monitoring the deep brain rhythms: from stimulation to recording," *Science Bulletin,* vol. 61, no. 19, pp. 1522-1524, 2016/10/01 2016, doi: 10.1007/s11434-016-1159-y.

[43] I. Bok *et al.*, "Wireless agents for brain recording and stimulation modalities," *Bioelectronic Medicine,* vol. 9, no. 1, p. 20, 2023/09/20 2023, doi: 10.1186/s42234-023-00122-5.

[44] B. P. Guiard and G. Gotti, "The High-Precision Liquid Chromatography with Electrochemical Detection (HPLC-ECD) for Monoamines Neurotransmitters and Their Metabolites: A Review," *Molecules,* vol. 29, no. 2, p. 496, 2024. [Online]. Available: https://www.mdpi.com/1420-3049/29/2/496.

[45] G.-W. Cheng, K.-C. Hsu, C.-F. Lee, H.-L. Wu, and Y.-L. Huang, "On-line Microdialysis Coupled with Liquid Chromatography for Biomedical Analysis," *Journal of Chromatographic Science,* vol. 47, no. 8, pp. 624-630, 2009, doi: 10.1093/chromsci/47.8.624.

[46] J. C. Cooley, M. W. Ducey, A. R. Regel, P. Nandi, S. M. Lunte, and C. E. Lunte, "Analytical Considerations for Microdialysis Sampling," in *Microdialysis in Drug Development*, M. Müller Ed. New York, NY: Springer New York, 2013, pp. 35-66.

[47] S. S. Wells, I. J. Bain, A. C. Valenta, A. E. Lenhart, D. J. Steyer, and R. T. Kennedy, "Microdialysis coupled with droplet microfluidics and mass spectrometry for determination of neurotransmitters in vivo with high temporal resolution," *Analyst,* 10.1039/D4AN00112E vol. 149, no. 8, pp. 2328-2337, 2024, doi: 10.1039/D4AN00112E.

[48] D. L. Krebs-Kraft, K. J. Frantz, and M. B. Parent, "In Vivo Microdialysis: A Method for Sampling Extracellular Fluid in Discrete Brain Regions," in *Handbook of Neurochemistry and Molecular Neurobiology: Practical Neurochemistry Methods*, A. Lajtha, G. Baker, S. Dunn, and A. Holt Eds. New York, NY: Springer US, 2007, pp. 219-256.

[49] C. M. Kho, S. K. Enche Ab Rahim, Z. A. Ahmad, and N. S. Abdullah, "A Review on Microdialysis Calibration Methods: the Theory and Current Related Efforts," *Molecular Neurobiology,* vol. 54, no. 5, pp. 3506-3527, 2017/07/01 2017, doi: 10.1007/s12035-016-9929-8.

[50] L. Meng *et al.*, "High-efficiency fluorescent and magnetic multimodal probe for long-term monitoring and deep penetration imaging of tumors," *Journal of Materials Chemistry B,* 10.1039/C9TB00638A vol. 7, no. 35, pp. 5345-5351, 2019, doi: 10.1039/C9TB00638A.

[51] T. Wang, Y. Chen, B. Wang, X. Gao, and M. Wu, "Recent Progress in Second Near-Infrared (NIR-II) Fluorescence Imaging in Cancer," *Biomolecules,* vol. 12, no. 8, p. 1044, 2022. [Online]. Available: https://www.mdpi.com/2218-273X/12/8/1044.

[52] A. Refaat *et al.*, "In vivo fluorescence imaging: success in preclinical imaging paves the way for clinical applications," *Journal of Nanobiotechnology,* vol. 20, no. 1, p. 450, 2022/10/15 2022, doi: 10.1186/s12951-022-01648-7.

[53] P. P. Mondal, "Temporal resolution in fluorescence imaging," (in English), *Frontiers in Molecular Biosciences,* Review vol. 1, 2014-September-09 2014, doi: 10.3389/fmolb.2014.00011.

[54] A. C. Sias *et al.*, "Dopamine projections to the basolateral amygdala drive the encoding of identity-specific reward memories," *Nature Neuroscience,* vol. 27, no. 4, pp. 728-736, 2024/04/01 2024, doi: 10.1038/s41593-024-01586-7.

[55] B. Halbout *et al.*, "Mesolimbic dopamine projections mediate cue-motivated reward seeking but not reward retrieval in rats," *eLife,* vol. 8, p. e43551, 2019/05/20 2019, doi: 10.7554/eLife.43551.

[56] M. E. Lacin and M. Yildirim, "Applications of multiphoton microscopy in imaging cerebral and retinal organoids," (in English), *Frontiers in Neuroscience,* Review vol. 18, 2024-March-05 2024, doi: 10.3389/fnins.2024.1360482.

[57] F. Feng, H. Mao, A. Wang, and L. Chen, "Two-Photon Fluorescence Imaging," in *Optical Imaging in Human Disease and Biological Research*, X. Wei and B. Gu Eds. Singapore: Springer Singapore, 2021, pp. 45-61.

[58] S. Chamberland *et al.*, "Fast two-photon imaging of subcellular voltage dynamics in neuronal tissue with genetically encoded indicators," *eLife,* vol. 6, p. e25690, 2017/07/27 2017, doi: 10.7554/eLife.25690.

[59] R. Huda, L. A. Ibrahim, and B. Bloem, "Two-Photon Microscopy for Studying RewardRewardsCircuits of the Brain," in *The Brain Reward System*, M. Fakhoury Ed. New York, NY: Springer US, 2021, pp. 339-363.

[60] Z. Yueyue, "Electrochemical Sensing of Neurotransmitters with High Temporal and Spatial Resolution," *Bulletin of Chinese Academy of Sciences,* vol. 32, no. 12, 2017.

[61] K. Jackowska and P. Krysinski, "New trends in the electrochemical sensing of dopamine," *Analytical and Bioanalytical Chemistry,* vol. 405, no. 11, pp. 3753-3771, 2013/04/01 2013, doi: 10.1007/s00216-012-6578-2.

[62] Y. Ou, A. M. Buchanan, C. E. Witt, and P. Hashemi, "Frontiers in electrochemical sensors for neurotransmitter detection: towards measuring neurotransmitters as chemical diagnostics for brain disorders," *Analytical Methods,* 10.1039/C9AY00055K vol. 11, no. 21, pp. 2738-2755, 2019, doi: 10.1039/C9AY00055K.

[63] P. Puthongkham and B. J. Venton, "Recent advances in fast-scan cyclic voltammetry," *Analyst,* 10.1039/C9AN01925A vol. 145, no. 4, pp. 1087-1102, 2020, doi: 10.1039/C9AN01925A.

[64] B. J. Venton and Q. Cao, "Fundamentals of fast-scan cyclic voltammetry for dopamine detection," *Analyst,* 10.1039/C9AN01586H vol. 145, no. 4, pp. 1158-1168, 2020, doi: 10.1039/C9AN01586H.

[65] D. L. Robinson, B. J. Venton, M. L. A. V. Heien, and R. M. Wightman, "Detecting Subsecond Dopamine Release with Fast-Scan Cyclic Voltammetry in Vivo," *Clinical Chemistry,* vol. 49, no. 10, pp. 1763-1773, 2003, doi: 10.1373/49.10.1763.

[66] K. E. Dunham and B. J. Venton, "Electrochemical and biosensor techniques to monitor neurotransmitter changes with depression," *Analytical and Bioanalytical Chemistry,* vol. 416, no. 9, pp. 2301-2318, 2024/04/01 2024, doi: 10.1007/s00216-024-05136-9.

[67] P. J. Clark and R. A. España, "Fast Scan Cyclic Voltammetry to Assess Dopamine Function: From Circuits to Behavior," in *Dopaminergic System Function and Dysfunction: Experimental Approaches*, J. A. Fuentealba-Evans and P. Henny Eds. New York, NY: Springer US, 2023, pp. 249-281.

[68] I. Anshori *et al.*, "Gold Nanospikes Formation on Screen-Printed Carbon Electrode through Electrodeposition Method for Non-Enzymatic Electrochemical Sensor," *Metals,* vol. 12, no. 12, p. 2116, 2022. [Online]. Available: https://www.mdpi.com/2075-4701/12/12/2116.

[69] Y. Liu, J. Du, M. Wang, J. Zhang, C. Liu, and X. Li, "Recent Progress in Quantitatively Monitoring Vesicular Neurotransmitter Release and Storage With

Micro/Nanoelectrodes," (in English), *Frontiers in Chemistry,* Review vol. 8, 2021-January-11 2021, doi: 10.3389/fchem.2020.591311.

[70] B. Si and E. Song, "Recent Advances in the Detection of Neurotransmitters," *Chemosensors,* vol. 6, no. 1, p. 1, 2018. [Online]. Available: https://www.mdpi.com/2227-9040/6/1/1.

[71] E. M. Richter and R. A. A. Munoz, "Amperometric Detection for Bioanalysis," in *Tools and Trends in Bioanalytical Chemistry*, L. T. Kubota, J. A. F. da Silva, M. M. Sena, and W. A. Alves Eds. Cham: Springer International Publishing, 2022, pp. 253-264.

[72] Z. Tavakolian-Ardakani, O. Hosu, C. Cristea, M. Mazloum-Ardakani, and G. Marrazza, "Latest Trends in Electrochemical Sensors for Neurotransmitters: A Review," *Sensors,* vol. 19, no. 9, p. 2037, 2019. [Online]. Available: https://www.mdpi.com/1424-8220/19/9/2037.

[73] T. Rajarathinam, M. Kang, S. Hong, and S.-C. Chang, "Nanocomposite-Based Electrochemical Sensors for Neurotransmitters Detection in Neurodegenerative Diseases," *Chemosensors,* vol. 11, no. 2, p. 103, 2023. [Online]. Available: https://www.mdpi.com/2227-9040/11/2/103.

[74] I. w. Huang, M. Clay, S. Wang, Y. Guo, J. Nie, and H. G. Monbouquette, "Electroenzymatic glutamate sensing at near the theoretical performance limit," *Analyst,* 10.1039/C9AN01969C vol. 145, no. 7, pp. 2602-2611, 2020, doi: 10.1039/C9AN01969C.

[75] C. Zhao *et al.*, "Implantable aptamer–field-effect transistor neuroprobes for in vivo neurotransmitter monitoring," *Science Advances,* vol. 7, no. 48, p. eabj7422, 2021, doi: doi:10.1126/sciadv.abj7422.

[76] X. Duan, "Nanoscale Field-Effect Transistors for Minimally Invasive, High Spatial Resolution, and Three-Dimensional Action Potential Recording," in *Nanotechnology and Neuroscience: Nano-electronic, Photonic and Mechanical Neuronal Interfacing*, M. De Vittorio, L. Martiradonna, and J. Assad Eds. New York, NY: Springer New York, 2014, pp. 13-43.

[77] M. Abrantes *et al.*, "Ultrasensitive dopamine detection with graphene aptasensor multitransistor arrays," *Journal of Nanobiotechnology,* vol. 20, no. 1, p. 495, 2022/11/24 2022, doi: 10.1186/s12951-022-01695-0.

[78] E. Castagnola *et al.*, "Glassy carbon microelectrode arrays enable voltage-peak separated simultaneous detection of dopamine and serotonin using fast scan cyclic voltammetry," *Analyst,* 10.1039/D1AN00425E vol. 146, no. 12, pp. 3955-3970, 2021, doi: 10.1039/D1AN00425E.

[79] J. Ding *et al.*, "Flexible silk-fibroin-based microelectrode arrays for high-resolution neural recording," *Materials Horizons,* 10.1039/D4MH00438H vol. 11, no. 18, pp. 4338-4347, 2024, doi: 10.1039/D4MH00438H.

[80] X. Liu, Y. Gong, Z. Jiang, T. Stevens, and W. Li, "Flexible high-density microelectrode arrays for closed-loop brain–machine interfaces: a review," (in English), *Frontiers in Neuroscience,* Review vol. 18, 2024-April-15 2024, doi: 10.3389/fnins.2024.1348434.

[81] S. Schulte, M. Gries, A. Christmann, and K.-H. Schäfer, "Using multielectrode arrays to investigate neurodegenerative effects of the amyloid-beta peptide," *Bioelectronic Medicine,* vol. 7, no. 1, p. 15, 2021/10/28 2021, doi: 10.1186/s42234-021-00078-4.

[82] E. Moutaux, B. Charlot, A. Genoux, F. Saudou, and M. Cazorla, "An integrated microfluidic/microelectrode array for the study of activity-dependent intracellular dynamics in neuronal networks," *Lab on a Chip,* 10.1039/C8LC00694F vol. 18, no. 22, pp. 3425-3435, 2018, doi: 10.1039/C8LC00694F.

[83] J. W. Kim *et al.*, "Microfluidic electrode array chip for electrical stimulation-mediated axonal regeneration," *Lab on a Chip,* 10.1039/D1LC01158H vol. 22, no. 11, pp. 2122-2130, 2022, doi: 10.1039/D1LC01158H.

[84] A. Scott, K. Weir, C. Easton, W. Huynh, W. J. Moody, and A. Folch, "A microfluidic microelectrode array for simultaneous electrophysiology, chemical stimulation, and imaging of brain slices," *Lab on a Chip,* 10.1039/C2LC40826K vol. 13, no. 4, pp. 527-535, 2013, doi: 10.1039/C2LC40826K.

[85] H. M. Dewey, A. Lamb, and J. Budhathoki-Uprety, "Recent advances on applications of single-walled carbon nanotubes as cutting-edge optical nanosensors for biosensing technologies," *Nanoscale,* 10.1039/D4NR01892C vol. 16, no. 35, pp. 16344-16375, 2024, doi: 10.1039/D4NR01892C.

[86] H. Ehtesabi and S.-O. Kalji, "Recent Advancements in 3D Graphene for Electrochemical Sensors," in *3D Graphene: Fundamentals, Synthesis, and Emerging Applications*, R. K. Gupta Ed. Cham: Springer Nature Switzerland, 2023, pp. 75-91.

[87] H. Rafi and A. G. Zestos, "Multiplexing neurochemical detection with carbon fiber multielectrode arrays using fast-scan cyclic voltammetry," *Analytical and Bioanalytical Chemistry,* vol. 413, no. 27, pp. 6715-6726, 2021/11/01 2021, doi: 10.1007/s00216-021-03526-x.

[88] Z. Fredj, B. Singh, M. Bahri, P. Qin, and M. Sawan, "Enzymatic Electrochemical Biosensors for Neurotransmitters Detection: Recent Achievements and Trends," *Chemosensors,* vol. 11, no. 7, p. 388, 2023. [Online]. Available: https://www.mdpi.com/2227-9040/11/7/388.

[89] L. Sellés Vidal, M. Isalan, J. T. Heap, and R. Ledesma-Amaro, "A primer to directed evolution: current methodologies and future directions," *RSC Chemical Biology,* 10.1039/D2CB00231K vol. 4, no. 4, pp. 271-291, 2023, doi: 10.1039/D2CB00231K.

[90] K. Voskarides, "Directed Evolution. The Legacy of a Nobel Prize," *Journal of Molecular Evolution,* vol. 89, no. 3, pp. 189-191, 2021/04/01 2021, doi: 10.1007/s00239-020-09972-y.

[91] J. S. Andon, B. Lee, and T. Wang, "Enzyme directed evolution using genetically encodable biosensors," *Organic & Biomolecular Chemistry,* 10.1039/D2OB00443G vol. 20, no. 30, pp. 5891-5906, 2022, doi: 10.1039/D2OB00443G.

[92] H. Du *et al.*, "Directed Evolution of 4-Hydroxyphenylpyruvate Biosensors Based on a Dual Selection System," *International Journal of Molecular Sciences,* vol. 25, no. 3, p. 1533, 2024. [Online]. Available: https://www.mdpi.com/1422-0067/25/3/1533.

[93] S. Chen *et al.*, "Ultrahigh-throughput screening-assisted in vivo directed evolution for enzyme engineering," *Biotechnology for Biofuels and Bioproducts,* vol. 17, no. 1, p. 9, 2024/01/22 2024, doi: 10.1186/s13068-024-02457-w.

Chapter 2 : Electrochemical Sensing of Dopamine by an Implantable Microelectrode Array Microprobe with an On-Probe Iridium Oxide Reference Electrode

Chapter 2 is a manuscript under review with the following citation:

D. Ruckodanov et al., "Electrochemical Sensing of Dopamine with an Implantable Microelectrode Array Microprobe including an On-Probe Iridium Oxide Reference Electrode." *ACS Chemical Neuroscience*, Submitted.

ABSTRACT

Inclusion of an on-probe iridium oxide (IrOx) reference electrode on an implantable microelectrode array (MEA) microprobe enabled dopamine (DA) sensing with high sensitivity, an ultralow limit of detection, and high selectivity against common electroactive interferents. The monitoring of DA signaling in vivo is important for the study of nervous system disorders such as Parkinson's disease and substance abuse. A post-fabrication method for electrochemical deposition of an IrOx film onto a targeted microelectrode enabled integration of an IrOx reference electrode (RE) onto the same MEA as the DA sensing, working electrode (WE). The on-probe IrOx RE is an attractive alternative to commonly used external Ag/AgCl wire REs, which can be unstable and can cause inflammatory responses in living tissue. The on-probe IrOx RE was tested for support of DA sensing performance in two-electrode (i.e., WE and RE) and three-electrode (i.e., WE, RE and counter electrode) configurations. The sensitivities of the integrated and externally referenced DA sensing microprobes were comparable at ~2500 nA/(μM·cm^2), however the integrated three-electrode configuration exhibited a 6-fold lower limit of detection of ~9 nM due to a significant,

82% reduction in baseline noise. In addition, excellent 1000:1 selectivity against common electroactive interferents makes these DA sensing microprobes attractive for implementation *in vivo*.

2.1 Introduction

Dopamine (DA) is an important neurotransmitter in the brain for regulation of motivation, cognition and motor behavior; and dysregulation of DA transmission has been associated with substance abuse, schizophrenia and Parkinson's disease, among other CNS disorders. Thus, it has long been a goal of neuroscientists to develop technologies to monitor DA signaling in the brain sensitively and selectively with high spatiotemporal resolution. Two primary approaches for electrochemical DA sensing have emerged, fast scan cyclic voltammetry (FSCV) and constant potential amperometry (CPA). In FSCV, the potential applied to a microelectrode (usually a carbon fiber) is ramped back and forth rapidly between two voltage set points, and the DA concentration is divined from the transients in current over the potential range characteristic of DA electrochemistry [1, 2]. CPA is a simpler electrochemical technique with a potentially faster response time, but permselective microelectrode coatings must be used to ensure acceptable selectivity [3, 4].

The desire to monitor multiple neurotransmitters simultaneously, including those not directly oxidizable at the electrode such as glutamate or acetylcholine, has led to the development of silicon wafer-based platinum microelectrode arrays (MEAs) that are fabricated using micro-electro-mechanical-systems (MEMS) technologies. Effective, implantable neurochemical sensing devices utilizing MEAs have been constructed that are based on immobilized oxidases (*e.g.*, for

glutamate, choline) or on direct electrooxidation of the analyte (e.g., for dopamine) [5-7]. The electrooxidation of dopamine occurs as follows,

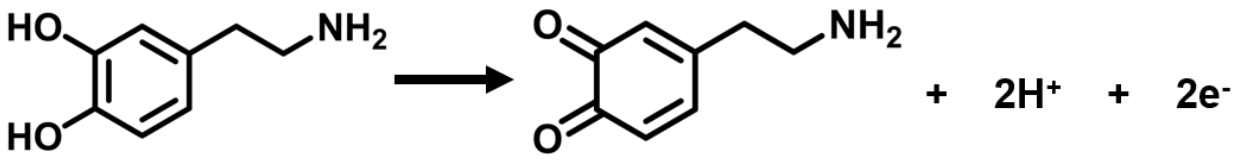

Dopamine (DA) Dopamine-o-quinone (DOQ)

where the flow of product electrons provides the sensor current signal. This signal may be correlated to the concentration of DA in the surrounding microenvironment. In previous work, we demonstrated the effective monitoring of DA, glutamate and choline concentration transients both in vitro and in vivo, using silicon MEA-based electrochemical sensors [8-10].

For these devices, a combination of Nafion and overoxidized polypyrrole (OPP) films on the surface of the microelectrode can prevent interfering responses from electroactive species common to brain extracellular fluid (ECF) including ascorbic acid (AA), uric acid (UA), L-3,4-dihydroxyphenylalanine (L-DOPA), and 3,4-dihydroxyphenylacetic acid (DOPAC) [4]. At near neutral pH, L-DOPA is a zwitterionic DA precursor, DOPAC is a negatively charged DA metabolite, and DA is positively charged. A polypyrrole film carries positive charge due to polarons and bipolarons associated with ring nitrogen atom [11]. However, when overoxidized, oxygen is added and some chain breakage occurs with the introduction of electronegativity to the overoxidized polypyrrole (OPP) film.

In contrast, Nafion is a negatively charged, sulfonated fluoropolymer-copolymer. The layered films of OPP and Nafion presumably reject potentially interfering species based on a combination of electrostatic repulsion and size exclusion. Previously, we reported a CPA sensor for DA utilizing a thin (~1 nm) OPP film with a Nafion overlayer exhibiting a limit of detection (LOD) of ~62 nM, a response time of ~1 s, and excellent selectivity against the potential

interferents listed above [4]. However, this LOD does not approach the reported lower end of the physiological range for DA in rodents in the single-digit nanomolar range [12], which has prompted our interest in alternative, permselective coatings for the working electrode (WE) including poly-m-phenylenediamine (m-PPD) and poly-o-phenylenediamine.

PPD films have been used successfully in the past, to create selective sensors for neurotransmitters [13-19], including DA [20-27]. Using PPD as the sole permselective film and square wave voltammetry, DA sensors with LODs of 10 nM and lower [21, 26] have been achieved that also may be selective against ascorbic acid and uric acid [21]. As in our prior experience with electroactive DA and OPP [4], reports suggest that it is important that the PPD film be thin and overoxidized as well for optimal DA sensing [22, 25]; as thicker films can prevent penetration of DA to the electrode surface and subsequent current signal generation. In this work, we strive to construct a DA sensor based on the simple CPA approach that exhibits selectivity against the broad spectrum of potential interfering species listed above and that attains a LOD approaching the lower end of the physiological range.

The reference electrode (RE) also is an important component of electrochemical sensing systems designed for optimal performance, but it usually is not integrated into the same micromachined probe with the working electrode (WE). Most commonly, biosensors used for studies in vivo make use of a separate Ag/AgCl RE [9, 15, 28-31]. However, there are key advantages to combining the WE and RE of an implantable biosensing system onto a single microprobe in an MEA geometry including simplified surgery, reduced tissue damage, and reduced noise, which leads to improved LODs. Although the integration of miniature Ag/AgCl REs onto microprobes has been achieved through wet chemical processing or plasma deposition [32, 33], these constructs are suboptimal due to the instability and toxicity of the deposited films.

AgCl films are often unstable due to delamination or dissolution of the chloride salt [34, 35], and the dissolved film is toxic leading to significant inflammatory responses [36, 37]. Successful implementation of an implantable RE in a MEA format requires several criteria to be met: (1) the RE fabrication method must be compatible with the MEA platform, (2) the RE must exhibit sufficient chemical and mechanical stability, (3) the RE must provide a stable reference potential over the applicable range of conditions associated with its intended use, and (4) the chosen RE must be biocompatible.

Many of the issues encountered with Ag/AgCl REs are avoided by using iridium oxide (IrOx) as the reference electrode material. Prior studies have addressed use of IrOx as a pH sensor, an electrode for electrophysiological recording and stimulation, and as a quasi-RE [38-43]. Although the potential at an IrOx electrode shows strong pH dependence [34], normal mammalian brain extracellular fluid pH is limited to a small dynamic range of 7.15–7.4. Also, IrOx films exhibit excellent mechanical stability and biocompatibility, both of which allow for long-term implantation with minimal adverse effects on living tissue [44, 45]. In this report, we describe IrOx deposition on platinum (Pt) microelectrodes of an MEA by a simple one-step electrochemical method [46] to give fully functional REs that improve DA sensing performance. We chose this method because it does not require any additional costly materials or any additional processing steps that are typically required for the electrochemical activation of a bulk Ir metal electrode or the sputtering of Ir film onto an appropriate substrate [45, 47-49].

2.2 Materials and Methods

2.2.1 Reagents and Equipment

Nafion (5 wt% solution in lower aliphatic alcohols/H2O mix), m-phenylenediamine (99%), 3-hydroxytyramine (dopamine, DA), L-3,4-dihydroxyphenylalanine (L-DOPA), 3,4-dihydroxyphenylacetic acid (DOPAC), L -ascorbic acid (AA), uric acid (UA), iridium tetrachloride hydrate, anhydrous oxalic acid (99%), hydrogen peroxide (30 wt% solution in water) and anhydrous potassium carbonate were purchased from Aldrich Chemical Co. (Milwaukee, WI, USA). Solutions of all neurotransmitters were formulated in phosphate buffered saline (PBS). PBS buffer consisted of 50 mM dibasic sodium phosphate with 100 mM sodium chloride adjusted to pH 7.4 with concentrated HCl. A Millipore Milli-Q Water System was used to generate ultrapure water for the preparation of all solutions used. Electrochemical preparations and calibration measurements were performed using a Versatile Multichannel Potentiostat equipped with the 'p' low current option and low current N'Stat box (VMP3, Bio-Logic USA LLC, Knoxville, TN, USA). For experiments in which an external reference electrode was necessary, Ag/AgCl glass-bodied reference electrodes with 3 M NaCl electrolyte and a 0.5 mm diameter platinum (Pt) wire auxiliary electrode were purchased from BASi (West Lafayette, IN).

2.2.2 Microelectrode Array Fabrication and Polymer Modification

Microelectrode arrays (MEAs) were fabricated on silicon probes in the UCLA Nanofabrication Laboratory (NanoLab) using MEMS technologies (Appendix A). The fabrication and array details are described in previous work [10]. The probe shafts were 150 μm thick, 140 μm wide, and 9 mm long with four 6000 μm^2 (40 μm × 150 μm) Pt microelectrode sites arranged

in pairs at the tip (Fig. 1). Each site was cleaned in 0.1 M H_2SO_4 solution by cycling the potential between -0.2 V and 1.5 V (vs. Ag/AgCl) at least 10× at a scan rate of 50 mV/s and rinsing in PBS. Subsequently, the microelectrodes were modified as needed to serve as working electrodes (WEs), reference electrodes (REs), or counter electrodes (CEs) (Appendix B).

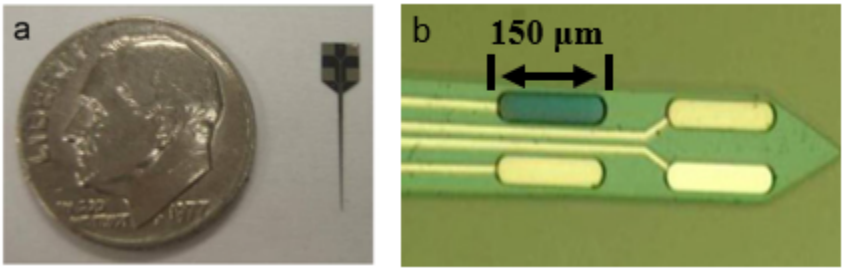

Figure 2.1 (a) A MEA probe with a 9 mm shank. (b) Four Pt microelectrode sites at the tip of a probe, each 6000 µm^2 in area. The dark site on the upper left was modified previously with electrodeposited IrOx.

Iridium oxide (IrOx) was electrodeposited to prepare REs (Appendix C) following the method of Yamanaka [46]. Briefly, a 20 mL aqueous solution of 4.5 mM iridium tetrachloride was stirred for 30 min followed by the addition of 200 µL of hydrogen peroxide and stirring for an additional 10 min. Oxalic acid dihydrate was then added to reach a concentration of 55.5 mM and stirred for another 10 min. Potassium carbonate was added in small aliquots until the solution reached a pH of 10.5. The resulting solution was allowed to sit quiescently for at least 48 h before electrodeposition, during which time the color shifted from yellow to purple.

IrOx was deposited anodically on an electrode site by cycling between 0.0 V and 0.6 V versus Ag/AgCl at a scan rate of 50 mV/s for 100 cycles resulting in a total charge transfer of ~1 C/cm^2. An image of the Pt microelectrode after electrodeposition of IrOx is shown in Fig. 1b. After RE creation, a poly-m-phenylenediamine (m-PPD) film was electrodeposited on designated WEs

from a 5 mM m-phenylenediamine solution in PBS by holding the voltage constant at 0.85 V vs. Ag/AgCl until the total transferred charge reached ~7.2 × 10-7 Coulombs. The m-PPD films were overoxidized by placing the sensor in 0.2 M NaOH and holding the voltage constant at 1.04 V vs. Ag/AgCl for 20 mins. Given the total of four microelectrode sites available, up to three could be used as WEs for redundant measurements. Nafion was deposited on all sites by dip-coating the probe tips into a 2% Nafion solution (diluted from 5% stock in 4:1 IPA:water solution) and immediately annealing at 115 °C for 20 minutes.[14] The sensors were sealed in a container with desiccant and stored dry at 4 °C prior to testing. A schematic of the final cross-sectional structures of the WE, RE, and CE sites is provided as Fig. 2.2.

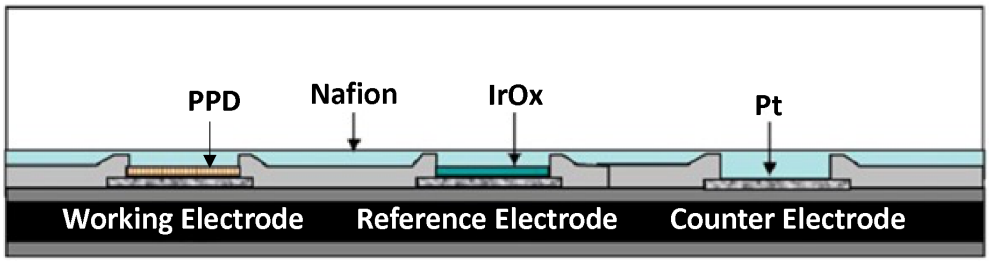

Figure 2.2 Representative cross-section of a multielectrode device (not to scale) for dopamine biosensing showing the Pt microelectrode modifications and permselective polymer coatings to create the WE, RE, and CE sites.

2.3 Sensor Calibration and Testing

The sensors were tested in two- and three-electrode configurations with the VMP3 potentiostat. When used, the CE consisted of an on-probe, Nafion-coated Pt site. DA sensor calibration and testing were conducted in a magnetically stirred 30 mL beaker in a Faraday cage. A potential of 0.6 V was applied to the DA sensors relative to the on-probe IrOx REs, which

corresponds to ~0.7 V vs. Ag/AgCl. The sensors were allowed to equilibrate until they achieved a steady-state current. After equilibration, steady current signals were recorded at DA concentrations sequentially increased by solution injection to generate data for calibration curves. Sensitivities were determined from the linear portion of the curves. Alternatively, interferents (AA, L-DOPA, DOPAC, EP, NEP, and UA) were injected sequentially to assess the selectivity of the sensors.

Noise measurement, analysis and filtering was performed once the sensors achieved a steady-state, baseline current using the built-in noise analysis tools of the BioLogic EC-lab software. Noise was analyzed by first applying a Fourier transform to the baseline current data [50, 51]. Ultralow noise frequency bands were removed using the frequency filter tool. The remaining noise in the filtered, steady-state, baseline current was quantified using the electrochemical corrosion tool of the software. This calculated rms noise was used subsequently in limit-of-detection (LOD) computations. The LOD was defined as the current change corresponding to 3× filtered rms noise. All sensitivity and LOD uncertainties in this work are reported as standard errors.

2.4 Results and Discussion

2.4.1 Three-Electrode Dopamine Sensing with an On-Probe IrOx Reference Electrode

Enhancement of dopamine (DA) sensing with an on-probe IrOx RE was assessed in vitro when the RE was incorporated with two DA working electrodes (WEs) and a platinum (Pt) counter electrode (CE) on our four-site, Pt microelectrode array (MEA). With this three-electrode (i.e., WE, RE, and CE) setup, the sensors gave current responses to DA that were approximately linear up to at least 40 μM (Fig. 2.3) at an operating potential of 0.6 V vs IrOx (~0.7 V vs Ag/AgCl). The composite performance of these three-electrode DA sensors using an on-probe IrOx RE showed a

mean sensitivity of 2650 ± 170 nA/(μM·cm^2) and a mean limit of detection (LOD) of 9 ± 4 nM (n = 10 working electrodes). This impressive LOD, achieved using simple constant potential amperometry (CPA), compares favorably to the typical LOD of ~15 nM attained with the more complex fast scan cyclic voltammetry (FSCV) technique [2].

The sensitivity of these DA sensors with the on-probe IrOx RE and on-probe Pt CE site is similar to what was achieved with an external Ag/AgCl RE and on-probe CE, 2450 ± 230 nA/(μM·cm^2) (n = 10 working electrodes) (Fig. 2.4); however, the LOD with the external Ag/AgCl RE was significantly higher at 54 ± 7 nM due to the greater rms noise of 2.6 ± 0.86 pA relative to the rms noise of 0.46 ± 0.18 pA with the on-probe IrOx RE. In earlier work with a three-electrode system for DA sensing based on Si probe-based Pt sites coated with OPP and Nafion and external REs and CEs based on Ag/AgCl and a Nafion-coated Pt wire, respectively, an LOD of 62 nM (at 2× rms noise) was achieved with background rms noise at ~5 pA [4]. Unfortunately, this data is not directly comparable, because neither the CE or RE were co-located on the probe and the noise was not pre-filtered. However, we also showed earlier that co-location of an IrOx RE, and a Nafion-coated Pt CE on our MEA probe with a glutamate sensing site resulted in a ~61% reduction in unfiltered noise, which approaches the ~82% reduction in pre-filtered noise achieved in this work [8].

2.4.2 Two-Electrode Dopamine Sensing with an On-Probe IrOx Reference Electrode

The current responses of our DA microsensors of ~6000 μm^2 in surface area to analyte in the physiological concentration range generally are in the nanoamp range and lower. Such low currents can allow for the use of a two-electrode configuration, where the RE also acts as the CE. DA sensing with an on-probe IrOx RE was assessed in vitro when the RE was incorporated with

three DA working electrodes (WEs) on our four-site, Pt microelectrode array (MEA). The composite performance (n = 10 working electrodes) of these two-electrode DA sensing microprobes with the on-probe IrOx RE was comparable to that of the three-electrode, on-probe system, as illustrated by a sensitivity of 2570 ± 230 nA/(μM·cm^2) in the linear range, yet the LOD was significantly higher at 35 ± 6 nM (Fig. 2.5). The higher LOD was due to greater rms noise of 1.3 ± 0.75 pA, which still is an improvement over the probes with external Ag/AgCl REs, but not as low as the noise achieved in three electrode systems on a single probe (0.46 ± 0.18 pA).

In the normal physiological DA concentration range up to 1 μM [52], the current response is linear with concentration. However, at DA concentrations above ~40 μM, the additional current alters the potential at the RE, which adversely affects linearity and sensitivity. Nevertheless, these results indicate that the two-electrode system with the on-probe IrOx RE is suitable for monitoring DA up to the expected maximum physiological concentration *in vivo*.

2.4.3 Calibration Curves

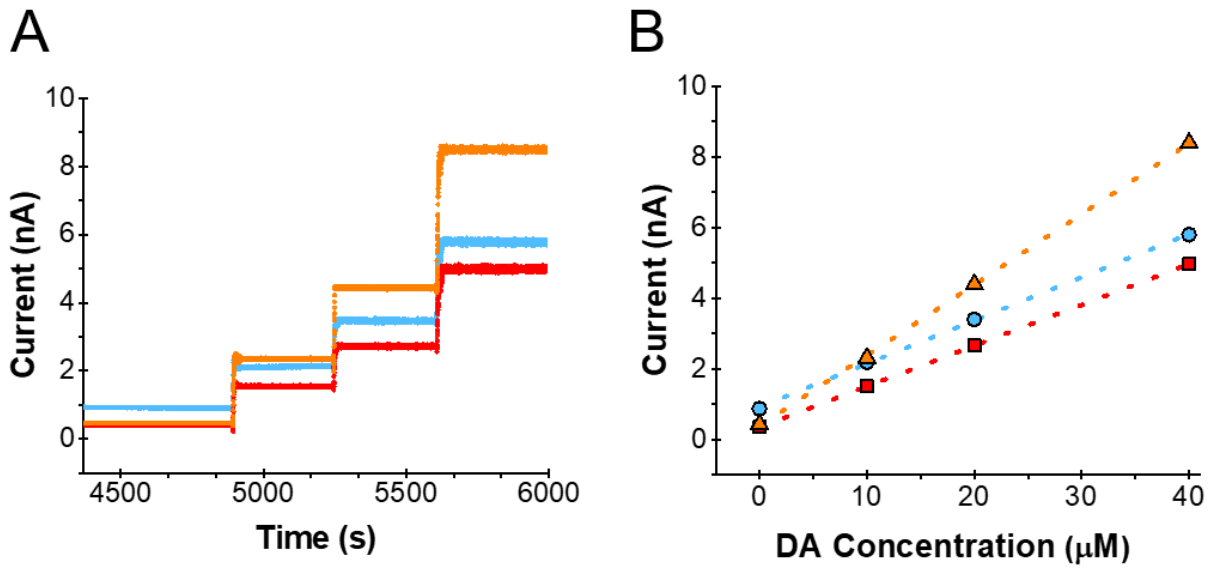

Figure 2.3 A) DA sensing on three representative working electrode sites on MEAs in a three-electrode configuration using an on-probe IrOx RE and an on-probe bare Pt microelectrode as CE. DA injections at 4850 s and 5200 s correspond to concentration increases of 10 μM each, while the final injection corresponds to an increase of 20 μM.

B) Calibrations plots are made by creating linear regressions ($R^2 = 0.994$) of the steady state current data (shown in A) as a function of the bulk injected dopamine concentration. DA sensing systems of this on-probe, three-electrode configuration showed an average sensitivity and limit of detection of 2650 ± 230 nA/(μM·cm^2) and 9 ± 4 nM (n = 10 working electrodes), respectively. The rms noise was 0.00046 nA.

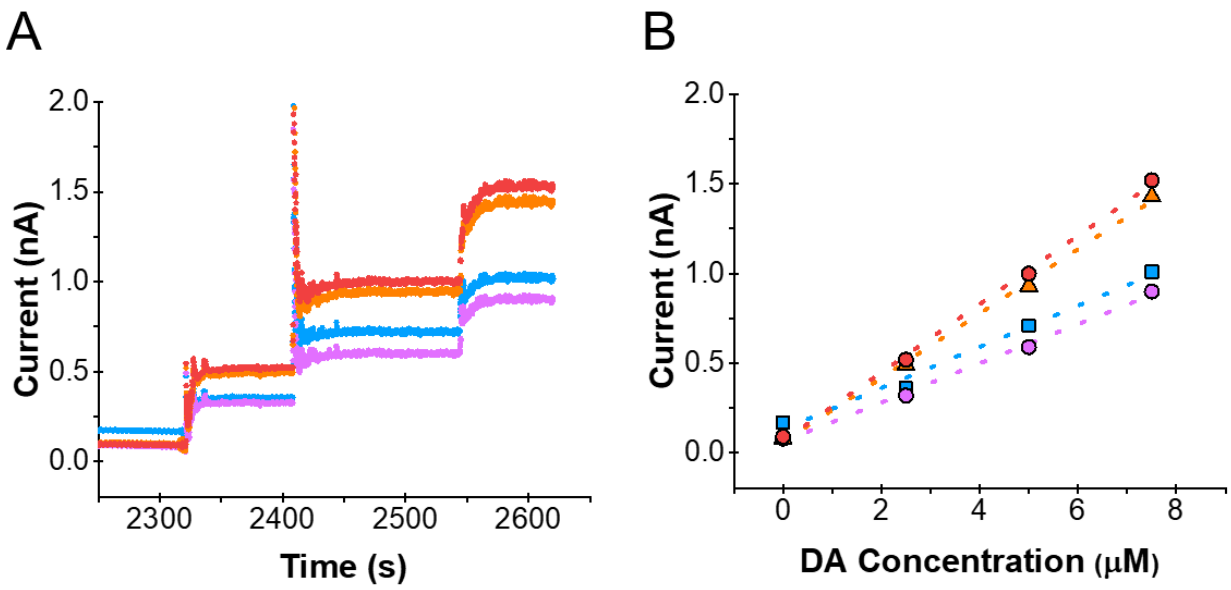

Figure 2.4 A) DA sensing on four representative working electrode sites on MEAs in a three-electrode configuration using an external Ag/AgCl electrode as the RE and an on-probe bare Pt microelectrode as the CE. All DA injections shown corresponded to 2.5 μM increases in concentration.

B) Calibrations plots are made by creating linear regressions ($R^2 = 0.998$) of the steady state current data (shown in A) as a function of the bulk injected dopamine concentration. The DA sensing systems of this three-electrode configuration with an external RE showed an average sensitivity and limit of detection of 2450 ± 230 nA/(μM·cm^2) and 54 ± 7 nM (n = 10 working electrodes), respectively. The rms noise was 0.0026 nA.

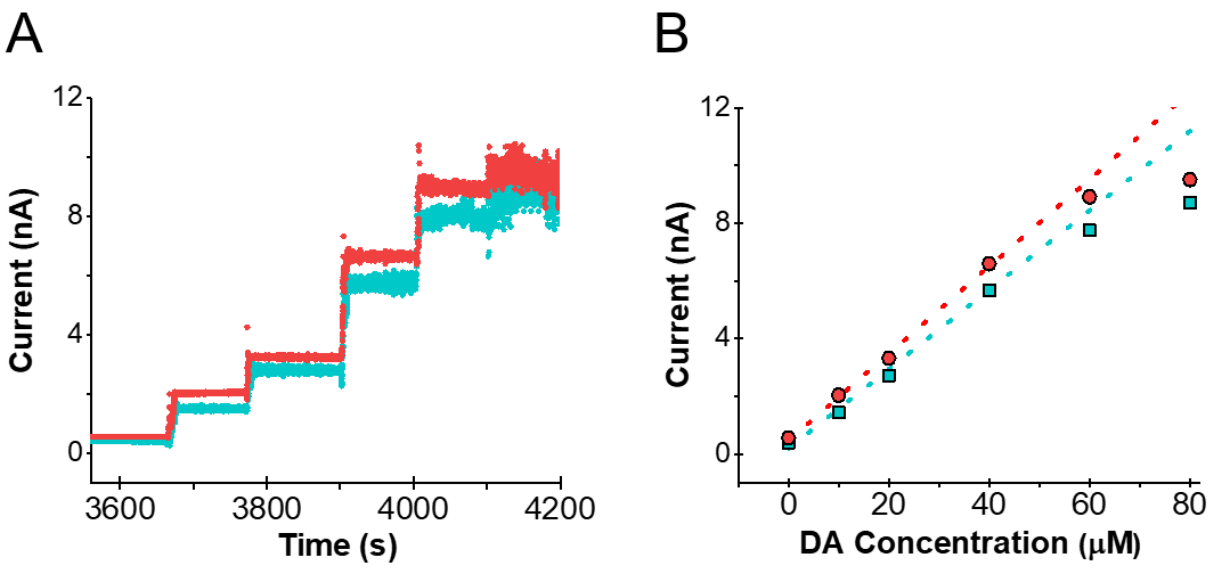

Figure 2.5 A) DA sensing on two representative working electrode sites on MEAs in a two-electrode configuration using an on-probe IrOx-coated microelectrode as both the RE and the CE. The IrOx film does not act as a stable RE at very high DA concentrations, which is illustrated by the nonlinearity of the current response above 40 μM DA. DA injections at 3650 s and 3750 s correspond to DA concentration increases of 10 μM, while all remaining injections correspond to DA concentration increases of 20 μM.

B) Representative calibration plots corresponding to the results shown in (A). The linear fits (R^2 = 0.997) shown were based on measurements up to 40 μM. DA sensing systems of this on-probe, two-electrode configuration showed an average sensitivity of 2570 ± 230 nA/(μM·cm^2) and a limit of detection of 35 ± 6 nM (n = 10 working electrodes), respectively. The rms noise was 0.0017 nA.

2.4.4 Selectivity Against Common Electroactive Interferents

In addition to detecting changes in physiological concentrations of DA, these biosensors also must be selective against common electroactive species in brain extracellular fluid. In this work, selectivity is defined as the ratio of the sensitivity to the analyte to that of the interferent. DA microsensors in the three-electrode configuration displayed excellent selectivity for DA against AA, DOPAC, DOPA, and UA at or above typical physiological concentrations (Fig. 2.6).

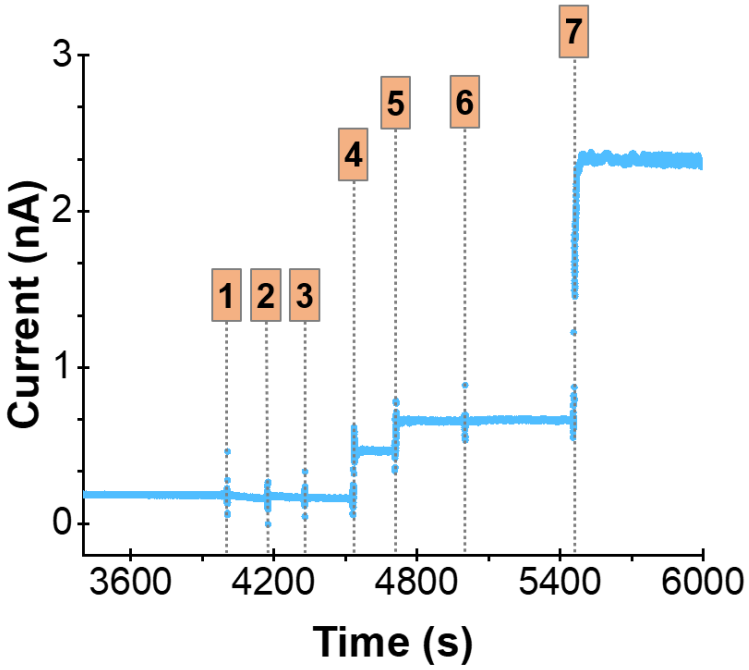

Figure 2.6 DA selectivity against common electroactive interferents found in brain ECF including 125 μM AA [1], 50 μM L-DOPA [2], 50 μM DOPAC [3], 12.5 μM EP [4], 12.5 μM NEP [5], 50 μM UA [6], and μM 10 DA [7]. The selectivity ratios of DA to AA, DOPAC, L-DOPA and UA all were more than 1000:1. The selectivities for DA over EP and NEP were ~6.7:1 and ~9.8:1, respectively; however, at biologically relevant concentrations in DA-rich brain regions such as the striatum, these species are not detectable by the DA sensor.

Average selectivity ratios of DA to AA, DOPAC, DOPA, and UA all were more than 1000:1 for our three-electrode system with on-probe IrOx RE. However, the selectivities for DA over EP and NEP were ~6.7 and ~9.8, respectively, due to their similar chemical structures and oxidation potentials. Fortunately, the estimated basal ECF concentrations of EP (~5 nM)[53] and NEP (~1 nM)[54] are well below the LODs of our DA sensor for these species (~75 nM and ~108 nM respectively). As a point of comparison, the popular FSCV method relies on differences in redox potential to distinguish electroactive interfering species from DA. It also cannot be used straightforwardly to differentiate EP or NEP from DA [55]. Thus, our upgraded DA sensor with on-probe IrOx RE offers a viable alternative to FSCV for monitoring DA using CPA both in vitro and *in vivo*.

2.5 Conclusions

A stable and reproducible IrOx film on a Pt microelectrode of a MEA can be used as an on-probe RE for highly sensitive and selective DA sensing in both 2-electrode and 3-electrode configurations. The electrochemical method employed for IrOx film deposition permits straightforward modification of selected microelectrodes in the MEA format. Other sites on the MEA were modified with a thin electropolymerized film of PPD, and all sites subsequently were dip-coated with Nafion to give high-performance DA microsensors. Inclusion of the IrOx RE on the same microprobe as the working electrodes reduces baseline rms noise levels by up to 82% compared to systems with a separate Ag/AgCl RE. The dramatic reduction in noise contributes to an ultralow detection limit of ~9 nM, which compares favorably with the more complex fast scan cyclic voltammetry (FSCV) technique [2]. These results were achieved while maintaining at least

1000:1 selectivity against the common electroactive interferents, ascorbic acid, L-DOPA, DOPAC, and uric acid. Further, epinephrine and norepinephrine in the physiological concentration range are below the LOD of the DA sensor. As such, this MEA-probe DA sensing system that is based on simple, CPA and avoids the complications of a separate Ag/AgCl RE offers an attractive alternative to FSCV for DA monitoring.

2.6 References

[1] J. A. Stamford, Z. L. Kruk, J. Millar, and R. M. Wightman, "Striatal Dopamine Uptake in the Rat - Invivo Analysis by Fast Cyclic Voltammetry," (in English), *Neurosci Lett,* vol. 51, no. 1, pp. 133-138, 1984, doi: Doi 10.1016/0304-3940(84)90274-X.

[2] B. J. Venton and Q. Cao, "Fundamentals of fast-scan cyclic voltammetry for dopamine detection," (in English), *Analyst,* vol. 145, no. 4, pp. 1158-1168, Feb 21 2020, doi: 10.1039/c9an01586h.

[3] S. J. Killoran and R. D. O'Neill, "Characterization of permselective coatings electrosynthesized on Pt-Ir from the three phenylenediamine isomers for biosensor applications," (in English), *Electrochimica Acta,* vol. 53, no. 24, pp. 7303-7312, Oct 15 2008, doi: 10.1016/j.electacta.2008.03.076.

[4] T. T. C. Tseng and H. G. Monbouquette, "Implantable microprobe with arrayed microsensors for combined amperometric monitoring of the neurotransmitters, glutamate and dopamine," (in English), *Journal of Electroanalytical Chemistry,* vol. 682, pp. 141-146, Aug 15 2012, doi: 10.1016/j.jelechem.2012.07.014.

[5] J. J. Burmeister, K. Moxon, and G. A. Gerhardt, "Ceramic-based multisite microelectrodes for electrochemical recordings," (in English), *Analytical Chemistry,* vol. 72, no. 1, pp. 187-192, Jan 1 2000, doi: DOI 10.1021/ac9907991.

[6] J. J. Burmeister, F. Pomerleau, M. Palmer, B. K. Day, P. Huettl, and G. A. Gerhardt, "Improved ceramic-based multisite microelectrode for rapid measurements of L-glutamate in the CNS," (in English), *J Neurosci Meth,* vol. 119, no. 2, pp. 163-171, Sep 30 2002, doi: Pii S0165-0270(02)00172-3

[7] J. J. Burmeister, M. Palmer, and G. A. Gerhardt, "Ceramic-based multisite microelectrode array for rapid choline measures in brain tissue," *Anal Chim Acta,* vol. 481, no. 1, pp. 65-74, 2003, doi: 10.1016/s0003-2670(03)00067-9.

[8] V. M. Tolosa, K. M. Wassum, N. T. Maidment, and H. G. Monbouquette, "Electrochemically deposited iridium oxide reference electrode integrated with an electroenzymatic glutamate sensor on a multielectrode array microprobe," (in English), *Biosensors & Bioelectronics,* vol. 42, pp. 256-260, Apr 15 2013, doi: 10.1016/j.bios.2012.10.061.

[9] K. M. Wassum, V. M. Tolosa, T. C. Tseng, B. W. Balleine, H. G. Monbouquette, and N. T. Maidment, "Transient Extracellular Glutamate Events in the Basolateral Amygdala Track Reward-Seeking Actions," (in English), *J Neurosci,* vol. 32, no. 8, pp. 2734-2746, Feb 22 2012, doi: 10.1523/Jneurosci.5780-11.2012.

[10] K. M. Wassum, V. M. Tolosa, J. Wang, E. Walker, H. G. Monbouquette, and N. T. Maidment, "Silicon Wafer-Based Platinum Microelectrode Array Biosensor for Near Real-Time Measurement of Glutamate in Vivo," *Sensors,* vol. 8, no. 8, pp. 5023-5036, 2008. [Online]. Available: https://www.mdpi.com/1424-8220/8/8/5023.

[11] C. Malitesta, I. Losito, L. Sabbatini, and P. G. Zambonin, "New findings on polypyrrole chemical structure by XPS coupled to chemical derivatization labelling," (in English), *Journal of Electron Spectroscopy and Related Phenomena,* vol. 76, pp. 629-634, Dec 29 1995, doi: Doi 10.1016/0368-2048(95)02438-7.

[12] S. M. Matt and P. J. Gaskill, "Where Is Dopamine and how do Immune Cells See it?: Dopamine-Mediated Immune Cell Function in Health and Disease," (in English), *Journal of Neuroimmune Pharmacology,* vol. 15, no. 1, pp. 114-164, Mar 2020, doi: 10.1007/s11481-019-09851-4.

[13] I. w. Huang, M. Clay, Y. Cao, J. Nie, Y. Guo, and H. G. Monbouquette, "Electroenzymatic choline sensing at near the theoretical performance limit," *Analyst,* 10.1039/D0AN01939A vol. 146, no. 3, pp. 1040-1047, 2021, doi: 10.1039/D0AN01939A.

[14] I. W. Huang, M. Clay, S. Q. Wang, Y. W. Guo, J. J. Nie, and H. G. Monbouquette, "Electroenzymatic glutamate sensing at near the theoretical performance limit," (in English), *Analyst,* vol. 145, no. 7, pp. 2602-2611, Apr 7 2020, doi: 10.1039/c9an01969c.

[15] J. P. Bruno *et al.*, "Second-by-second measurement of acetylcholine release in prefrontal cortex," (in English), *Eur J Neurosci,* vol. 24, no. 10, pp. 2749-2757, Nov 2006, doi: 10.1111/j.1460-9568.2006.05176.x.

[16] K. M. Mitchell, "Acetylcholine and choline amperometric enzyme sensors characterized in vitro and in vivo," (in English), *Analytical Chemistry,* vol. 76, no. 4, pp. 1098-1106, Feb 15 2004, doi: 10.1021/ac034757v.

[17] B. Wang, B. Koo, L.-w. Huang, and H. G. Monbouquette, "Microbiosensor fabrication by polydimethylsiloxane stamping for combined sensing of glucose and choline," *Analyst (Cambridge, U. K.),* 10.1039/c8an01343h vol. 143, no. 20, pp. 5008-5013, // 2018, doi: 10.1039/c8an01343h.

[18] N. Wahono, S. Qin, P. Oomen, T. I. Cremers, M. G. de Vries, and B. H. Westerink, "Evaluation of permselective membranes for optimization of intracerebral amperometric glutamate biosensors," *Biosens Bioelectron,* vol. 33, no. 1, pp. 260-6, Mar 15 2012, doi: 10.1016/j.bios.2012.01.019.

[19] J. M. Cooper and D. J. Pritchard, "Biomolecular Sensors for Neurotransmitter Determination - Electrochemical Immobilization of Glutamate Oxidase at Microelectrodes in a Poly(O-Phenylenediamine) Film," (in English), *Journal of Materials Science-Materials in Electronics,* vol. 5, no. 2, pp. 111-116, Apr 1994. [Online]. Available: <Go to ISI>://WOS:A1994NF71200009.

[20] T. Dhanasekaran *et al.*, "Recent advances in polymer supporting layered double hydroxides nanocomposite for electrochemical biosensors," *Materials Research Express,* vol. 5, no. 1, 2018, doi: 10.1088/2053-1591/aaa538.

[21] N. Dükar *et al.*, "Highly sensitive and selective dopamine sensing in biological fluids with one-pot prepared graphene/poly(o-phenylenediamine) modified electrodes," *Materials Chemistry and Physics,* vol. 228, pp. 357-362, 2019, doi: 10.1016/j.matchemphys.2019.02.043.

[22] E. Ekinci, G. Erdogdu, and A. E. Karagözler, "Preparation, optimization, and voltammetric characteristics of poly(o-phenylenediamine) film as a dopamine-selective polymeric membrane," *Journal of Applied Polymer Science,* vol. 79, no. 2, pp. 327-332, 2001, doi: 10.1002/1097-4628(20010110)79:2<327::Aid-app150>3.0.Co;2-z.

[23] S. Liu, B. Yu, and T. Zhang, "Preparation of crumpled reduced graphene oxide–poly(p-phenylenediamine) hybrids for the detection of dopamine," *Journal of Materials Chemistry A,* vol. 1, no. 42, 2013, doi: 10.1039/c3ta12594g.

[24] X. Liu, H. Zhu, and X. Yang, "An electrochemical sensor for dopamine based on poly(o-phenylenediamine) functionalized with electrochemically reduced graphene oxide," *RSC Adv.,* vol. 4, no. 8, pp. 3743-3749, 2014, doi: 10.1039/c3ra45234d.

[25] E. Ekinci, G. Erdogdu, and A. E. Karagözler, "Investigation of polymerization parameters affecting dopamine selectivity of a polymeric membrane," (in English), *Polymer Bulletin,* vol. 44, no. 5-6, pp. 547-553, Jul 2000, doi: DOI 10.1007/s002890070077.

[26] J. W. Mo and B. Ogorevc, "Simultaneous measurement at dopamine and ascorbate at their physiological levels using voltammetric microprobe based on overoxidized poly(1,2-phenylenediamine)-coated carbon fiber," (in English), *Analytical Chemistry,* vol. 73, no. 6, pp. 1196-1202, Mar 15 2001, doi: 10.1021/ac0010882.

[27] T. Selvaraju and R. Ramaraj, "Simultaneous determination of dopamine and serotonin in the presence of ascorbic acid and uric acid at poly(m-phenylenediamine) modified electrode," (in English), *Journal of Applied Electrochemistry,* vol. 33, no. 8, pp. 759-762, Aug 2003, doi: Doi 10.1023/A:1025096309274.

[28] Y. B. Hu, K. M. Mitchell, F. N. Albahadily, E. K. Michaelis, and G. S. Wilson, "Direct Measurement of Glutamate Release in the Brain Using a Dual Enzyme-Based Electrochemical Sensor," (in English), *Brain Res,* vol. 659, no. 1-2, pp. 117-125, Oct 3 1994, doi: Doi 10.1016/0006-8993(94)90870-2.

[29] K. H. Lee *et al.*, "High-frequency stimulation of the subthalamic nucleus increases glutamate in the subthalamic nucleus of rats as demonstrated by enzyme-linked glutamate sensor," (in English), *Brain Res,* vol. 1162, pp. 121-129, Aug 8 2007, doi: 10.1016/j.brainres.2007.06.021.

[30] T. C. Thomas, D. K. Grandy, G. A. Gerhardt, and P. E. A. Glaser, "Decreased Dopamine D4 Receptor Expression Increases Extracellular Glutamate and Alters Its Regulation in Mouse Striatum," (in English), *Neuropsychopharmacol,* vol. 34, no. 2, pp. 436-445, Jan 2009, doi: 10.1038/npp.2008.74.

[31] E. Walker, J. Wang, N. Hamdi, H. G. Monbouquette, and N. T. Maidment, "Selective detection of extracellular glutamate in brain tissue using microelectrode arrays coated with over-oxidized polypyrrole," (in English), *Analyst,* vol. 132, no. 11, pp. 1107-1111, 2007, doi: 10.1039/b706880h.

[32] S. I. Park, S. B. Jun, S. Park, H. C. Kim, and S. J. Kim, "Application of a new Cl-plasma-treated Ag/AgCl reference electrode to micromachined glucose sensor," (in English), *Ieee Sens J,* vol. 3, no. 3, pp. 267-273, Jun 2003, doi: 10.1109/Jsen.2003.814649.

[33] H. Suzuki, T. Hirakawa, S. Sasaki, and I. Karube, "Micromachined liquid-junction Ag/AgCl reference electrode," (in English), *Sensor Actuat B-Chem,* vol. 46, no. 2, pp. 146-154, Feb 15 1998, doi: Doi 10.1016/S0925-4005(98)00110-5.

[34] R. K. Franklin *et al.*, "Iridium oxide reference electrodes for neurochemical sensing with MEMS microelectrode arrays," (in English), *2005 Ieee Sensors, Vols 1 and 2,* pp. 1400-1403, 2005. [Online]. Available: <Go to ISI>://WOS:000237003500350.

[35] H. Yang, S. K. Kang, D. H. Shin, H. Kim, and Y. T. Kim, "Microfabricated iridium oxide reference electrode for continuous glucose monitoring sensor," (in English), *Boston Transducers'03: Digest of Technical Papers, Vols 1 and 2,* pp. 103-106, 2003. [Online]. Available: <Go to ISI>://WOS:000184567300026.

[36] A. M. Dymond, L. E. Kaechele, J. M. Jurist, and P. H. Crandall, "Brain Tissue Reaction to Some Chronically Implanted Metals," (in English), *Journal of Neurosurgery,* vol. 33, no. 5, pp. 574-&, 1970, doi: DOI 10.3171/jns.1970.33.5.0574.

[37] R. Cooper and H. J. Crow, "Toxic effects of intra-cerebral electrodes," *Med Biol Eng,* vol. 4, no. 6, pp. 575-581, 1966, doi: 10.1007/BF02474827.

[38] I. A. Ges, I. A. Dzhura, and F. J. Baudenbacher, "On-chip acidification rate measurements from single cardiac cells confined in sub-nanoliter volumes," (in English), *Biomedical Microdevices,* vol. 10, no. 3, pp. 347-354, Jun 2008, doi: 10.1007/s10544-007-9142-7.

[39] J. Li, Y. Du, and C. Fang, "Developing an Iridium Oxide Film Modified Microelectrode for Microscale Measurement of pH," *Electroanalysis,* vol. 19, no. 5, pp. 608-611, 2007, doi: https://doi.org/10.1002/elan.200603753.

[40] R. D. Meyer, S. E. Cogan, T. H. Nguyen, and R. D. Rauh, "Electrodeposited iridium oxide for neural stimulation and recording electrodes," (in English), *Ieee T Neur Sys Reh,* vol. 9, no. 1, pp. 2-11, Mar 2001, doi: Doi 10.1109/7333.918271.

[41] P. Vanhoudt, Z. Lewandowski, and B. Little, "Iridium Oxide Ph Microelectrode," (in English), *Biotechnol Bioeng,* vol. 40, no. 5, pp. 601-608, Aug 20 1992, doi: DOI 10.1002/bit.260400507.

[42] D. O. Wipf, F. Y. Ge, T. W. Spaine, and J. E. Bauer, "Microscopic measurement of pH with iridium oxide microelectrodes," (in English), *Analytical Chemistry,* vol. 72, no. 20, pp. 4921-4927, Oct 15 2000, doi: 10.1021/ac000383j.

[43] H. S. Yang *et al.*, "An iridium oxide reference electrode for use in microfabricated biosensors and biochips," (in English), *Lab on a Chip,* vol. 4, no. 1, pp. 42-46, 2004, doi: 10.1039/b309899k.

[44] S. A. M. Marzouk, S. Ufer, R. P. Buck, T. A. Johnson, L. A. Dunlap, and W. E. Cascio, "Electrodeposited iridium oxide pH electrode for measurement of extracellular myocardial acidosis during acute ischemia," (in English), *Analytical Chemistry,* vol. 70, no. 23, pp. 5054-5061, Dec 1 1998, doi: DOI 10.1021/ac980608e.

[45] E. Slavcheva, R. Vitushinsky, W. Mokwa, and U. Schnakenberg, "Sputtered iridium oxide films as charge injection material for functional electrostimulation," (in English),

Journal of the Electrochemical Society, vol. 151, no. 7, pp. E226-E237, 2004, doi: 10.1149/1.1747881.

[46] K. Yamanaka, "Anodically Electrodeposited Iridium Oxide-Films (Aeirof) from Alkaline-Solutions for Electrochromic Display Devices," (in English), *Japanese Journal of Applied Physics Part 1-Regular Papers Short Notes & Review Papers,* vol. 28, no. 4, pp. 632-637, Apr 1989, doi: Doi 10.1143/Jjap.28.632.

[47] S. Glab, A. Hulanicki, G. Edwall, and F. Ingman, "Metal-Metal Oxide and Metal-Oxide Electrodes as Ph Sensors," (in English), *Critical Reviews in Analytical Chemistry,* vol. 21, no. 1, pp. 29-47, 1989, doi: Doi 10.1080/10408348908048815.

[48] T. Katsube, I. Lauks, and J. N. Zemel, "Ph-Sensitive Sputtered Iridium Oxide-Films," (in English), *Sensors and Actuators,* vol. 2, no. 4, pp. 399-410, 1982, doi: Doi 10.1016/0250-6874(81)80060-1.

[49] K. G. Kreider, M. J. Tarlov, and J. P. Cline, "Sputtered Thin-Film Ph Electrodes of Platinum, Palladium, Ruthenium, and Iridium Oxides," (in English), *Sensor Actuat B-Chem,* vol. 28, no. 3, pp. 167-172, Sep 1995, doi: Doi 10.1016/0925-4005(95)01655-4.

[50] F. Guenther, "Solving noise control problems," (in English), *Ashrae Journal-American Society of Heating Refrigerating and Air-Conditioning Engineers,* vol. 40, no. 2, pp. 34-+, Feb 1998. [Online]. Available: <Go to ISI>://WOS:000071926000007.

[51] D. M. Morgan and S. G. Weber, "Noise and Signal-to-Noise Ratio in Electrochemical Detectors," (in English), *Analytical Chemistry,* vol. 56, no. 13, pp. 2560-2567, 1984, doi: DOI 10.1021/ac00277a065.

[52] S. H. Walters, E. M. Robbins, and A. C. Michael, "Kinetic Diversity of Striatal Dopamine: Evidence from a Novel Protocol for Voltammetry," (in English), *Acs Chemical Neuroscience,* vol. 7, no. 5, pp. 662-667, May 2016, doi: 10.1021/acschemneuro.6b00020.

[53] B. R. Dev, P. A. Mason, and C. R. Freed, "Drug-Induced Changes in Blood-Pressure Lead to Changes in Extracellular Concentrations of Epinephrine, Dihydroxyphenylacetic Acid, and 5-Hydroxyindoleacetic Acid in the Rostral Ventrolateral Medulla of the Rat," (in English), *Journal of Neurochemistry,* vol. 58, no. 4, pp. 1386-1394, Apr 1992, doi: DOI 10.1111/j.1471-4159.1992.tb11354.x.

[54] R. W. Roosevelt, D. C. Smith, R. W. Clough, R. A. Jensen, and R. A. Browning, "Increased extracellular concentrations of norepinephrine in cortex and hippocampus following vagus nerve stimulation in the rat," (in English), *Brain Res,* vol. 1119, pp. 124-132, Nov 13 2006, doi: 10.1016/j.brainres.2006.08.048.

[55] M. L. A. V. Heien, M. A. Johnson, and R. M. Wightman, "Resolving neurotransmitters detected by fast-scan cyclic voltammetry," (in English), *Analytical Chemistry,* vol. 76, no. 19, pp. 5697-5704, Oct 1 2004, doi: 10.1021/ac0491509.

Chapter 3 : Multi-Organ-on-Chip Device for Modeling Opioid Reinforcement and Withdrawal and the Negative Component of Pain: A Therapeutic Screening Tool

ABSTRACT

The escalating opioid crisis underscores the urgent need for new therapeutics targeting opioid use disorder (OUD) and non-addictive pain treatments. To advance drug discovery and better understand addiction neurobiology, a multi-organ, microphysiological system (MPS) is being developed so that key components of the midbrain's dopaminergic and GABAergic circuitry can be modeled. This system incorporates human-induced, pluripotent stem cell (iPSC)-derived neurons; microglia; a mock blood-brain barrier (BBB), and liver metabolism components to enable high-throughput drug screening. The platform is further enhanced with integrated dopamine (DA) sensors, capable of real-time monitoring within the MPS. Preliminary results demonstrate the sensors' ability to produce current signals in response to varying DA concentrations within the microfluidic chip, laying the groundwork for future in-depth studies with neuronal cultures.

3.1 Introduction

The opioid abuse epidemic has emerged as one of the most pressing public health crises, with profound implications for individuals and society [1]. The development of effective therapeutics for opioid use disorder (OUD) and non-addictive pain treatments is paramount. However, the complexity of addiction, particularly the neurobiological mechanisms underlying it, presents significant challenges for therapeutic development [2]. Traditional models for studying

these mechanisms are limited by their inability to fully capture the intricate interactions between different cell types and physiological systems involved in addiction [3].

To address these challenges, we have engaged in the development of a multi-organ, microphysiological system (MPS) that leverages recent advances in organ-on-a-chip and iPSC technologies. This MPS will focus on the dopaminergic and GABAergic neurons of the midbrain, which play a critical role in mediating the reinforcing properties of opioids and other drugs of abuse [4-6]. By incorporating human iPSC-derived neurons, microglia, BBB, and liver metabolism components, this platform will provide a more accurate and dynamic model of the neurobiological processes involved in addiction.

The system will enable the study of chronic opioid-induced plasticity in dopamine (DA) responsiveness, a key factor in the development of opioid addiction. By examining the effects of both mu opioid receptor agonists and kappa-mediated opioid effects on DA transmission, the MPS will offer insights into the mechanisms underlying opioid withdrawal, chronic pain states, and the potential for relapse [7-9]. Furthermore, the integration of RNA sequencing (RNAseq) and metabolomics analyses will support the identification of novel therapeutic targets and mechanisms [10].

This project will also focus on the development of high-throughput screening capabilities, facilitated by the incorporation of online sensors for real-time detection of DA and other key analytes. The platform's ability to screen a curated set of kinase inhibitors and other compounds will be informed by the RNAseq and metabolomics data, providing a targeted approach to addiction treatment development [11]. The potential to use this device to test the abuse liability of novel antinociceptive agents further expands its utility, making it a valuable tool in the ongoing fight against opioid addiction [12-14].

With an interdisciplinary team of scientists and engineers, this project builds upon recent technological advancements to create innovative MPSs with the potential to make significant clinical impacts in the future.

3.2 Materials and Methods

3.2.1 Dopamine Microelectrode Fabrication and Calibration

Initially, two sensor configurations were tested for integration into the microfluidic chip. The first configuration involved platinum wire sensors [15-17] coated with poly-*m*-phenylenediamine (*m*-PPD) and Nafion, similar to those used in microelectrode arrays (MEAs). An external Ag/AgCl reference electrode was prepared by dipping silver wire into sodium hypochlorite solution [18]. A counterelectrode was prepared by using a strip of platinum wire without any coatings.

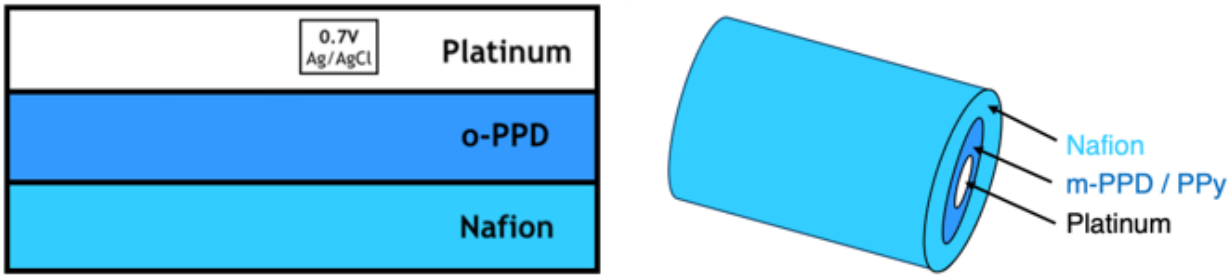

Figure 3.1 Comparison illustration of the dopamine working electrode geometries showing the planar MEA (left) and cylindrical/wire (right) geometries. The major advantage of the cylindrical design is that the surface area of the platinum site is significantly larger (0.016 cm^2) vs. that of the traditional MEA design (0.00006 cm^2).

The 250-fold enhancement in surface area confers one significant benefit from an analyte detection standpoint, which is that the limit of detection (1-10 nM) is comfortably within the physiological range [19]. Unfortunately, this improvement is to the detriment of several other desirable properties. Mostly notably, the noise on these probes was measured to be 0.079 nA, which is almost an order of magnitude higher than the standard MEA probes. In addition, the sensitivity was approximately half an order of magnitude lower than that of MEA probes with a similar formulation.

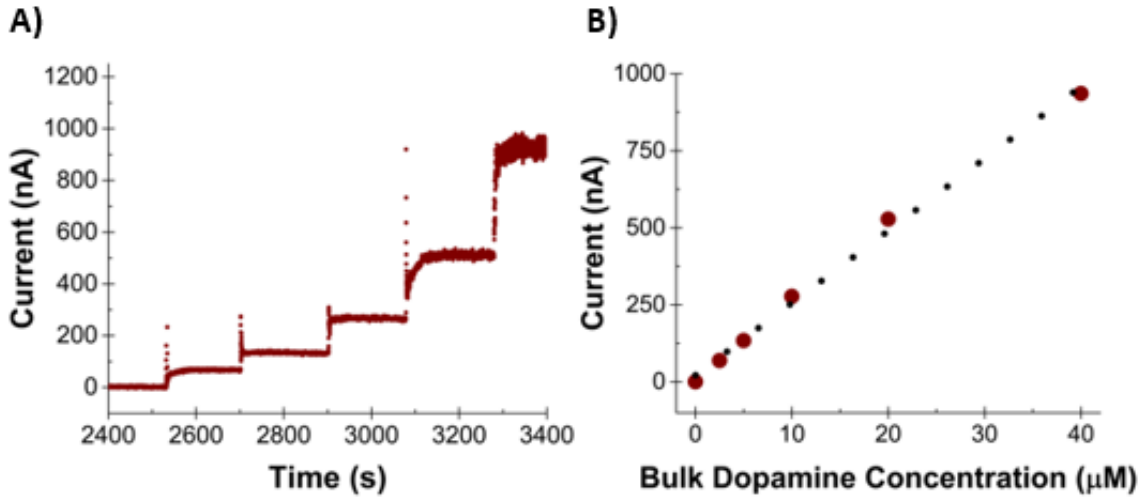

Figure 3.2 A) DA sensing on a single platinum dopamine wire sensor using a three-electrode configuration. A silver wire dipped in bleach is used as the reference electrode and a bare platinum wire is used as a counterelectrode. B) Calibration plots are made by creating linear regressions (R^2 = 0.997) of the steady state current data (shown in A) as a function of the bulk injected dopamine concentration. The DA sensing systems of this three-electrode configuration with an external RE showed an average sensitivity and limit of detection of 790 ± 50 nA/(μM·cm^2) and 5 ± 3 nM (n = 10 working electrodes), respectively. The rms noise was 0.079 nA.

Second, the silver wire needed for RE wire fabrication is sold with a perfluoroalkoxy alkane (PFA) coating. Even after careful removal, the sheared edges of the coating appeared to interfere with the sensor's ability to maintain a stable baseline current, further diminishing its reliability. Third, despite the cylindrical geometry's impressive performance metrics *in vitro*, inserting the wire into the chamber of the microfluidic channels of the chip is not a straightforward endeavor. Without a cannula, it is challenging not to bend the wire sensor while inserting it into the chip. With a cannula, it is difficult to seal the sensor in the chip in a way that maintains the flow pressures of the fluidic elements. The final problematic consideration is that this particular geometry requires three distinct micromachined channels to insert the working, reference, and counterelectrodes of the complete electrochemical system. Even though this revised sensor incorporated the same electrochemical design components and achieved an improved limit of detection, the aforementioned issues rendered the configuration unsuitable for precise dopamine detection within the microfluidic environment.

Therefore, the platinum wire working electrode was replaced with the microelectrode array geometry used in previous studies. The dopamine sensors were fabricated and calibrated following established protocols described in Chapter 2. MEA-based dopamine sensors with an integrated iridium oxide (IrOx) reference electrode offer the distinct advantage of incorporating all three electrode types onto a single probe, thereby requiring only a single micromachined channel. Although smaller in surface area, these sensors offer significant advantages in terms of noise reduction and stability[20], despite the modest increase in their limit of detection. The ability to maintain a stable baseline current, combined with reduced noise levels, made this configuration particularly effective for dopamine detection within the microfluidic chip. As a result, the MEA sensor configuration with the integrated IrOx reference electrode was selected for all subsequent

experiments due to its superior performance in minimizing noise, maintaining a stable baseline, and enhancing sensitivity.

3.2.2 Microfluidic Chip Design and Assembly

The microfluidic chip utilized in this study was meticulously designed and fabricated by the Terasaki Institute for Biomedical Innovation, which contributed their expertise in organ-on-a-chip technologies. The primary objective of the chip's design was to emulate the blood-brain barrier (BBB) and provide a platform for the future integration of neurochemical sensors, particularly those for dopamine detection.

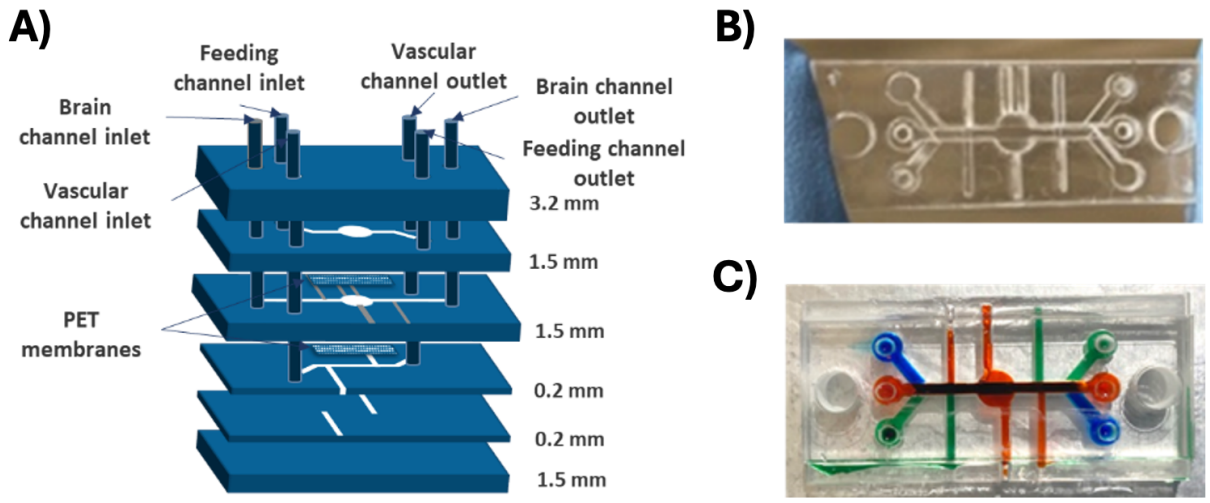

Figure 3.3 PMMA-based BBB chip. (A) Schematic of the multi-layer chip. (B) Assembled chip. (C) Assembled chip with distinct coloring for each channel: green (bottom, vascular), orange (middle, brain), and blue (top, feed).

The Terasaki team employed advanced microfabrication techniques to produce the microfluidic chips. Initially, polydimethylsiloxane (PDMS) was chosen for its favorable properties, including biocompatibility and the ability to easily form microchannels[21-23]. However, to address concerns about the adsorption of small hydrophobic molecules and to improve the overall durability of the chip, polymethylmethacrylate (PMMA) was ultimately selected as the primary material for fabrication[24-26]. The final chip design featured three distinct channels: the vascular channel (bottom layer), the brain channel (middle layer), and the feeding channel (top layer). These channels were engineered to replicate the physiological flow of nutrients and waste products across the BBB, with a central chamber within the brain channel designated for housing sensors and ensuring consistent exposure to the cultured neurons.

To ensure the integrity of the BBB within the microfluidic chip, platinum (Pt) electrodes were embedded by the Terasaki team into the microchannels to facilitate transendothelial electrical resistance (TEER) measurements [27]. These TEER measurements provided critical real-time data on the barrier function of the endothelial cell layers within the chip, thereby confirming that the experimental setup closely mirrored the physiological environment of the human brain.

3.2.3 Sensor Integration into Microfluidic Chip

The integration of the dopamine sensors into the microfluidic chip was a critical step in enabling real-time neurochemical monitoring within the blood-brain barrier (BBB) model. Following the fabrication of the microfluidic chips, the sensors were carefully inserted into the designated micromachined channels leading to the central chamber of the brain channel (Fig. 3.4).

The dopamine sensors were inserted through the micromachined access channels into the central chamber of the microfluidic chip. This central chamber was specifically designed to ensure

optimal exposure of the sensors to the cultured neurons and to facilitate accurate monitoring of dopamine release. Once positioned, the sensors were securely sealed in place using a layer of polydimethylsiloxane (PDMS) to prevent any leakage and to maintain the flow pressure of the microfluidic environment.

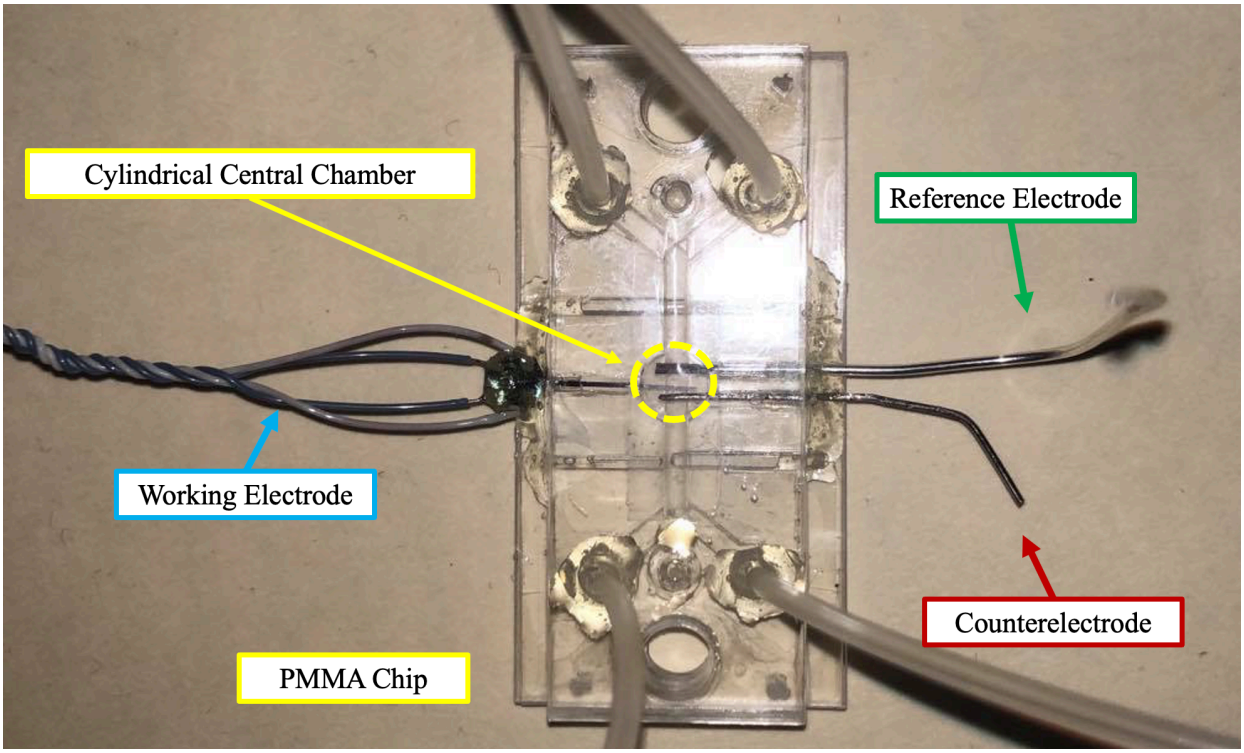

Figure 3.4 The cylindrical central chamber of the PMMA chip has substantially greater volume than the microfluidic channel. This chamber can accommodate three electrodes without the risk of grazing the PMMA surface and shearing off the polymer coatings on the surface of the working electrode.

Data collection from the integrated sensors was conducted using the same methodology outlined in the dopamine sensor study. The VMP3 potentiostat (Bio-Logic USA LLC, Knoxville, TN) was employed to apply a constant potential of 0.6 V vs. IrOx (equivalent to 0.7 V vs.

Ag/AgCl). This setup allowed for the real-time recording of current responses corresponding to dopamine concentrations within the chip. The data were collected and analyzed using the EC-Lab software.

3.3 Results and Discussion

3.3.1 Preliminary Sensor Validation in Microfluidic Environment

Before testing the dopamine sensor within a microphysiological system (MPS) containing cultured neurons, an initial control experiment was conducted to evaluate the sensor's performance in the microfluidic chip using phosphate-buffered saline (PBS) solutions with varying dopamine concentrations. This was intended to verify that the sensor could reliably detect transient dopamine concentrations under controlled conditions in the microfluidic environment. The dopamine sensor was integrated into the central chamber of the chip through micromachined channels. A constant potential of 0.6 V vs. IrOx (equivalent to 0.7 V vs. Ag/AgCl) was applied and PBS solutions with varying bulk concentrations of dopamine were sequentially pushed and pulled through the chip. The sensor's amperometric response was measured using the VMP3 potentiostat.

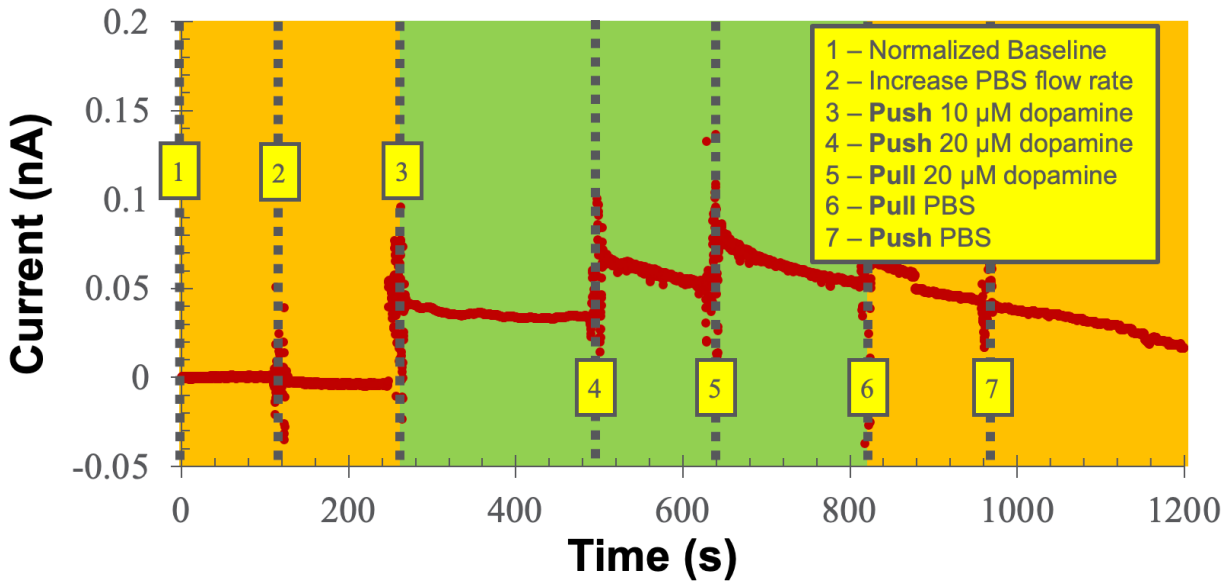

Figure 3.5 The dopamine microelectrode array sensor's current signals respond directly to transient local concentrations of dopamine. The steady state current recordings appear to be independent of the choice of flow orientation (push = green, pull = orange).

The sensor's current response modulated in direct proportion to the local concentration of dopamine. However, the sensitivity of the sensor in this setup was notably lower than the values observed in previous *in vitro* testing. This reduction in sensitivity is believed to result from the original design of the central chamber. The initial chamber geometry, which maintained the same height as the flow channels, likely caused a rapid flow rate through the chamber. This fast flow resulted in a very short residence time for dopamine molecules near the sensor surface[28], limiting the local concentration of dopamine available for detection. These results suggested that the sensor was not fully optimized for dopamine detection under these flow conditions, as the dopamine molecules were swiftly swept away from the sensor before they could be effectively measured.

3.3.2 Design Revision and Optimization

To address this issue, the design of the central chamber was revised in subsequent iterations. The revised geometry incorporated a tapered conical shape with the sensor placed at the bottom of the cone. In this configuration, dopaminergic neurons or other relevant cells can be cultured immediately above the sensor. The conical design allows dopamine released by the neurons to accumulate in the vicinity of the sensor, significantly increasing the local concentration of dopamine and preventing it from being swept away quickly by the flow [29-31]. This design increases the residence time of dopamine near the sensor, thereby improving the likelihood of detection and enhancing sensitivity. Although these control experiments were performed before the chamber redesign, the findings have informed critical design changes that are expected to significantly improve the sensor's performance when the system is tested with cultured neurons.

3.3.3 Preliminary Recommendations for Future Work

The next immediate step will involve repeating a similar experiment, but with the inclusion of actual dopaminergic neurons in the microfluidic chip. For the first test, neurons will be cultured on the surface of the sensor in the central chamber. No drugs will be introduced in this phase; instead, buffers will be used, with one buffer containing a high concentration of potassium ions to depolarize the neurons. This depolarization will trigger the neurons to release large amounts of dopamine into the chamber, effectively flooding the system with dopamine [32]. This high dopamine release will act as a robust positive control to confirm that the sensors can detect neuron-released dopamine in the chip, rather than just dopamine introduced into the system via buffer solutions.

It is important to note that the exact sensor geometry and design used in this study has been successfully implemented *in vivo* in rat models for a variety of neurotransmitter measurements,

including dopamine. Given the sensor's proven ability to function reliably in the complex biochemical environment of living brain tissue [33-35], there is strong reason to believe that it will perform just as well, if not better, in the simplified biochemical environment of the neurons within the microfluidic chip. This prior success in more challenging conditions further supports the expectation that the sensor will effectively detect dopamine in future experiments involving neuron cultures.

Once this neuronal control experiment is successfully completed, the next phase will involve repeating the experiment using different buffer solutions containing pharmacological agents, such as opioids or other drugs of interest. This will allow the system to model the effects of drug treatments on dopamine release, giving researchers insight into how various pharmacological agents influence dopaminergic signaling in this microphysiological context. These future experiments will bring the project closer to its goal of developing a reliable platform for studying the neurobiological mechanisms of opioid addiction and for screening potential therapeutics in a high-throughput, *in vitro* system that emulates the blood-brain barrier [30].

3.3 Conclusions

The integration of dopamine sensors into a microfluidic MPS represents a significant advancement in the development of platforms for studying addiction neurobiology and screening potential therapeutics for opioid use disorder. The preliminary results demonstrate the feasibility of using these sensors to monitor dopamine dynamics within a controlled microenvironment, paving the way for more complex studies involving real neuronal cultures. The success of this

project could provide a powerful tool for drug discovery, offering insights into the neurochemical processes underlying addiction and facilitating the development of more effective treatments.

3.4 References

[1] M. B. Mohammad S. Jalali, Rachael C. Hwang, Howard K. Koh, R. Kathryn McHugh, "The opioid crisis: a contextual, social-ecological framework," *Health Research Policy and Systems,* vol. 18, no. 87, pp. 1-9, 2020.

[2] L. Schmaal *et al.*, "ENIGMA MDD: seven years of global neuroimaging studies of major depression through worldwide data sharing," *Translational Psychiatry,* vol. 10, no. 1, p. 172, 2020/05/29 2020, doi: 10.1038/s41398-020-0842-6.

[3] L. A. Low, M. Sutherland, N. Lumelsky, S. Selimovic, M. S. Lundberg, and D. A. Tagle, "Organs-on-a-Chip," in *Biomaterials- and Microfluidics-Based Tissue Engineered 3D Models*, J. M. Oliveira and R. L. Reis Eds. Cham: Springer International Publishing, 2020, pp. 27-42.

[4] C. W.-B. Emily Frances Mendez, "Postmortem-derived iPSC models in substance use disorders research," *Neuropsychopharmacology,* vol. 49, pp. 349-350, 2024.

[5] N. Picollet-D'hahan, A. Zuchowska, I. Lemeunier, and S. Le Gac, "Multiorgan-on-a-Chip: A Systemic Approach To Model and Decipher Inter-Organ Communication," (in eng), *Trends Biotechnol,* vol. 39, no. 8, pp. 788-810, Aug 2021, doi: 10.1016/j.tibtech.2020.11.014.

[6] M. G. Otero *et al.*, "Organ-Chips Enhance the Maturation of Human iPSC-Derived Dopamine Neurons," (in eng), *Int J Mol Sci,* vol. 24, no. 18, Sep 18 2023, doi: 10.3390/ijms241814227.

[7] S. S. Liu *et al.*, "Kappa Opioid Receptors Drive a Tonic Aversive Component of Chronic Pain," (in eng), *J Neurosci,* vol. 39, no. 21, pp. 4162-4178, May 22 2019, doi: 10.1523/jneurosci.0274-19.2019.

[8] M. R. Bruchas, B. B. Land, and C. Chavkin, "The dynorphin/kappa opioid system as a modulator of stress-induced and pro-addictive behaviors," (in eng), *Brain Res,* vol. 1314, pp. 44-55, Feb 16 2010, doi: 10.1016/j.brainres.2009.08.062.

[9] A. Matsui and J. T. Williams, "Opioid-Sensitive GABA Inputs from Rostromedial Tegmental Nucleus Synapse onto Midbrain Dopamine Neurons," *The Journal of Neuroscience,* vol. 31, no. 48, pp. 17729-17735, 2011, doi: 10.1523/jneurosci.4570-11.2011.

[10] T. Ivanisevic and R. N. Sewduth, "Multi-Omics Integration for the Design of Novel Therapies and the Identification of Novel Biomarkers," (in eng), *Proteomes,* vol. 11, no. 4, Oct 20 2023, doi: 10.3390/proteomes11040034.

[11] Y. Wang *et al.*, "Systematic identification of non-coding pharmacogenomic landscape in cancer," *Nature Communications,* vol. 9, no. 1, p. 3192, 2018/08/09 2018, doi: 10.1038/s41467-018-05495-9.

[12] A. S. Yekkirala, D. P. Roberson, B. P. Bean, and C. J. Woolf, "Breaking barriers to novel analgesic drug development," *Nature Reviews Drug Discovery,* vol. 16, no. 8, pp. 545-564, 2017/08/01 2017, doi: 10.1038/nrd.2017.87.

[13] E. W. Esch, A. Bahinski, and D. Huh, "Organs-on-chips at the frontiers of drug discovery," (in eng), *Nat Rev Drug Discov,* vol. 14, no. 4, pp. 248-60, Apr 2015, doi: 10.1038/nrd4539.

[14] N. Franzen, W. H. van Harten, V. P. Retèl, P. Loskill, J. van den Eijnden-van Raaij, and I. J. M, "Impact of organ-on-a-chip technology on pharmaceutical R&D costs," (in eng), *Drug Discov Today,* vol. 24, no. 9, pp. 1720-1724, Sep 2019, doi: 10.1016/j.drudis.2019.06.003.

[15] K. Jackowska and P. Krysinski, "New trends in the electrochemical sensing of dopamine," *Analytical and Bioanalytical Chemistry,* vol. 405, no. 11, pp. 3753-3771, 2013/04/01 2013, doi: 10.1007/s00216-012-6578-2.

[16] A. Yorita, "Microfabricated Devices for the Detection of Neurotransmitters and Nucleic Acids," Ph.D., Chemical and Biomolecular Engineering, University of California - Los Angeles, 2016.

[17] W.-T. Chiu *et al.*, "Real-Time Electrochemical Recording of Dopamine Release under Optogenetic Stimulation," *PLOS ONE,* vol. 9, no. 2, p. e89293, 2014, doi: 10.1371/journal.pone.0089293.

[18] D. S. Macedo, M. Vepsäläinen, T. Rodopoulos, S. Peacock, and C. F. Hogan, "A sulphide resistant Ag|AgCl reference electrode for long-term monitoring," *Analyst,* 10.1039/D4AN01076K 2024, doi: 10.1039/D4AN01076K.

[19] K. Wiencke, A. Horstmann, D. Mathar, A. Villringer, and J. Neumann, "Dopamine release, diffusion and uptake: A computational model for synaptic and volume transmission," *PLOS Computational Biology,* vol. 16, no. 11, p. e1008410, 2020, doi: 10.1371/journal.pcbi.1008410.

[20] V. M. Tolosa, K. M. Wassum, N. T. Maidment, and H. G. Monbouquette, "Electrochemically deposited iridium oxide reference electrode integrated with an electroenzymatic glutamate sensor on a multi-electrode array microprobe," (in eng), *Biosens Bioelectron,* vol. 42, pp. 256-60, Apr 15 2013, doi: 10.1016/j.bios.2012.10.061.

[21] L. Lin and C.-K. Chung, "PDMS Microfabrication and Design for Microfluidics and Sustainable Energy Application: Review," *Micromachines,* vol. 12, no. 11, p. 1350, 2021. [Online]. Available: https://www.mdpi.com/2072-666X/12/11/1350.

[22] A. Borók, K. Laboda, and A. Bonyár, "PDMS Bonding Technologies for Microfluidic Applications: A Review," *Biosensors,* vol. 11, no. 8, p. 292, 2021. [Online]. Available: https://www.mdpi.com/2079-6374/11/8/292.

[23] A. Shakeri, S. Khan, and T. F. Didar, "Conventional and emerging strategies for the fabrication and functionalization of PDMS-based microfluidic devices," *Lab on a Chip,* 10.1039/D1LC00288K vol. 21, no. 16, pp. 3053-3075, 2021, doi: 10.1039/D1LC00288K.

[24] F. Kotz *et al.*, "Fused Deposition Modeling of Microfluidic Chips in Polymethylmethacrylate," *Micromachines,* vol. 11, no. 9, p. 873, 2020. [Online]. Available: https://www.mdpi.com/2072-666X/11/9/873.

[25] X. Ma, R. Li, Z. Jin, Y. Fan, X. Zhou, and Y. Zhang, "Injection molding and characterization of PMMA-based microfluidic devices," *Microsystem Technologies,* vol. 26, no. 4, pp. 1317-1324, 2020/04/01 2020, doi: 10.1007/s00542-019-04662-2.

[26] S.-C. Li, C.-C. Chiang, Y.-S. Tsai, C.-J. Chen, and T.-H. Lee, "Fabrication of a Three-Dimensional Microfluidic System from Poly(methyl methacrylate) (PMMA) Using an Intermiscibility Vacuum Bonding Technique," *Micromachines,* vol. 15, no. 4, p. 454, 2024. [Online]. Available: https://www.mdpi.com/2072-666X/15/4/454.

[27] O. l. Y. Waithe, X. Peng, E. W. Childs, and B. Tharakan, "Measurement of Transendothelial Electrical Resistance in Blood-Brain Barrier Endothelial Cells," in *Vascular Hyperpermeability: Methods and Protocols*, B. Tharakan Ed. New York, NY: Springer US, 2024, pp. 199-203.

[28] M. D. Johnson *et al.*, "Understanding Residence Time, Residence Time Distribution, and Impact of Surge Vessels," in *Continuous Pharmaceutical Processing*, Z. K. Nagy, A. El Hagrasy, and J. Litster Eds. Cham: Springer International Publishing, 2020, pp. 51-85.

[29] S. Nuh, A. Numnuam, P. Thavarungkul, and T. Phairatana, "A Novel Microfluidic-Based OMC-PEDOT-PSS Composite Electrochemical Sensor for Continuous Dopamine Monitoring," *Biosensors,* vol. 13, no. 1, p. 68, 2023. [Online]. Available: https://www.mdpi.com/2079-6374/13/1/68.

[30] P. Pattanayak *et al.*, "Microfluidic chips: recent advances, critical strategies in design, applications and future perspectives," *Microfluidics and Nanofluidics,* vol. 25, no. 12, p. 99, 2021/10/26 2021, doi: 10.1007/s10404-021-02502-2.

[31] J. Mukherjee, D. Chaturvedi, S. Mishra, R. Jain, and P. Dandekar, "Microfluidic technology for cell biology–related applications: a review," *Journal of Biological Physics,* vol. 50, no. 1, pp. 1-27, 2024/03/01 2024, doi: 10.1007/s10867-023-09646-y.

[32] Y.-W. Cho, J.-H. Park, K.-H. Lee, T. Lee, Z. Luo, and T.-H. Kim, "Recent advances in nanomaterial-modified electrical platforms for the detection of dopamine in living cells," *Nano Convergence,* vol. 7, no. 1, p. 40, 2020/12/22 2020, doi: 10.1186/s40580-020-00250-7.

[33] M. Malvaez *et al.*, "Basolateral amygdala rapid glutamate release encodes an outcome-specific representation vital for reward-predictive cues to selectively invigorate reward-seeking actions," *Scientific Reports,* vol. 5, no. 1, p. 12511, 2015/07/27 2015, doi: 10.1038/srep12511.

[34] K. M. Wassum, V. M. Tolosa, J. Wang, E. Walker, H. G. Monbouquette, and N. T. Maidment, "Silicon Wafer-Based Platinum Microelectrode Array Biosensor for Near Real-Time Measurement of Glutamate in Vivo," (in eng), *Sensors (Basel),* vol. 8, no. 8, pp. 5023-5036, 2008, doi: 10.3390/s8085023.

[35] B. Wang *et al.*, "An implantable multifunctional neural microprobe for simultaneous multi-analyte sensing and chemical delivery," *Lab on a Chip,* 10.1039/D0LC00021C vol. 20, no. 8, pp. 1390-1397, 2020, doi: 10.1039/D0LC00021C.

Chapter 4 : Directed Evolution of a γ-Aminobutyric Acid Oxidase via Ultra-High Throughput Functional Enrichment of Enzyme Libraries by Fluorescence Activated Cell Sorting

ABSTRACT

Directed evolution (DE) has become an indispensable tool for enzyme optimization across biotechnological applications, yet the screening of large libraries of flavin adenine dinucleotide (FAD)-dependent oxidases poses distinct challenges. Conventional activity-based screening methods, such as colorimetric assays and colony-based screens, often are based on cumbersome assay methods and are limited to throughputs that are insufficient to detect nuanced catalytic improvements within extensive variant libraries. In this study, we refined and applied a fluorescence-activated cell sorting (FACS)-based platform specifically for the directed evolution of *in vivo* GABA oxidase activity in *Escherichia coli*. This approach circumvents the need for cell surface expression, emulsion formation, or the addition of extracellular peroxidases, thus streamlining the DE workflow and achieving a throughput of over 10^6 variants per day. The platform effectively enriched libraries in functional variants, ultimately producing GABA oxidase mutants with 40-fold improved Michaelis constants (95 ± 43 mM) when compared to the wild type enzyme (3100 ± 160 mM). Sensors employing these evolved enzymes demonstrated order of magnitude improvements in sensitivity (to 247 ± 41 nA/(mM·cm^2)) and limit of detection (to 80 ± 21 μM). The integration of an engineered GABA oxidase into biosensing technologies offers a promising tool for neurochemical research and exemplifies the transformative potential of directed evolution to advance next-generation biosensors.

4.1 Introduction

γ-Aminobutyric acid (GABA) is a critical inhibitory neurotransmitter, integral to various neurological processes including motor control, vision, and anxiety regulation [1]. Dysregulation of GABA signaling has been implicated in a spectrum of central nervous system (CNS) disorders [2-4], notably epilepsy, schizophrenia, and addiction. Consequently, real-time monitoring of GABA concentrations *in vivo* presents significant value, both in advancing neurochemical research and in potential clinical applications. However, the non-electroactive nature of GABA [5], coupled with the biochemical complexity of the brain's extracellular matrix, poses substantial challenges for continuous, selective, and sensitive detection. Discovering or creating a selective oxidase for GABA represents a critical step toward overcoming these limitations [6] and developing the robust electroenzymatic sensor needed to investigate GABA-related mechanisms for many neurological disorders.

Directed evolution (DE) provides an effective strategy for enhancing and optimizing enzymes [7] for specialized applications such as GABA sensing. Engineered enzymes are widely employed across biotechnology and synthetic biology due to their versatility and ability to catalyze complex reactions with specificity and efficiency [8-10]. In DE, the typical workflow involves three primary stages [11-13]: (1) identifying a suitable parent enzyme; (2) generating genetic diversity; and (3) screening or selecting for variants with enhanced functionality. This process may be repeated over several cycles until an enzyme with optimal properties is obtained. For biosensing applications, large and diverse libraries of enzyme variants are essential for efficiently navigating the complex fitness landscape [14]. However, screening or selecting from vast libraries (often $>10^6$ variants) represents a significant bottleneck in DE. Advances in ultra-high throughput screening techniques, particularly fluorescence-activated cell sorting (FACS) [15-19] and fluorescence-

activated droplet sorting (FADS) [20], have become instrumental in expanding DE's applicability, especially for enzymes such as GABA oxidase that require high sensitivity and selectivity in complex biological contexts.

Despite these advances, there are still many classes of biotechnologically important enzymes for which a generally applicable, ultra-high throughput assay is not available. Prior to the FACS-centric work of Sadler *et al*. [21], no ultra-high throughput workflow existed for the directed evolution of flavin adenine dinucleotide (FAD)-dependent oxidases. This enzyme class encompasses a large and diverse group that catalyzes the transfer of electrons from their substrates, removing a hydride equivalent and passing it to an electron acceptor. Within this group of enzymes, those that transfer electrons to oxygen to produce hydrogen peroxide are particularly useful in biosensors because hydrogen peroxide can be oxidized or reduced at an electrode to yield a current signal. Alternative high-throughput methods, such as those developed for the directed evolution of glucose oxidase and monoamine oxidase (MAO-N) from *Aspergillus niger* [22-24], have been used effectively to engineer enzymes with catalytic function on primary, secondary, and tertiary amines. However, these methods often involve complex systems requiring yeast surface expression [25], emulsion formation [26], or the addition of exogenous peroxidases, thus limiting their widespread application.

To address the inherent limitations of traditional colony-based screening, we adapted protocols from Sadler *et al*. [21] to enable the sensitive detection of GABA oxidase activity at the single-cell level in *Escherichia coli*. By leveraging fluorescence-activated cell sorting (FACS), this approach allowed for significantly higher throughput and sensitivity than conventional colony assays, enabling efficient screening of large enzyme variant libraries [27]. A critical prerequisite for implementing this methodology was the identification of a starting enzyme with the capability

to oxidize GABA or structurally similar substrates, alongside the production of hydrogen peroxide (H_2O_2) as a byproduct for subsequent electrooxidation.

The search for a suitable starting enzyme initially included pursuing reports of a "novel GABA oxidase" that was purported to exhibit high activity and selectivity for GABA oxidation [28]. However, repeated efforts to acquire the specific *Penicillium* strain, the enzyme itself, or its genetic sequence were ultimately unsuccessful. This led to the establishment of a defined set of criteria for selecting alternative enzyme candidates. These criteria included: (1) an ability to directly oxidize GABA or compounds with close structural similarity [29]; (2) activity toward GABA analogues, such as deaminated, hydroxylated, β-substituted, or aromatized derivatives [13, 30, 31]; and (3) demonstrated capacity to oxidize amino acids, neurotransmitters, or their metabolites, ensuring H_2O_2 generation for electrooxidation [29, 32, 33]. Ultimately, 4-methylaminobutyrate oxidase (MABO) was selected as the starting enzyme for directed evolution due to the structural resemblance between its primary substrate, methyl-GABA, and GABA itself, differing only by a single methyl group (Fig. 1). This structural similarity provided an ideal foundation for tailoring specificity toward GABA. Furthermore, MABO's role in the nicotine degradation pathway in *Arthrobacter nicotinovorans* has been documented, and its gene sequence is accessible via UniProt (Q8GAJ0). Prior studies by Chiribau *et al*. [34] reported robust catalytic activity with methyl-GABA (k_{cat} = 1230 s^{-1}, K_M = 250 μM) and substantial activity with GABA (k_{cat} = 878 s^{-1}, K_M = 6.66 mM) at pH 9.8, a condition optimized for redox enzymes. Together, these attributes established MABO as an excellent candidate for the subsequent directed evolution efforts aimed at engineering a GABA oxidase optimized for biosensing applications.

It is important to address a notable mischaracterization on UniProt (Q8GAJ0), regarding this enzyme, which is referred to as methylamino*butanoate* oxidase (MABO). The enzyme's

native substrate, methyl-GABA, is a GABA precursor wherein one of the hydrogen atoms on the amine group is replaced with a methyl group. This substrate contains no ester groups, contradicting the implication of the enzyme's nomenclature. The MABO enzyme catalyzes the oxidative deamination of GABA-like molecules. A more accurate designation would be methylamino*butyrate* oxidase, reflecting the correct substrate structure and reaction mechanism. This clarification is critical for avoiding further propagation of inaccuracies in the characterization of this enzyme.

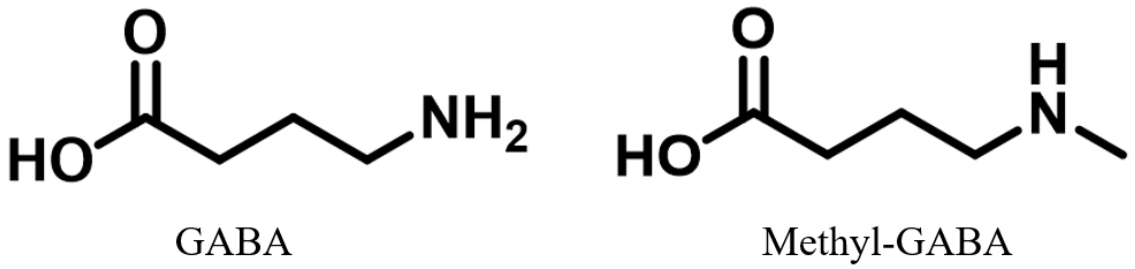

Figure 4.1 Chemical structures of GABA and methyl-GABA. GABA, the primary inhibitory neurotransmitter in the central nervous system, consists of a four-carbon backbone with an amine group at one end and a carboxylic acid group at the other. Methyl-GABA, the native substrate for methylaminobutyrate oxidase (MABO), is structurally similar to GABA but features a methyl group in place of one of the hydrogen atoms on the amine group, providing a basis for enzymatic specificity and affinity engineering.

In this work, *E. coli* cells were transformed with plasmids containing MABO and libraries of its variants. After the cells are transformed such that each cell harbored a single variant of the enzyme, expression was induced. Finally, the cell membranes were stained with a fluorogenic dye. After enzyme-catalyzed oxidation occurred, the product reactive oxygen species (ROS) reacted

with the dye and fluorescence was emitted [35-37]. Cells encoding for variant enzymes with improved catalytic activity generated even higher levels of fluorescence. FACS-based techniques could then sort out the mutants with improved activity.

This ultra-high throughput screening methodology (>10^6 variants per day) is broadly applicable to the directed evolution of FAD dependent oxidases in *E. coli*. By applying this innovative approach, new mutants of MABO with enhanced activity towards GABA were identified. This advancement significantly improves the capabilities of constant potential amperometry (CPA)-based neurotransmitter biosensors, enabling precise and reliable detection of non-electroactive substrates with high specificity and sensitivity. This work exemplifies the transformative potential of directed evolution in developing next generation biosensing technologies.

4.2 Materials and Methods

4.2.1 Reagents and Equipment

Methyl 4-aminobutyrate hydrochloride (methyl-GABA), γ-aminobutyric acid (GABA), isopropyl β-D-1-thiogalactopyranoside (IPTG), kanamycin sulfate, ascorbic acid, catalase from bovine liver, and the 5(6)-carboxy-2′,7′-dichlorofluorescein diacetate dye were purchased from MilliporeSigma (Burlington, MA, USA). The codon-optimized gene for methylaminobutyrate oxidase (MABO) was purchased from Twist Bioscience (South San Francisco, CA, USA) and cloned into the pET28a expression vector provided by Professor Yi Tang's laboratory. Ultrapure water for all solution preparations was produced with a Millipore Milli-Q Water System

(MilliporeSigma, Burlington, MA, USA). Lysogeny broth (LB) and agar were purchased from Fisher Scientific (Waltham, MA, USA).

Cloning-optimized 5-alpha competent cells, SoluBL21 expression-optimized competent cells, the HiFi DNA Assembly Kit, the Q5 Site-Directed Mutagenesis Kit, and Taq polymerase (NEB M0273S) were obtained from New England Biolabs (NEB, Ipswich, MA, USA). For DNA purification, the Zymo Zyppy Plasmid Miniprep Kit (Zymo Research, Irvine, CA, USA) was used, with DNA sequencing conducted by Laragen (Culver City, CA, USA) and/or Plasmidsaurus (Arcadia, CA, USA).

Protein purification employed 5 mL EconoFit Profinity IMAC columns and the Native IMAC Buffer Kit from Bio-Rad (Hercules, CA, USA). Enzyme kinetics and absorbance-based measurements were performed using the MAK166 Fluorometric Hydrogen Peroxide Assay Kit (Sigma Aldrich, St. Louis, MO, USA) in a Tecan Infinite M1000 plate reader (Tecan Group Ltd., Männedorf, Switzerland). Flow cytometry experiments were conducted on a Sony SH800S cytometer at the UCLA Jonsson Comprehensive Cancer Center (JCCC).

4.2.2 Preparation of GABA Oxidase Gene Construct

The codon-optimized gene sequence for MABO was derived from UniProt (Q8GAJ0), synthesized by Twist Bioscience (South San Francisco, CA, USA), and cloned into the pET28a expression vector (Appendix D). This vector is useful for protein expression due to its T7 promoter, which enables high levels of protein production in *E. coli* [38]. It also incorporates the lac operon, allowing for tightly controlled expression through the lac repressor and induction with isopropyl β-D-1-thiogalactopyranoside (IPTG) [39]. Additionally, the vector contains an N-terminal His_6-tag sequence, which facilitates the eventual purification of promising mutant proteins with

improved catalytic activity for GABA oxidation by metal affinity chromatography. Variants were created using both site-directed and random mutagenesis strategies. As before, these variants were cloned into the pET28a vector, with the resulting libraries encoding $>10^6$ variants. All cloning reactions were performed using the HiFi DNA Assembly Cloning Kit according to the supplier's protocol.

4.2.3 Preparation of Cell Samples for Flow Cytometry

SoluBL21 *E. coli* cells in 50 µL aliquots were transformed with 1–5 ng plasmid DNA (Appendix E) according to the supplier's protocol. Three mL of lysogeny broth (LB) containing 50 µg/mL kanamycin and 0.4% glycerol (v/v) was inoculated with a single colony from the transformation, incubated at 37 °C, with agitation at 180 rpm (2.5 cm orbit diameter) and grown to an OD_{600} of 0.6 before inducing protein expression by the addition of IPTG solution (100 mM in sterile H_2O) to a final concentration of 100 nM. Cultures were then incubated at 37 °C, with agitation at 180 rpm (2.5 cm orbit diameter) for 3 hours before harvesting the cells by centrifugation (17,000 × g, 5 minutes, 4 °C). The supernatant was discarded, and the cell pellet was stored at −80 °C for at least 3 hours prior to thawing and analysis by flow cytometry. This freeze-thaw step was crucial for reproducible probe uptake and eventual cell fluorescence, as it exploited the physical properties of cell membranes. The rapid freezing and thawing process disrupted cell membranes, causing many cells to die, but leaving most just sufficiently compromised to more easily uptake the dye and substrate [21]. Further detail on the preparation of the flow cytometry assay stocks is provided in Appendix H.

4.2.4 Preparation of Site Directed Mutagenesis Variant Libraries

The crystal structure of MABO co-crystallized with bound FAD first was analyzed using PyMOL (Schrödinger, LLC, New York, NY, USA). In oxidase enzymes, aromatic "cages" are commonly observed motifs surrounding the active site, playing a crucial role in substrate binding and specificity [40]. These cages are typically formed by aromatic residues—such as phenylalanine, tyrosine, and tryptophan—that create a stabilizing environment through π-stacking interactions [41, 42] and hydrophobic effects [40]. Such interactions help orient substrates correctly within the active site, facilitating the transfer of electrons during the oxidation process. In MABO, this aromatic cage is positioned adjacent to the isoalloxazine ring of FAD, contributing both to the proper orientation of the substrate and to electron transfer efficiency, ultimately enhancing catalytic function. By examining the spatial arrangement of these aromatic residues, we sought to identify potential residues for mutation that might enhance the enzyme's affinity and selectivity toward GABA.

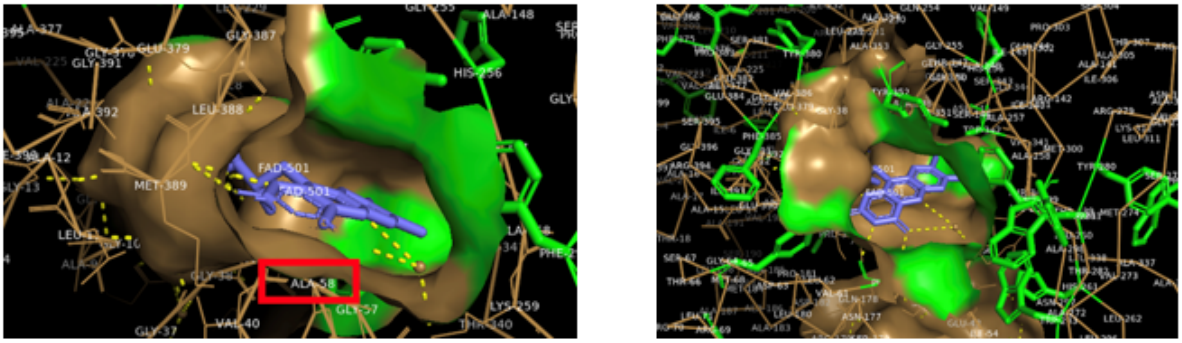

Figure 4.2 Alanine-58 is adjacent to the aromatic cage (green) and the FAD isoalloxazine ring (blue). This residue presumably participates in orienting the methyl-GABA and GABA amine groups near the isoalloxazine nitrogen, which influences the enzyme's preference for methyl-GABA over GABA.

To generate the library for site-directed mutagenesis, the New England BioLabs (NEB) Q5 Site-Directed Mutagenesis kit was used. Forward and reverse primers were designed to survey the sequence space in proximity to alanine-58. The site directed library was generated according to the supplier's protocol in which the targeted mutations were inserted as indicated by the designed primers (Appendix F). Moreover, the Q5 Site-Directed Mutagenesis kit works best with a template plasmid already containing the native MABO gene. As such, the PCR step amplifies both the MABO gene fragment and the pET28a vector backbone and ligates them back together. As a result, a separate cloning step was not necessary.

E. coli protein expression optimized strain (SoluBL21) cells in 50 µL aliquots were transformed with 1–5 ng of plasmid DNA containing site-directed mutations. After transformation, 3 mL of LB containing 50 µg/mL kanamycin was inoculated with 900 µL of the outgrowth (SOC medium) culture and incubated at 37 °C overnight. Subsequently, 3 mL of LB containing 50 µg/mL kanamycin and 0.4% glycerol (v/v) was inoculated with 1% (v/v) of the overnight culture and incubated at 37 °C with agitation at 180 rpm (2.5 cm orbit diameter) until an OD_{600} of 0.6 was reached. Protein expression was induced by the addition of IPTG solution (100 mM in sterile H_2O) to a final concentration of 100 µM and the cells were collected by centrifugation (17,000×g, 5 minutes, 4 °C). The supernatant was discarded, and the cell pellet was stored at −80 °C for at least 3 hours prior to analysis by flow cytometry. Further detail on the preparation of the flow cytometry assay stocks is provided in Appendix H.

4.2.5 Preparation of Random Mutagenesis Variant Libraries

Random mutagenesis is a less straightforward process compared to site-directed mutagenesis, as it cannot be accomplished with a commercial kit. Mutations were introduced into

the MABO gene fragment using an error-prone PCR (epPCR) recipe from the literature (Appendix G) [43]. To achieve this, a Taq polymerase (NEB M0273S) was used with a skewed dNTP ratio (5:1 TC/AG) to increase the likelihood of nucleotide misincorporation during DNA amplification. In addition, $MnCl_2$ was added immediately before inserting the mixture into the thermocycler due to its interference with the $MgCl_2$ buffer-DNA polymerase system, further reducing the polymerase's fidelity and increasing the mutation rate. The resulting randomly mutated MABO variant gene fragments were cloned into the pET28a vector using the HiFi DNA Assembly Cloning Kit according to the supplier's protocol.

SoluBL21 *E. coli* cells in 50 µL aliquots were transformed with 1–5 ng of plasmid DNA containing randomly generated mutations. After transformation, 3 mL of LB containing 50 µg/mL kanamycin was inoculated with 900 µL of the outgrowth (SOC medium) culture and incubated at 37 °C overnight. Subsequently, 3 mL of LB containing 50 µg/mL kanamycin and 0.4% glycerol (v/v) was inoculated with 1% (v/v) of the overnight culture and incubated at 37 °C with agitation at 180 rpm and 2.5 cm orbit diameter until an OD_{600} of 0.6 was reached. Protein expression was induced by the addition of IPTG solution (100 mM in sterile H_2O) to a final concentration of 100 µM, and the cells were collected by centrifugation (17,000×g, 5 minutes, 4 °C). The supernatant was discarded, and the cell pellet was stored at −80 °C for at least 3 hours prior to analysis by flow cytometry.

4.2.6 Analysis by Flow Cytometry

Cell pellets were thawed on ice and resuspended in 100 mM potassium phosphate buffer (pH 6.2) containing 100 mM KCl, 3 mM $MgCl_2$, and 1% (v/v) 1-butanol. A 10 mM solution of 5(6)-Carboxy-2′,7′-dichlorofluorescein diacetate (C-DCFDA) in DMSO was added to achieve

a final concentration of 250 μM, and the cells were incubated at 37 °C with shaking at 180 rpm (2.5 cm orbit diameter) for 1 hour. The cells were harvested by centrifugation (17,000×g, 5 minutes, 4 °C), and the supernatant was discarded. The cell pellet was resuspended in 50 mM potassium phosphate buffer (pH 7.5) containing 100 mM KCl and 3 mM $MgCl_2$. The reaction was initiated by adding GABA solution (variable concentration in 100 mM potassium phosphate buffer with 100 mM KCl and 3 mM $MgCl_2$).

To scavenge extracellular hydrogen peroxide and minimize potential cross-talk between cells, catalase from bovine liver was added to a final concentration of 0.01 mg/mL at the time of substrate addition. The reaction was quenched by adding ascorbic acid solution (100 mM in Milli-Q water) to a final concentration of 10 mM [44]. Flow cytometric cell sorting was performed using the Sony SH800S at the UCLA Jonsson Comprehensive Cancer Center (JCCC) and Center for AIDS Research Flow Cytometry Core Facility. The fluorescein product was excited by a 488 nm laser and detected in the FL2 channel (525/50 nm). Forward scatter (FSC) and side scatter (SSC) data also were collected; cells were gated on FSC-A vs. SSC-A, and singlets were identified by sub-gating on FSC-A vs. FSC-H. Flow cytometric data were analyzed, and figures were prepared using the FlowJo v10 software package (FlowJo, LLC, Ashland, OR, USA).

4.2.7 Functional Enrichment of Libraries by FACS

For the isolation of functional variants from GABA oxidase libraries, 1000 cells in the 99th percentile of fluorescence intensity (FL2-H channel) were sorted into an empty collection tube. The gene variants were outgrown in super optimal broth with catabolite repression (SOC medium) at 37 °C for 1 hour before inoculating into 3 mL of LB containing 50 μg/mL kanamycin with subsequent incubation at 37 °C overnight. This enriched cultured library was then purified using

a Zyppy Plasmid Miniprep kit (Zymo Research) according to the manufacturer's instructions, eluting in 20 μL of sterile H_2O.

When it was desirable to identify the gene sequences of improved variants, 100 μL of the aforementioned SOC culture was plated onto LB kanamycin agar media and incubated overnight at 37 °C. Individual colonies from these plates were then used to inoculate 3 mL of LB containing 50 μg/mL kanamycin. These cultures also were grown overnight at 37 °C, and the DNA was subsequently purified using the Zyppy Plasmid Miniprep kit. Gene sequencing was performed by either Laragen Inc. (Culver City, CA) or Plasmidsaurus Inc. (Arcadia, CA).

4.2.8 Enzyme Purification and Characterization

The 4-methylaminobutyrate oxidase (MABO) protein was purified using immobilized metal ion affinity chromatography (IMAC) with Bio-Scale Mini Profinity IMAC Cartridges (Bio-Rad, Hercules, CA). *E. coli* cultures expressing histidine-tagged MABO were grown for 16 hours at 15°C, harvested by centrifugation, and resuspended in lysis buffer (300 mM KCl, 50 mM KH_2PO_4, 5 mM Imidazole). Following resuspension, the cells were lysed by sonication on ice, with multiple rounds of brief pulses, to ensure efficient breakage while minimizing heat generation. After centrifuging to remove cellular debris, the clarified lysate was filtered and immediately applied to the pre-equilibrated IMAC column to capture the histidine-tagged protein.

The IMAC cartridge was then flushed with wash buffers (300 mM KCl, 50 mM KH_2PO_4, 5-10 mM Imidazole) containing low concentrations of imidazole to remove any non-specifically bound proteins and to enhance the purity of the final product. MABO was eluted from the column using a high-imidazole concentration elution buffer (300 mM KCl, 50 mM KH_2PO_4, 250 mM Imidazole), and imidazole was removed by buffer exchange to avoid interference in subsequent

spectrophotometric measurements. The purified protein was stored at 4 °C. The detailed workflow can be found in Appendix I.

Protein concentration was determined using the Coomassie (Bradford) Protein Assay (Thermo Fisher Scientific, Waltham, MA), with bovine serum albumin (BSA) as the standard (Appendix J). A series of BSA standards, spanning concentrations from 0 to 2000 μg/mL, was prepared and added to individual wells in a microplate, alongside the purified MABO samples. Each well received varying amounts of Coomassie reagent, which binds to protein and produces a color change. After a brief 10-minute incubation at room temperature, absorbance was measured at 595 nm. Using the BSA standard curve, absorbance readings were correlated with protein concentration.

To characterize the kinetic parameters of MABO, a fluorometric hydrogen peroxide assay (Sigma-Aldrich, Catalog No. MAK166) was employed, which offers a sensitive approach for detecting hydrogen peroxide as a byproduct of the enzyme-catalyzed oxidation reaction. The assay relies on a fluorogenic substrate and horseradish peroxidase (HRP) to generate a fluorescent signal proportional to the concentration of hydrogen peroxide produced by the enzyme-catalyzed reaction. A range of substrate concentrations was prepared for both methyl-GABA and GABA activity assays to capture behavior across environmentally relevant conditions, specifically focusing on values near the enzyme's K_M at both pH 7.4 and 9.8. Reaction mixtures were prepared by combining MABO with the assay's master mix, which included infrared peroxidase substrate and HRP, in a 96-well plate format. Reactions were initiated by adding the substrate to each well, and fluorescence emission was monitored (λ_{ex} = 640 nm, λ_{em} = 680 nm) using a Tecan Infinite M1000 plate reader (Tecan, Männedorf, Switzerland). Data were collected at regular intervals, and hydrogen peroxide production was quantified using a calibration curve. Apparent kinetic

parameters, K_M and k_{cat}, were determined by analyzing the initial reaction rates across a range of substrate concentrations using a fluorometric hydrogen peroxide assay without control of oxygen concentration. Initial reaction rates were calculated from the linear region of absorbance vs. time data, where the reaction exhibited a consistent rate of H_2O_2 production. These initial rates were then plotted against substrate concentration and fitted to the Michaelis-Menten equation to estimate V_{max} and K_M. k_{cat} was calculated by normalizing V_{max} to the total enzyme concentration, providing a comprehensive assessment of catalytic efficiency under the specified conditions (Appendix K).

4.3 Results and Discussion

4.3.1 Preliminary Characterization of MABO Kinetic Parameters

A comprehensive evaluation of MABO's potential as a GABA oxidase was conducted through detailed kinetic characterization, employing Michaelis-Menten analysis to quantify its catalytic properties with both its native substrate, methyl-GABA, and the target substrate, GABA. Given the role of dissolved O_2 as an uncontrolled co-substrate in these reactions, the kinetic constants reported here represent apparent values [45]. As depicted in Figure 4.3, MABO demonstrated a high turnover frequency (k_{cat}) for both substrates, achieving optimal performance at pH 9.8—a condition that aligns well with the activity profile of many redox enzymes. However, MABO's apparent K_M for GABA, particularly at physiological pH, was significantly elevated, indicating a limited substrate binding affinity that constrains its applicability in electroenzymatic sensing. This elevated apparent K_M underscored the need for enzyme optimization to enhance GABA affinity for biosensing applications at physiologically relevant conditions.

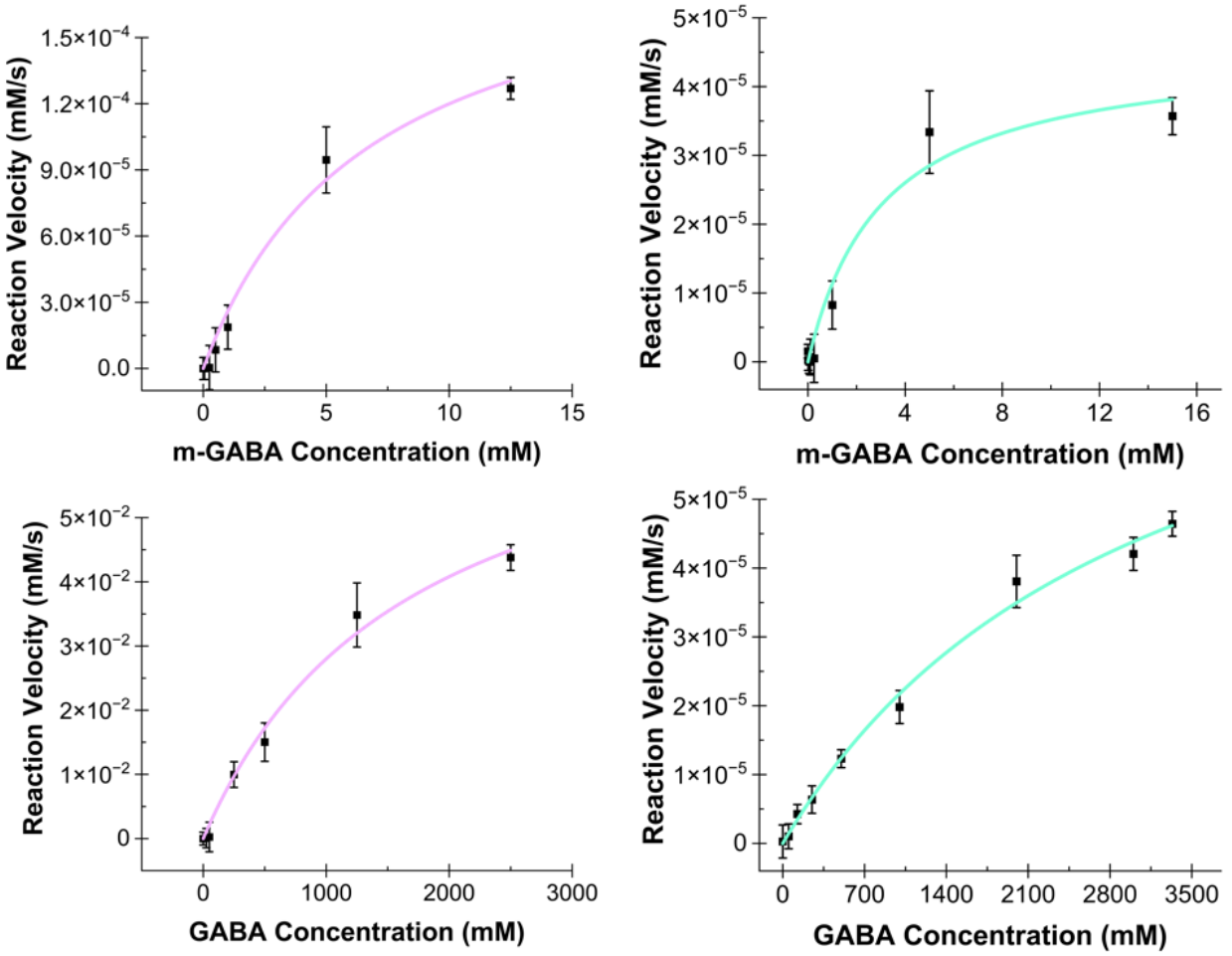

Figure 4.3 Preliminary Michaelis-Menten characterization of MABO's catalytic activity for methyl-GABA and GABA at pH 9.8 (pink) and pH 7.4 (green).

pH	Substrate	k_{cat} (s^{-1})	K_M (mM)
7.4	methyl-GABA	11.2 ± 0.56	3.05 ± 0.23
	GABA	1.8 ± 0.08	3100 ± 160
9.8	methyl-GABA	40.2 ± 2.3	6.74 ± 0.45
	GABA	15 ± 0.82	1690 ± 95
9.8 [34]	methyl-GABA	1230	0.250
	GABA	878	6.66

Table 4.1 At pH 9.8, MABO exhibited high turnover for methyl-GABA and moderate turnover for GABA, comparable to glutamate oxidase with glutamate substrate at pH 7.4 ($k_{cat} \approx 40\ s^{-1}$, $K_M \approx 200\ \mu M$) [46]. However, MABO's binding affinity for GABA was low, with high apparent K_M values at both pH 9.8 and physiological pH 7.4, indicating a need for further optimization.

Effective *in vivo* neurochemical sensing requires enzymes that operate efficiently at the physiological pH of brain extracellular fluid (pH 7.4). At this pH, the apparent K_M of MABO for GABA considerably exceeds the preferred threshold for practical electroenzymatic applications, ideally below 200 μM to achieve sensitive detection. This limitation highlights the central aim of this work: to refine MABO's substrate affinity through targeted engineering, thereby enhancing both the enzyme and sensor's performance in neurochemical sensing under physiological conditions. Through a strategic, directed evolution campaign, the goal was to generate a GABA oxidase variant with improved binding affinity, ultimately yielding an enzyme with significantly enhanced potential for real-time, *in vivo* monitoring of GABA dynamics.

In comparison to the literature, our findings revealed substantial discrepancies in kinetic parameters. Chiribau *et al*. [34] reported a $k_{cat} = 1230\ s^{-1}$ and $K_M = 250$ μM for methyl-GABA as well as $k_{cat} = 878\ s^{-1}$ and $K_M = 6.66$ mM for GABA (both at pH 9.8). In contrast, our experimentally derived parameters yielded notably lower turnover rates and higher K_M values. This deviation may stem from several factors. Firstly, the absorbance versus time data exhibited very steep initial slopes, suggesting rapid reaction kinetics in early stages. However, this behavior might not have been fully captured through traditional Michaelis-Menten analysis. Furthermore, the complexity of MABO's reaction mechanism—relying on O_2 and water as additional reactants—likely exacerbates the limitations of the Michaelis-Menten model when applied to this multi-substrate system [47]. Since co-substrate concentrations were not rigorously controlled, the derived parameters represent apparent values that may differ substantially from those obtained under ideal controlled conditions.

4.3.2 Assay Condition Optimization

The assay development and optimization procedures were based on the comprehensive work of Sadler *et al*. This detailed protocol was instrumental in determining varying levels of GABA oxidation activity across diverse mutant MABO libraries. The previously published work provided a simple and sensitive method for screening enzyme activity, greatly facilitating this work and validating this method for future studies in mapping structure-activity relationships in oxidase enzymes.

The method of Sadler *et al*. for the detection of oxidase activity *in vivo* relied on various non-fluorescent 'dihydro' dyes that become fluorescent in the presence of reactive oxygen species (ROS). Their work included the identification of suitable ROS probes, such as dihydrorhodamine123 (DHR), 2',7' - dichlorodihydrofluorescein diacetate (H_2DCFDA), and carboxy-2',7'-dichlorodihydrofluorescein diacetate (C-H_2DCFDA). It should be noted that the latter two acetylated molecules require deacetylation by endogenous esterases prior to oxidation and eventual fluorescence. In their work, C-H_2DCFDA was identified as the most effective probe, because it displayed higher fluorescence in positive populations compared to negative ones. This work incorporated carboxy-DCFDA, a very similar molecule that only differs by the omission of the "dihydro" group, using the same justification (Fig. 4.4).

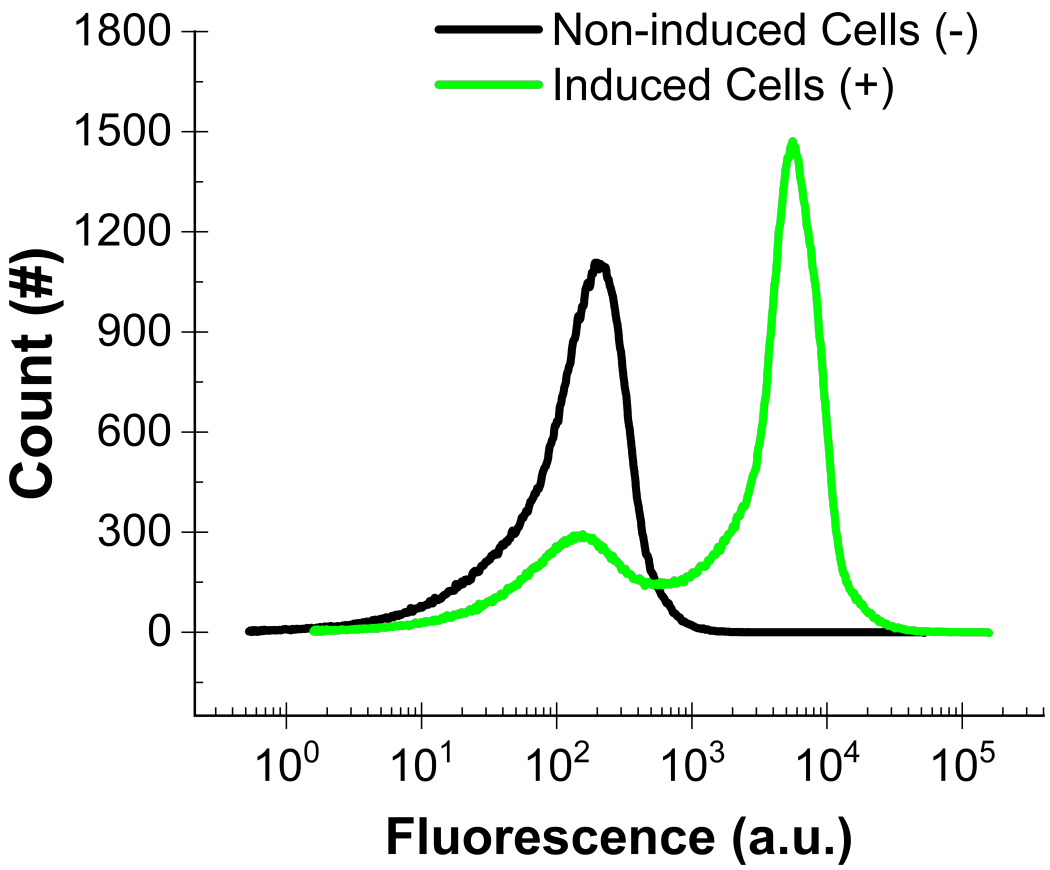

Figure 4.4 Fluorescence of carboxy-DCFDA stained *E. coli* that have been transformed with mutant MABO libraries. The positive population (green) was induced with 100 μM IPTG and the negative population (black) was not induced. Both samples were incubated with 1 M GABA for 30 minutes and quenched with 10 mM ascorbic acid prior to data collection.

The optimized assay conditions included a 3-hour induction period at 37 °C, which resulted in a high proportion of cells exhibiting positive fluorescence. The linear range of the assay was extended by using higher concentrations (250 μM) of carboxy-DCFDA, allowing for the faster detection of mutants prior to system saturation. Additionally, the assay's time sensitivity was addressed by incorporating ROS scavenging agents, with ascorbic acid identified as an effective

quencher, enabling sample analysis up to an hour after quenching without changes in fluorescence. The freeze-thaw step, essential for probe uptake, was also a critical part of the protocol, ensuring reproducibility by perforating the cell membrane to enable dye penetration.

4.3.3 Screening and Identification of Improved Site Directed Enzyme Variants

A significant benefit of the flow cytometric assay for analyzing oxidase activity, compared to the solid phase assay, is its ability to rapidly analyze large numbers of variants (up to 10,000 cells per second with the Sony SH800S instrument). This feature is especially valuable in directed evolution projects, where screening extensive variant libraries is essential to effectively navigate the complex sequence spaces. Coupling flow cytometry with fluorescence-activated cell sorting (FACS) allowed for the isolation of cells exhibiting high fluorescence. MABO variants with higher GABA turnover frequency showed increased fluorescence under the assay conditions, so FACS was used to isolate improved variants.

To validate the efficacy of our approach, a site-directed mutagenesis library of 20 variants was constructed according to previously established protocols (4.2.4) and subsequently screened for activity using the flow cytometric assay, with 1 M GABA as the substrate. Non-induced cells containing the native protein encoding sequence served as a negative control, while induced cells with the native sequence provided a positive control. Cells from the library exhibiting elevated fluorescence were sorted into a functionally enriched sub-library (4.2.7) and sequenced to identify promising variants.

Through this process, alanine-58 emerged as a focal point of interest due to its strategic position near both the aromatic cage and the electron mediator, the FAD isoalloxazine ring. This unique positioning places alanine-58 in close proximity to essential residues that facilitate

substrate binding and catalysis, suggesting it plays a key role in regulating access to the enzyme's active site. As illustrated in Figure 4.2, the active site of MABO is configured so that the amine groups of both methyl-GABA and GABA align with the isoalloxazine nitrogen—a precise orientation necessary for effective electron transfer during catalysis. Recognizing the importance of this spatial arrangement for catalytic function, we hypothesized that the hydrophobic pocket adjacent to alanine-58 contributes significantly to the enzyme's inherent catalytic preference for methyl-GABA over GABA. This insight guided further mutagenesis efforts to enhance GABA affinity and turnover.

To assess whether the observed distribution of genotypes in the site-directed mutagenesis experiment deviated significantly from a random distribution, a chi-squared goodness-of-fit test was performed. The null hypothesis proposed that each of the 20 potential genotypes resulting from the site-directed mutagenesis had an equal likelihood of being represented among the sequenced colonies. Under this assumption, each genotype would be expected to appear in approximately 1.5 out of the 30 sequenced colonies. However, sequencing results showed that 22 of the 30 colonies expressed the A58Y mutation, 8 expressed the A58G mutation, and the remaining 18 possible variants were entirely absent. This distribution of observed frequencies, compared to the expected frequency of 1.5 per genotype under the null hypothesis, highlights the non-random enrichment of specific variants, further validating the functional importance of mutations at alanine-58 in optimizing GABA oxidase activity. The degrees of freedom for the chi-squared (χ^2) test were calculated based on the number of possible genotypes. Since there are 20 canonical amino acids, there are 20 possible genotypes that could result from the mutagenesis of alanine-58, leading to 19 degrees of freedom. A χ^2 statistic of 335.34 was calculated with 19 degrees of freedom, yielding a p-value of approximately 1.085×10^{-59}. This p-value is far below

any conventional threshold for significance, so the null hypothesis is convincingly rejected, which supports the conclusion that the observed distribution of genotypes is not due to random chance. Instead, the results strongly suggested that the A58Y and A58G mutants were preferentially selected during the FACS process because of their enhanced catalytic activity for GABA oxidation. This indicated that the flow cytometer effectively filtered out background noise, allowing for a clear distinction between true signal and spurious fluctuations, thereby isolating the most functionally improved variants.

Figure 4.5 provides a visual representation of key K_M values obtained for wild type and mutant forms of the enzyme at pH 7.4. Panel A illustrates the substantial reductions in K_M achieved with A58Y (568 mM) and A58G (160 mM) compared to the wild type (3100 mM), highlighting alanine-58 as a critical locus for enhancing catalysis for GABA oxidation. The corresponding k_{cat} values for A58Y ($10.2 \pm 0.35\ s^{-1}$) and A58G ($5.7 \pm 0.42\ s^{-1}$) also improved by an order of magnitude and half an order of magnitude, respectively, under the same environmental conditions. These mutations not only address affinity improvements (aligning with the engineering goal of reducing K_M), but also modestly improve turnover frequency (increasing k_{cat}). Encouraged by these findings, further combinatorial saturation mutagenesis was conducted on residues 57, 58, and 59. A sample of these results is shown in Panel B, where it became evident that none of the additional mutations surpassed the GABA affinity achieved by the A58Y or A58G mutations alone.

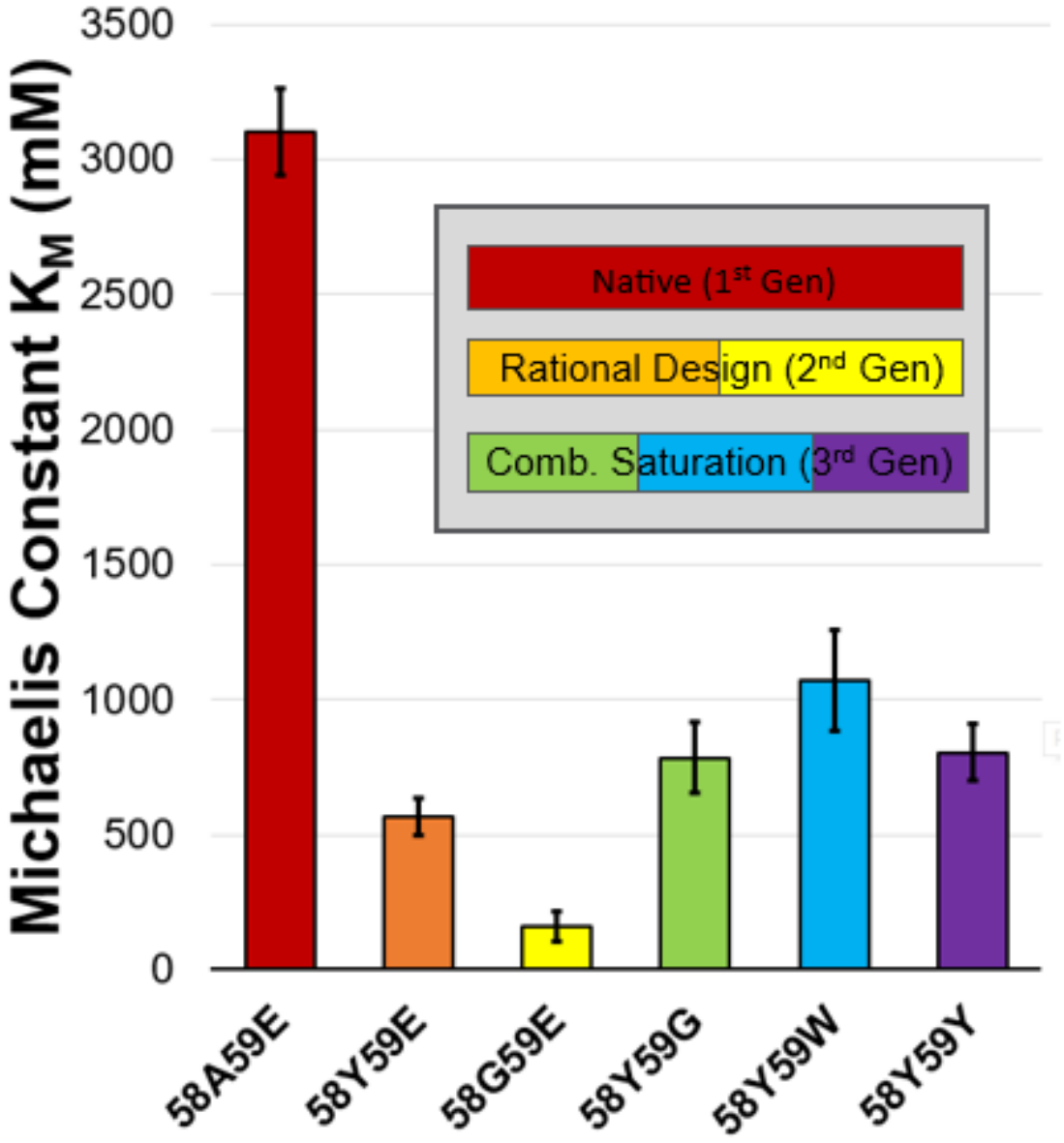

Figure 4.5 K_M values are presented as bar graphs for each variant: wild type (3100 mM), A58Y (568 mM), and A58G (160 mM). This significant enhancement in GABA affinity (based on lower K_M values) underscores the potential of alanine-58 as a critical binding site. Combinatorial active site saturation (CASS) was performed across residues 57, 58, and 59. None of these selected mutants surpassed the GABA affinity of A58Y or A58G. These findings suggested that the A58 site represents a local fitness peak in the enzyme's binding landscape for GABA.

While these findings suggested potential for further exploration around the alanine-58 residue, such as investigating adjacent positions 56 and 60, the pursuit of a local fitness peak around this specific site did not guarantee the identification of the global maximum for GABA oxidation activity. Consequently, a more extensive approach through random mutagenesis was prioritized to obtain a broader and more comprehensive understanding of the protein structure-function relationship, potentially uncovering variants with significantly enhanced GABA oxidase activity across the entire enzyme fitness landscape.

4.3.4 Screening and Identification of Improved Random Enzyme Variants

While site-directed mutagenesis provided valuable insights, it inherently focused on a limited portion of the enzyme's evolutionary potential. Concentrating on specific residues, such as alanine-58, narrowed the exploration to a small, predefined area within a vast and complex fitness landscape. This targeted approach uncovered a local fitness peak, offering modest improvements in GABA oxidase activity, but it restricted our ability to identify more significant enhancements that might arise from broader structural changes. The enzyme's performance could be influenced by interactions occurring far from the active site or through subtle modifications across multiple regions that site-directed mutagenesis might miss [48]. To overcome these limitations and fully explore the enzyme's evolutionary landscape, random mutagenesis was employed. This technique introduced mutations throughout the entire sequence, enabling a more comprehensive examination of the protein's structure-function relationship. By allowing a more stochastic and expansive exploration, random mutagenesis increased the likelihood of discovering variants with significantly enhanced GABA oxidase activity, potentially revealing global fitness peaks that remain hidden within unexplored regions of the protein's sequence space.

Random mutagenesis libraries were generated and prepared as described (4.2.5), and subsequently screened using the same flow cytometric assay as that discussed above for the site-directed mutagenesis approach. To ensure the selection of mutants with improved affinity for GABA, the substrate concentration was gradually reduced in subsequent generations, favoring variants with lower K_M values for GABA oxidation. The screening process mirrored the approach used for the site-directed mutagenesis library: non-induced cells containing the native protein encoding sequence served as the negative control, while induced cells with the native sequence functioned as the positive control. Cells from the library exhibiting fluorescence at or above the 99^{th} percentile were sorted into a functionally enriched sub-library (4.2.7). These enriched sub-libraries then served as templates for generating subsequent rounds of random mutants, further refining the search for optimized enzyme variants.

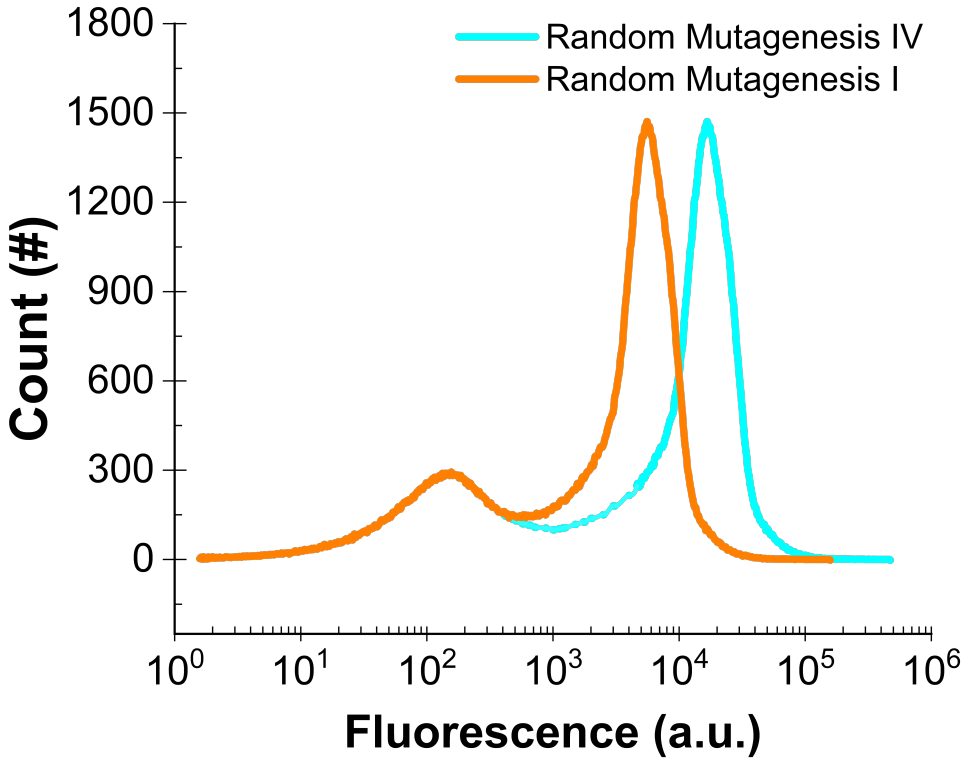

Figure 4.6 Iteratively selecting the top 1% of variants from each generation caused the fluorescence of the positive population to consistently shift to the right. After four mutation and selection cycles, there was a discernible improvement in the enzyme's catalytic efficiency for GABA oxidation. The concentration of the GABA substrate in the FACS assay decreased in sequential generations: 1 M, 800 mM, 650 mM, 500 mM.

While catalytic efficiency is conventionally defined as k_{cat}/K_M, the primary objective of this study was to reduce K_M, given that the native enzyme exhibited a reasonable turnover frequency (k_{cat}) despite its poor substrate affinity for GABA. For the affinity optimized double mutant A58G-I393T, k_{cat} was determined to be 2.2 ± 0.36 s^{-1}, a value similar to the native enzyme under similar conditions. However, it is worth noting that this is a reduction when compared to the mutants isolated from site directed mutagenesis (A58G and A58Y). These results suggested that

the improvements achieved through both site-directed and random mutagenesis efforts were predominantly driven by enhanced substrate affinity rather than changes in turnover frequency. This outcome aligns with the inherent biochemical principle that improving substrate binding affinity is often more accessible than modulating turnover frequency, particularly when the starting enzyme exhibits weak affinity for the target substrate. Collectively, these findings underscore the efficacy of targeted mutagenesis strategies in tailoring enzyme functionality, with a specific emphasis on optimizing substrate affinity to meet physiological and analytical requirements.

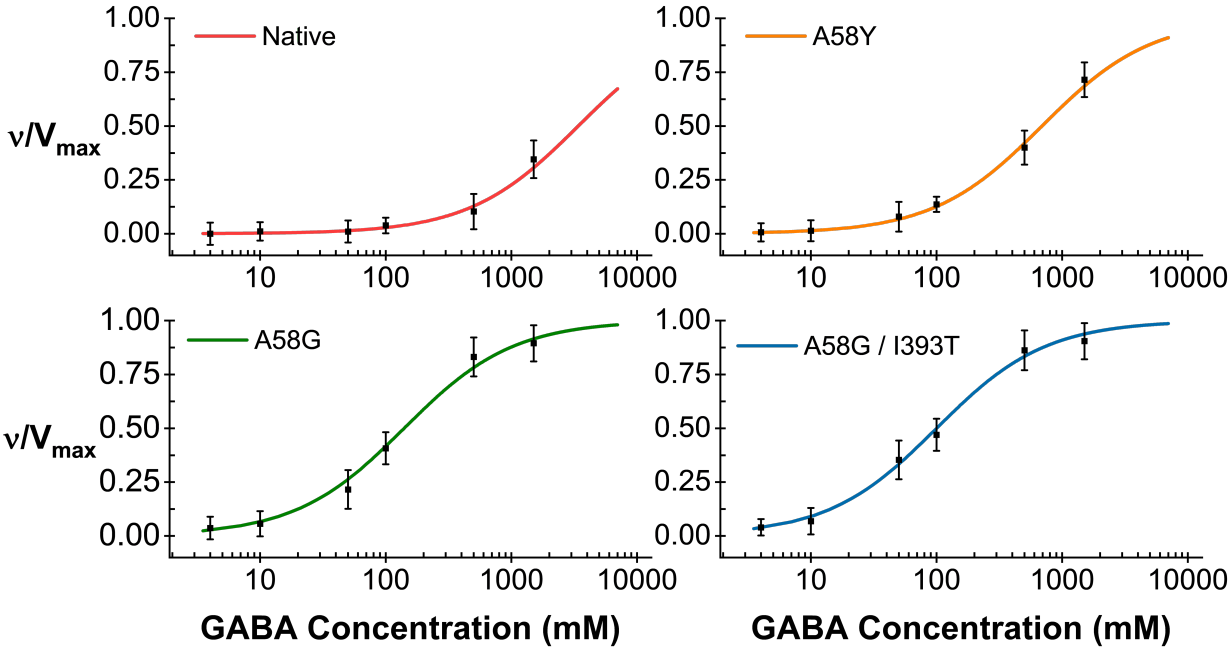

Figure 4.7 The above semilog Michaelis-Menten plots illustrate the evolution of kinetic parameters across key GABA oxidase variants, including the native enzyme, A58G, A58Y, and the double mutant A58G-I393T, derived from the 4th round of random mutagenesis. The x-axis represents substrate concentration on a logarithmic scale. The y-axis is plotted as a nondimensionalized reaction rate for a more straightforward comparison.

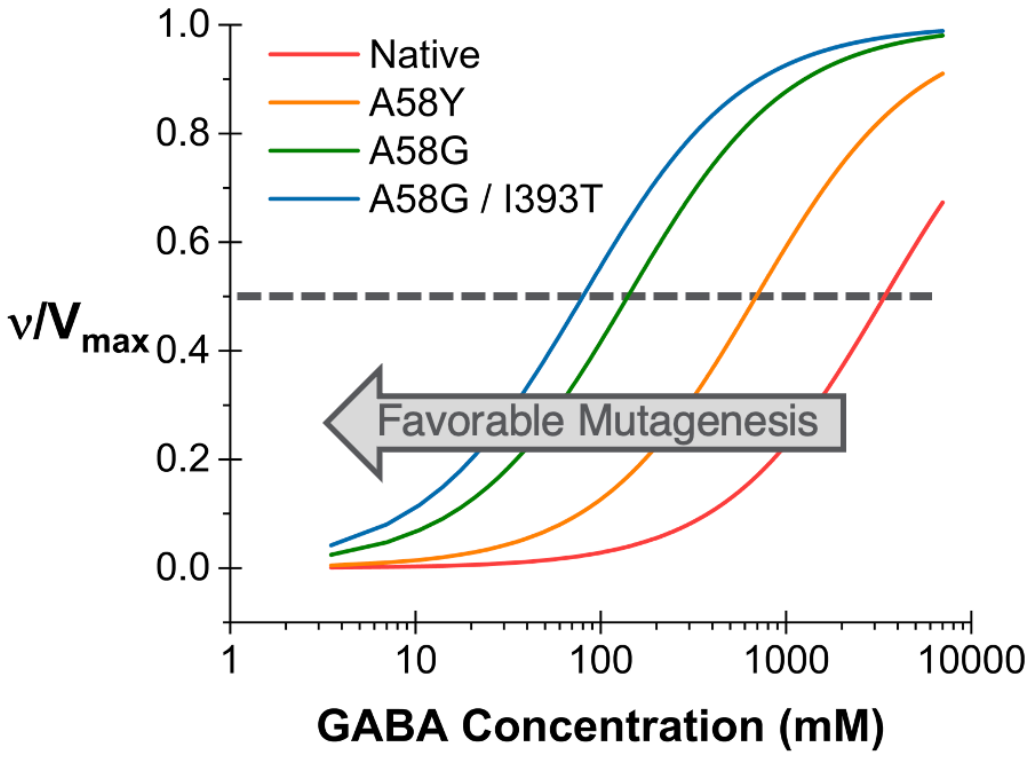

Figure 4.8 The superimposition of the plots shown in figure 4.7 indicates a clear, progressive leftward shift across generations. This is representative of an iterative reduction in K_M (the x value that corresponds to $\nu/V_{max} = 0.5$ for each curve) that spans multiple orders of magnitude. Notably, the A58G-I393T double mutant exhibits the most significant improvement in affinity, indicating the efficacy of combining site directed and random mutagenesis strategies.

Enzyme Variant	Native	A58Y	A58G	A58G/I393T
k_{cat} (s^{-1})	1.8 ± 0.08	10.2 ± 0.35	5.7 ± 0.42	2.2 ± 0.36
K_M (mM)	3100 ± 160	570 ± 71	160 ± 54	95 ± 43
V_{max} (µM/s)	0.15 ± 0.02	0.27 ± 0.01	0.34 ± 0.2	0.21 ± 0.03

Table 4.2 Summary of GABA oxidase kinetic parameters across key variants assayed at physiological pH (7.4). Varying concentrations of GABA were tested as the substrate and the reported uncertainties correspond to standard error computations.

Despite undergoing four rounds of random mutagenesis, the optimized A58G-I393T variant retained only two functionally impactful amino acid substitutions, while numerous silent mutations accumulated across cycles. Although these silent mutations did not alter the amino acid sequence, their presence reflects the inherent randomness of mutational processes and underscores the fidelity of this directed evolution experiment to natural evolutionary mechanisms. The iterative screening process effectively eliminated variants harboring mutations that reduced catalytic performance while selectively retaining only mutations with neutral impacts or those that contributed to improved function.

The recurrent identification of the A58G mutation, initially targeted during site-directed mutagenesis, reinforces the critical importance of alanine-58 for GABA affinity and catalysis, suggesting that this residue is indeed a pivotal site within the enzyme's active configuration. The subsequent discovery of the I393T mutation highlights the power of random mutagenesis to reveal synergistic modifications that, when combined with A58G, yield superior GABA affinity. This selective combination of mutations underscores the advantage of integrating site-directed and random mutagenesis approaches to identify variants with markedly enhanced substrate affinity, with the final A58G-I393T variant achieving a K_M of 95 ± 43 mM. Together, these findings illustrate that directed evolution, even through multiple cycles, reliably captures both the diversity and selectivity observed in natural evolution, ultimately yielding an enzyme variant that is better suited for biosensing applications, such as those discussed in Chapter 5. As it stands, further rounds of mutagenesis will be required to refine the kinetics of GABA oxidase, advancing its performance to a level where sensors utilizing this enzyme can reliably detect GABA concentrations at the lower end of the physiological range.

4.4 Conclusions

In conclusion, the combined approaches of site-directed and random mutagenesis have effectively advanced the understanding and optimization of GABA oxidase activity. Site-directed mutagenesis provided valuable insights into specific residues, such as alanine-58, that play a crucial role in enzyme function. However, random mutagenesis enabled a broader investigation of the enzyme's fitness landscape [49]. Through iterative selection and screening, significant improvements were made in the enzyme's catalytic efficiency, particularly by reducing the K_M for GABA, which was a critical limitation of the native enzyme.

The observed shift in fluorescence across successive generations of random mutants underscored the success of this strategy in identifying variants with enhanced GABA oxidation activity. Notably, A58G-I393T exhibited significantly improved GABA oxidase activity compared to the wild-type enzyme. These alterations contributed to the observed improvements in catalytic efficiency, particularly in reducing the K_M for GABA oxidation.

The ability to detect and sort variants with improved function directly within a prokaryotic system highlights the robustness of the assay employed. The iterative FACS-based selection process enriched for enzyme variants with superior catalytic properties, effectively demonstrating the utility of this approach in directed evolution studies. The work presented here not only demonstrates the successful application of a flow cytometric assay for the enrichment of high-performing GABA oxidase variants but also lays the groundwork for future studies focused on refining and optimizing enzymes for various biotechnological applications.

These findings underscore the potential for further refinement of enzyme activity through both targeted and broad-based mutagenesis techniques. The successful identification of a novel, high-activity GABA oxidase variant illustrates the power of random mutagenesis in uncovering

unexpected and valuable enzyme characteristics. This research provides a strong foundation for future efforts to engineer enzymes with tailored properties, particularly for applications in biosensing and other critical areas of biotechnology. By leveraging these mutagenesis strategies, the potential for optimizing enzyme function across a wide range of substrates is significantly expanded, opening new avenues for research, development, and application.

4.5 References

[1] R. B. Lydiard, "The role of GABA in anxiety disorders," (in eng), *J Clin Psychiatry,* vol. 64 Suppl 3, pp. 21-7, 2003.

[2] Y. Feng *et al.*, "Genetic variations in GABA metabolism and epilepsy," *Seizure - European Journal of Epilepsy,* vol. 101, pp. 22-29, 2022, doi: 10.1016/j.seizure.2022.07.007.

[3] L. M. Levy and A. J. Degnan, "GABA-Based Evaluation of Neurologic Conditions: MR Spectroscopy," *American Journal of Neuroradiology,* vol. 34, no. 2, pp. 259-265, 2013, doi: 10.3174/ajnr.A2902.

[4] M. Jahangir, J.-S. Zhou, B. Lang, and X.-P. Wang, "GABAergic System Dysfunction and Challenges in Schizophrenia Research," (in English), *Frontiers in Cell and Developmental Biology,* Review vol. 9, 2021-May-14 2021, doi: 10.3389/fcell.2021.663854.

[5] J. Hou, R. Strand-Amundsen, and G. Martinsen Ø, "Detection of physiological concentrations of GABA using dielectric spectroscopy - A pilot study," (in eng), *J Electr Bioimpedance,* vol. 14, no. 1, pp. 47-52, Jan 2023, doi: 10.2478/joeb-2023-0006.

[6] T. K. Le *et al.*, "Biosensor-Based Directed Evolution of Methanol Dehydrogenase from Lysinibacillus xylanilyticus," (in eng), *Int J Mol Sci,* vol. 22, no. 3, Feb 2 2021, doi: 10.3390/ijms22031471.

[7] F. H. Arnold and A. A. Volkov, "Directed evolution of biocatalysts," (in eng), *Curr Opin Chem Biol,* vol. 3, no. 1, pp. 54-9, Feb 1999, doi: 10.1016/s1367-5931(99)80010-6.

[8] V. G. H. Eijsink, S. Gåseidnes, T. V. Borchert, and B. van den Burg, "Directed evolution of enzyme stability," *Biomolecular Engineering,* vol. 22, no. 1, pp. 21-30, 2005/06/01/ 2005, doi: https://doi.org/10.1016/j.bioeng.2004.12.003.

[9] R. A. Sheldon and D. Brady, "The limits to biocatalysis: pushing the envelope," *Chemical Communications,* 10.1039/C8CC02463D vol. 54, no. 48, pp. 6088-6104, 2018, doi: 10.1039/C8CC02463D.

[10] P. A. Dalby, "Optimising enzyme function by directed evolution," *Current Opinion in Structural Biology,* vol. 13, no. 4, pp. 500-505, 2003/08/01/ 2003, doi: https://doi.org/10.1016/S0959-440X(03)00101-5.

[11] A. Currin, N. Swainston, P. J. Day, and D. B. Kell, "Synthetic biology for the directed evolution of protein biocatalysts: navigating sequence space intelligently," *Chemical Society Reviews,* 10.1039/C4CS00351A vol. 44, no. 5, pp. 1172-1239, 2015, doi: 10.1039/C4CS00351A.

[12] Y. Wang, P. Xue, M. Cao, T. Yu, S. T. Lane, and H. Zhao, "Directed Evolution: Methodologies and Applications," *Chemical Reviews,* vol. 121, no. 20, pp. 12384-12444, 2021/10/27 2021, doi: 10.1021/acs.chemrev.1c00260.

[13] U. Markel, K. D. Essani, V. Besirlioglu, J. Schiffels, W. R. Streit, and U. Schwaneberg, "Advances in ultrahigh-throughput screening for directed enzyme evolution," *Chemical Society Reviews,* 10.1039/C8CS00981C vol. 49, no. 1, pp. 233-262, 2020, doi: 10.1039/C8CS00981C.

[14] D. B. Kell, "Scientific discovery as a combinatorial optimisation problem: how best to navigate the landscape of possible experiments?," (in eng), *Bioessays,* vol. 34, no. 3, pp. 236-44, Mar 2012, doi: 10.1002/bies.201100144.

[15] G. Yang and S. G. Withers, "Ultrahigh-throughput FACS-based screening for directed enzyme evolution," (in eng), *Chembiochem,* vol. 10, no. 17, pp. 2704-15, Nov 23 2009, doi: 10.1002/cbic.200900384.

[16] T. H. Yoo, M. Pogson, B. L. Iverson, and G. Georgiou, "Directed Evolution of Highly Selective Proteases by Using a Novel FACS-Based Screen that Capitalizes on the p53 Regulator MDM2," *ChemBioChem,* vol. 13, no. 5, pp. 649-653, 2012, doi: https://doi.org/10.1002/cbic.201100718.

[17] S. J. Kwon, R. Petri, A. L. DeBoer, and C. Schmidt-Dannert, "A high-throughput screen for porphyrin metal chelatases: application to the directed evolution of ferrochelatases for metalloporphyrin biosynthesis," (in eng), *Chembiochem,* vol. 5, no. 8, pp. 1069-74, Aug 6 2004, doi: 10.1002/cbic.200400051.

[18] J. M. Duarte, I. Barbier, and Y. Schaerli, "Bacterial Microcolonies in Gel Beads for High-Throughput Screening of Libraries in Synthetic Biology," (in eng), *ACS Synth Biol,* vol. 6, no. 11, pp. 1988-1995, Nov 17 2017, doi: 10.1021/acssynbio.7b00111.

[19] A. Espargaró, R. Sabate, and S. Ventura, "Thioflavin-S staining coupled to flow cytometry. A screening tool to detect in vivo protein aggregation," (in eng), *Mol Biosyst,* vol. 8, no. 11, pp. 2839-44, Nov 2012, doi: 10.1039/c2mb25214g.

[20] P.-Y. Colin *et al.*, "Ultrahigh-throughput discovery of promiscuous enzymes by picodroplet functional metagenomics," *Nature Communications,* vol. 6, no. 1, p. 10008, 2015/12/07 2015, doi: 10.1038/ncomms10008.

[21] J. C. Sadler, A. Currin, and D. B. Kell, "Ultra-high throughput functional enrichment of large monoamine oxidase (MAO-N) libraries by fluorescence activated cell sorting," *Analyst,* 10.1039/C8AN00851E vol. 143, no. 19, pp. 4747-4755, 2018, doi: 10.1039/C8AN00851E.

[22] K. E. Atkin *et al.*, "The structure of monoamine oxidase from Aspergillus niger provides a molecular context for improvements in activity obtained by directed evolution," (in eng), *J Mol Biol,* vol. 384, no. 5, pp. 1218-31, Dec 31 2008, doi: 10.1016/j.jmb.2008.09.090.

[23] H. Gaweska and P. F. Fitzpatrick, "Structures and Mechanism of the Monoamine Oxidase Family," (in eng), *Biomol Concepts,* vol. 2, no. 5, pp. 365-377, Oct 1 2011, doi: 10.1515/bmc.2011.030.

[24] K. Markošová, A. Camattari, M. Rosenberg, A. Glieder, N. J. Turner, and M. Rebroš, "Cloning and upscale production of monoamine oxidase N (MAO-N D5) by Pichia pastoris," (in eng), *Biotechnol Lett,* vol. 40, no. 1, pp. 127-133, Jan 2018, doi: 10.1007/s10529-017-2450-y.

[25] R. Ostafe, R. Prodanovic, J. Nazor, and R. Fischer, "Ultra-High-Throughput Screening Method for the Directed Evolution of Glucose Oxidase," *Chemistry & Biology,* vol. 21, no. 3, pp. 414-421, 2014/03/20/ 2014, doi: https://doi.org/10.1016/j.chembiol.2014.01.010.

[26] R. Prodanovic, R. Ostafe, M. Blanusa, and U. Schwaneberg, "Vanadium bromoperoxidase-coupled fluorescent assay for flow cytometry sorting of glucose oxidase gene libraries in double emulsions," (in eng), *Anal Bioanal Chem,* vol. 404, no. 5, pp. 1439-47, Sep 2012, doi: 10.1007/s00216-012-6234-x.

[27] T. F. Edgardo, "Fluorescence Activated Cell Sorting for Enzymatic Activity," *Combinatorial Chemistry & High Throughput Screening,* vol. 9, no. 4, pp. 321-328, 2006, doi: http://dx.doi.org/10.2174/138620706776843200.

[28] A. Yamamura, Y. Kimura, S. Tamai, and K. Matsumoto, "Gamma-Aminobutyric acid (GABA) sensor using GABA oxidase from Penicillium sp. KAIT-M-117," *ECS Meeting Abstracts,* vol. MA2008-02, no. 46, p. 2832, 2008/08/29 2008, doi: 10.1149/MA2008-02/46/2832.

[29] F. H. Arnold, "Design by Directed Evolution," *Accounts of Chemical Research,* vol. 31, no. 3, pp. 125-131, 1998/03/01 1998, doi: 10.1021/ar960017f.

[30] S. H. Albayati *et al.*, "Main Structural Targets for Engineering Lipase Substrate Specificity," *Catalysts,* vol. 10, no. 7, p. 747, 2020. [Online]. Available: https://www.mdpi.com/2073-4344/10/7/747.

[31] M. T. Reetz, "Directed evolution of selective enzymes and hybrid catalysts," *Tetrahedron,* vol. 58, no. 32, pp. 6595-6602, 2002/08/05/ 2002, doi: https://doi.org/10.1016/S0040-4020(02)00668-3.

[32] S. Sen, V. Venkata Dasu, and B. Mandal, "Developments in Directed Evolution for Improving Enzyme Functions," *Applied Biochemistry and Biotechnology,* vol. 143, no. 3, pp. 212-223, 2007/12/01 2007, doi: 10.1007/s12010-007-8003-4.

[33] M. T. Reetz and K.-E. Jaeger, "Superior Biocatalysts by Directed Evolution," in *Biocatalysis - From Discovery to Application*, W.-D. Fessner *et al.* Eds. Berlin, Heidelberg: Springer Berlin Heidelberg, 1999, pp. 31-57.

[34] C.-B. Chiribau, M. Mihasan, P. Ganas, G. L. Igloi, V. Artenie, and R. Brandsch, "Final steps in the catabolism of nicotine," *The FEBS Journal,* vol. 273, no. 7, pp. 1528-1536, 2006/04/01 2006, doi: https://doi.org/10.1111/j.1742-4658.2006.05173.x.

[35] S. G. Rhee, T. S. Chang, W. Jeong, and D. Kang, "Methods for detection and measurement of hydrogen peroxide inside and outside of cells," (in eng), *Mol Cells,* vol. 29, no. 6, pp. 539-49, Jun 2010, doi: 10.1007/s10059-010-0082-3.

[36] J. P. Robinson *et al.*, "High-Throughput Secondary Screening at the Single-Cell Level," *Journal of Laboratory Automation,* vol. 18, no. 1, pp. 85-98, 2013, doi: 10.1177/2211068212456978.

[37] B. Kalyanaraman, M. Hardy, R. Podsiadly, G. Cheng, and J. Zielonka, "Recent developments in detection of superoxide radical anion and hydrogen peroxide: Opportunities, challenges, and implications in redox signaling," (in eng), *Arch Biochem Biophys,* vol. 617, pp. 38-47, Mar 1 2017, doi: 10.1016/j.abb.2016.08.021.

[38] P. J. Shilling, K. Mirzadeh, A. J. Cumming, M. Widesheim, Z. Köck, and D. O. Daley, "Improved designs for pET expression plasmids increase protein production yield in Escherichia coli," *Communications Biology,* vol. 3, no. 1, p. 214, 2020/05/07 2020, doi: 10.1038/s42003-020-0939-8.

[39] D. J. Wurm, L. Veiter, S. Ulonska, B. Eggenreich, C. Herwig, and O. Spadiut, "The E. coli pET expression system revisited-mechanistic correlation between glucose and lactose uptake," (in eng), *Appl Microbiol Biotechnol,* vol. 100, no. 20, pp. 8721-9, Oct 2016, doi: 10.1007/s00253-016-7620-7.

[40] M. A. Tararina and K. N. Allen, "Bioinformatic Analysis of the Flavin-Dependent Amine Oxidase Superfamily: Adaptations for Substrate Specificity and Catalytic Diversity," *Journal of Molecular Biology,* vol. 432, no. 10, pp. 3269-3288, 2020/05/01/ 2020, doi: https://doi.org/10.1016/j.jmb.2020.03.007.

[41] D. E. Edmondson, C. Binda, and A. Mattevi, "Structural insights into the mechanism of amine oxidation by monoamine oxidases A and B," *Archives of Biochemistry and Biophysics,* vol. 464, no. 2, pp. 269-276, 2007/08/15/ 2007, doi: https://doi.org/10.1016/j.abb.2007.05.006.

[42] S. N. Muellers, M. A. Tararina, U. Kuzmanovic, J. E. Galagan, and K. N. Allen, "Structural Insights into the Substrate Range of a Bacterial Monoamine Oxidase," (in eng), *Biochemistry,* vol. 62, no. 3, pp. 851-862, Feb 7 2023, doi: 10.1021/acs.biochem.2c00540.

[43] F. H. Arnold and G. Georgiou, *Directed evolution library creation : methods and protocols* (Methods in molecular biology ; 231). Totowa, N.J: Humana Press, 2003.

[44] S. Hosaka, M. Obuki, J. Nakajima, and M. Suzuki, "Comparative study of antioxidants as quenchers or scavengers of reactive oxygen species based on quenching of MCLA-dependent chemiluminescence," (in eng), *Luminescence,* vol. 20, no. 6, pp. 419-27, Nov-Dec 2005, doi: 10.1002/bio.867.

[45] J. Wang, E. Erdem, and J. M. Woodley, "Effect of Nitrogen, Air, and Oxygen on the Kinetic Stability of NAD(P)H Oxidase Exposed to a Gas–Liquid Interface," *Organic Process Research & Development,* vol. 27, no. 6, pp. 1111-1121, 2023/06/16 2023, doi: 10.1021/acs.oprd.3c00095.

[46] H. Cao and J.-C. Chiao, "Nanowire Modification to Enhance the Performance of Neurotransmitter Sensors," *Journal of Nanotechnology in Engineering and Medicine,* vol. 1, no. 4, 2010, doi: 10.1115/1.4002500.

[47] R. T. K. Ariyawansha, B. F. A. Basnayake, A. K. Karunarathna, and M. I. M. Mowjood, "Extensions to Michaelis-Menten Kinetics for Single Parameters," *Scientific Reports,* vol. 8, no. 1, p. 16586, 2018/11/08 2018, doi: 10.1038/s41598-018-34675-2.

[48] A. N. Naganathan, "Modulation of allosteric coupling by mutations: from protein dynamics and packing to altered native ensembles and function," *Current Opinion in Structural Biology,* vol. 54, pp. 1-9, 2019/02/01/ 2019, doi: https://doi.org/10.1016/j.sbi.2018.09.004.

[49] R. M. P. Siloto and R. J. Weselake, "Site saturation mutagenesis: Methods and applications in protein engineering," *Biocatalysis and Agricultural Biotechnology,* vol. 1, no. 3, pp. 181-189, 2012/07/01/ 2012, doi: https://doi.org/10.1016/j.bcab.2012.03.010.

Chapter 5 : A Microelectrode Array Microprobe for Electroenzymatic GABA Sensing with an Engineered GABA Oxidase and an On-Probe Iridium Oxide Reference Electrode

ABSTRACT

The integration of an on-probe iridium oxide (IrOx) reference electrode on a microelectrode array (MEA) microprobe with electroenzymatic γ-aminobutyric acid (GABA) sensing sites based on an engineered GABA oxidase enables selective monitoring of GABA levels *in vivo* with response times on the order of ~1 s. Precise detection and quantitation of GABA is critical for studying inhibitory pathways in the central nervous system, with implications for epilepsy, anxiety, and addiction disorders. A post-fabrication electrochemical deposition process allows for the direct integration of an IrOx reference electrode (RE) onto the same MEA as the GABA-sensing working electrode (WE), enhancing stability and reducing noise compared to external Ag/AgCl REs, which are prone to instability and can induce inflammatory responses *in vivo*. The engineered GABA oxidase, immobilized on the MEA, facilitates the electroenzymatic oxidation of GABA, generating hydrogen peroxide as a byproduct, which in turn is electrooxidized thereby generating a current signal detectable using constant potential amperometry (CPA). This IrOx-referenced GABA sensor demonstrates a sensitivity of 247 ± 41 nA/mM·cm^2 and limit of detection of 80 ± 21 μM. The rms noise of 0.00048 nA was similar to that of implantable microelectrode array dopamine sensing devices. Furthermore, permselective films on the WE inhibit interference from common electroactive species while the engineered GABA oxidase is selective for GABA, thereby providing a highly selective tool for GABA measurement in the

physiological milieu. The on-probe IrOx RE and high selectivity make this GABA sensor suitable for neurochemical studies *in vivo*, supporting the development of targeted therapies and interventions in neuropsychiatric disorders.

5.1 Introduction

γ-Aminobutyric acid (GABA) serves as the principal inhibitory neurotransmitter within the mammalian central nervous system (CNS) [1, 2], playing an indispensable role in regulating neuronal excitability, balancing excitatory input, and maintaining network stability. Disruptions in GABAergic signaling pathways are closely associated with a range of CNS disorders [3], including epilepsy, anxiety disorders, depression, and substance addiction [4]. Monitoring fluctuations in GABA levels within specific brain regions could thus provide critical insights into the pathophysiology of these conditions [5], ultimately aiding in the development of therapeutic interventions. However, existing electrochemical detection methods present substantial challenges inhibiting the sensitive and selective detection of GABA *in vivo*, primarily due to GABA's non-electroactive nature [6]. Among the electrochemical techniques available for neurotransmitter sensing, fast-scan cyclic voltammetry (FSCV) and constant potential amperometry (CPA) have proven highly effective for monitoring electroactive neurotransmitters like dopamine [7]. However, use of FSCV requires application to electroactive analytes. In contrast, CPA is both a simpler and potentially faster technique, suitable for continuous real-time monitoring. However, CPA-based neurotransmitter sensors require the application of permselective polymer coatings to exclude electroactive interfering species [8-13] and the electrochemical coupling of an analyte-specific enzyme (*e.g.*, an oxidase) to the electrode for detection of non-electroactive analytes like GABA.

Existing multi-step GABA sensors rely on enzymatic conversion of GABA into secondary metabolites, such as succinic semialdehyde or glutamate, which are subsequently detected via electrochemical oxidation [14]. However, these approaches are inherently limited by the presence of pre-existing physiological concentrations of these metabolites in the extracellular environment, which compromises accuracy and prevents reliable detection of transient GABA fluctuations [6]. These considerations have motivated the development of an enzyme-based, electrochemical GABA sensor to enable effective monitoring of GABA dynamics in the brain [15]. Among potential enzymes, methylaminobutyrate oxidase (MABO) emerged as a promising foundation for sensor development due to its structural and functional compatibility with GABA oxidation. The native form of MABO exhibits moderate catalytic activity toward GABA, as detailed in earlier studies [16]. However, directed evolution was employed to enhance its substrate specificity and affinity for GABA [17], resulting in an optimized variant with significantly improved performance metrics (Chapter 4). This engineered MABO, hereafter referred to as GABAOx, was adapted for integration into the electrochemical sensor platform described in this chapter.

The reaction catalyzed by GABAOx forms the basis of the electroenzymatic GABA sensor, where the production of hydrogen peroxide (H_2O_2) enables downstream electrooxidation at the underlying electrode.

$$\text{GABA} + H_2O + O_2 \longrightarrow NH_3 + H_2O_2 + \text{Succinic Semialdehyde}$$

The resulting current signal directly correlates with the concentration of GABA in the surrounding microenvironment. This electroenzymatic approach was implemented using silicon-based platinum microelectrode array (MEA) microprobes, leveraging advanced micro-electro-mechanical-systems (MEMS) fabrication technology to create a robust platform for neurotransmitter sensing. MEAs have been widely used for neurotransmitter detection due to their

precise microfabrication capabilities, compatibility with enzyme immobilization techniques, and proven performance *in vivo* [18-20]. This electroenzymatic approach has been extensively validated for the detection of non-electroactive analytes, including glucose [21], lactate [22], glutamate [9], and choline [10], providing a robust precedent for the detection of GABA using the engineered MABO variant.

To achieve high selectivity in the complex chemical milieu of brain extracellular fluid (ECF), the MEA-based electrochemical sensors are further modified with permselective polymer coatings. Nafion, a perfluorinated sulfonate polymer with anionic properties, was applied to selectively repel negatively charged interferents [23-25] such as ascorbic acid (AA) and uric acid (UA), which are present in high concentrations in the ECF and would otherwise interfere with the sensor response. m-PPD was electrodeposited onto the sensor surface as a thin film to act as a size-exclusion filter, selectively impeding the access of electroactive molecules larger than H_2O_2 (Fig. 5.1). Permselective coatings like m-PPD play a critical role in ensuring sensor selectivity by rejecting interfering species [26] while facilitating the efficient transport of the target analyte's electroactive byproducts. In this work, m-PPD was chosen for its demonstrated efficacy in electroenzymatic sensor applications [27-29], particularly for rejecting interferents such as dopamine (DA) and ascorbic acid (AA), which are prevalent in brain extracellular fluid at physiologically relevant concentrations.

The use of m-PPD also allowed for the deposition of thinner secondary coatings, such as Nafion, without compromising the rejection of interfering species. Previous studies have shown that this combination improves H_2O_2 sensitivity by reducing diffusion resistance [9]. Compared to overoxidized polypyrrole (OPP) [30], another commonly employed permselective film, m-PPD offers superior transport properties, enhancing sensor sensitivity and response time. These

attributes make m-PPD an optimal choice for the GABA sensor, aligning with the platform's dual objectives of high selectivity and sensitivity.

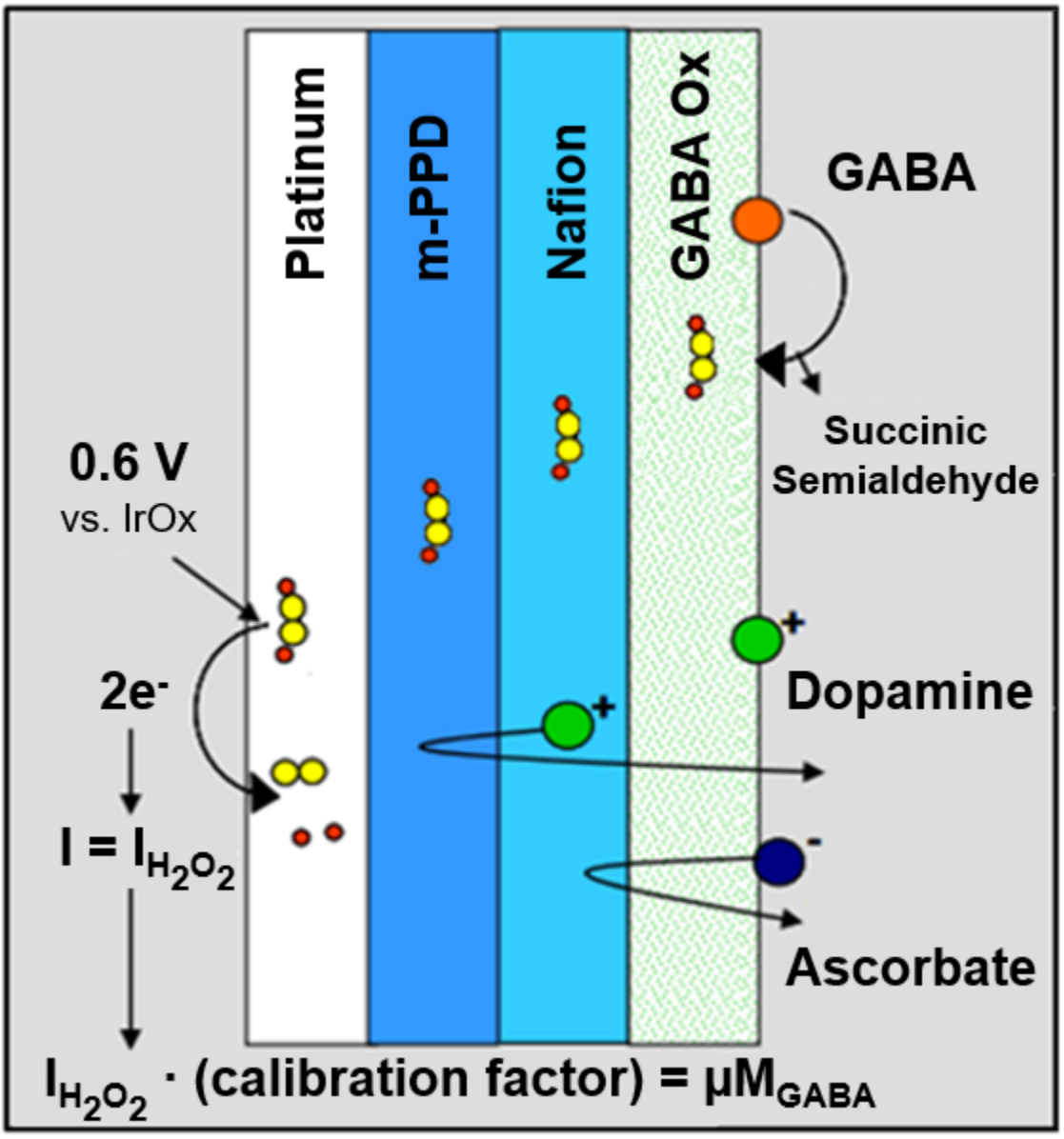

Figure 5.1 Cross-sectional schematic of the GABA sensing working electrode surface. The permselective Nafion and m-PPD coatings ensure that only the H_2O_2 electroactive byproduct of GABA oxidation reaches the platinum working electrode surface.

An iridium oxide (IrOx) reference electrode (RE) was integrated directly onto the MEA probe to address the limitations inherent in conventional Ag/AgCl REs, which are prone to instability [31] and can provoke inflammatory responses in tissue [32]. IrOx offers numerous advantages as a quasi-reference electrode material [33-35], including excellent stability, mechanical robustness, and biocompatibility. Although the steady-state potential of IrOx displays modest pH dependence [36], the small dynamic range of physiological pH (7.15–7.4 in brain ECF) ensures a nearly invariant reference potential under test conditions. By replacing the external Ag/AgCl RE with an integrated IrOx electrode, the electrochemical performance of MEA-based sensors is significantly enhanced, with improvements in baseline stability and reduced noise (Chapter 2).

The present study describes the adaptation of the MEA-based neurotransmitter detection platform to selective GABA detection using GABA oxidase as the biorecognition element. The aim of this work is to establish an implantable GABA sensor with high sensitivity, selectivity, and stability suitable for the real-time monitoring of GABA transients *in vivo*. The design leverages the advantages of the IrOx reference electrode and advanced permselective polymer coatings to address the complex demands of neurotransmitter sensing *in vivo*. This GABA sensor represents a significant step forward in neurochemical sensing technologies, offering a new tool for investigating inhibitory neurotransmission and its role in CNS disorders. Through the combination of MEMS-fabricated MEAs, enzyme-based detection, and IrOx reference integration, this platform paves the way for further advancements for the *in vivo* analysis of complex neurotransmitter systems.

5.2 Materials and Methods

5.2.1 Reagents and Equipment

Nafion (5 wt% solution in lower aliphatic alcohols/H_2O mix), m-phenylenediamine (99%), 3-hydroxytyramine (dopamine, DA), L-3,4-dihydroxyphenylalanine (L-DOPA), 3,4-dihydroxyphenylacetic acid (DOPAC), L -ascorbic acid (AA), uric acid (UA), iridium tetrachloride hydrate, anhydrous oxalic acid (99%), hydrogen peroxide (30 wt% solution in water), anhydrous potassium carbonate, and γ-aminobutyric acid (GABA) were purchased from Sigma (Milwaukee, WI, USA). Solutions of all neurotransmitters, metabolites, and interferents were formulated in phosphate buffered saline (PBS). PBS buffer consisted of 50 mM dibasic sodium phosphate with 100 mM sodium chloride adjusted to pH 7.4 with concentrated HCl. A Millipore Milli-Q Water System was used to generate ultrapure water for the preparation of all solutions used. Enzyme kinetics and absorbance-based measurements were performed using the MAK166 Fluorometric Hydrogen Peroxide Assay Kit (Sigma Aldrich, St. Louis, MO, USA) in a Tecan Infinite M1000 plate reader (Tecan Group Ltd., Männedorf, Switzerland). Electrochemical preparations and calibration measurements were performed using a Versatile Multichannel Potentiostat equipped with the 'p' low current option and low current N'Stat box (VMP3, Bio-Logic USA LLC, Knoxville, TN, USA). GABA oxidase and its variants were purified as per the protocols in Appendix I.

5.2.2 Microelectrode Array Fabrication and Polymer Modification

Microelectrode arrays (MEAs) were fabricated on silicon probes in the UCLA Nanofabrication Laboratory (NanoLab) using MEMS technologies. The fabrication and array

details are described in previous work [20]. The probe shafts were 150 µm thick, 140 µm wide, and 9 mm long with four 6000 µm^2 (40 µm × 150 µm) Pt microelectrode sites arranged in pairs at the tip (Fig. 5.2). Each site was cleaned in 0.1 M H_2SO_4 solution by cycling the potential between -0.2 V and 1.5 V (vs. Ag/AgCl) at least 10× at a scan rate of 50 mV/s and rinsing in PBS. Subsequently, the microelectrodes were modified as needed to serve as working electrodes (WEs), reference electrodes (REs), or counter electrodes (CEs).

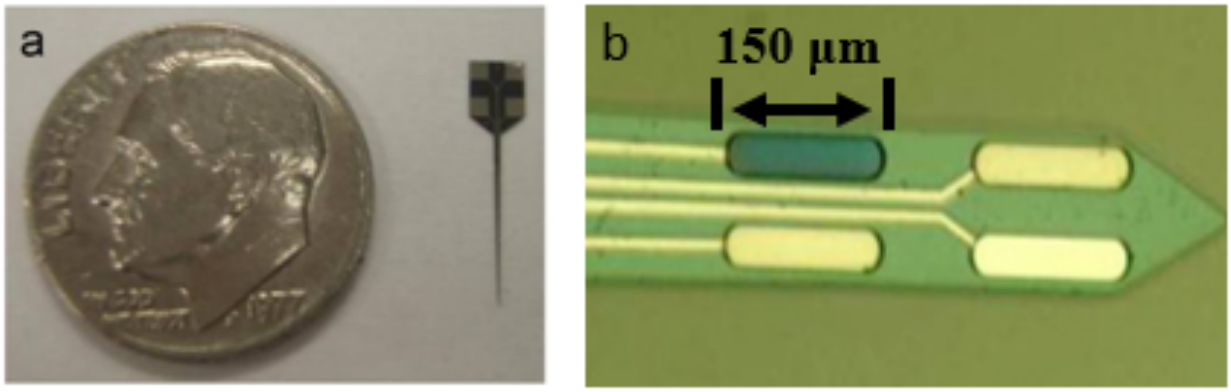

Figure 5.2 (a) A MEA probe with a 9 mm shank. (b) Four Pt microelectrode sites at the tip of a probe, each 6000 µm^2 in area. The dark site on the upper left was modified previously with electrodeposited IrOx to give an on-probe RE.

Iridium oxide (IrOx) was electrodeposited to prepare REs following the method of Yamanaka [37]. Briefly, a 20 mL aqueous solution of 4.5 mM iridium tetrachloride was stirred for 30 min followed by the addition of 200 µL of hydrogen peroxide and stirring for an additional 10 min. Oxalic acid dihydrate was then added to reach a concentration of 55.5 mM and stirred for another 10 min. Potassium carbonate was added in small aliquots until the solution reached a pH of 10.5. The resulting solution was allowed to sit quiescently for at least 48 h before electrodeposition, during which time the color shifted from yellow to purple. IrOx was deposited

anodically on an electrode site by cycling between 0.0 V and 0.6 V versus Ag/AgCl at a scan rate of 50 mV/s for 100 cycles resulting in a total charge transfer of ~1 C/cm^2. An image of the Pt microelectrode after electrodeposition of IrOx is shown in Fig. 5.2b.

After RE creation, an m-PPD film was electrodeposited on designated WEs from a 5 mM m-phenylenediamine solution in PBS by holding the voltage constant at 0.85 V vs. Ag/AgCl until the total charge transferred reached 7.2 x 10^{-7} Coulombs. Given the total of four microelectrode sites available, up to three could be used as WEs for redundant measurements. Nafion was deposited on all sites by dip-coating the probe tips into a 2% Nafion solution (diluted from 5% stock in 4:1 IPA:water solution) and immediately annealing at 115 °C for 20 minutes. The sensors were sealed in a container with desiccant and stored dry at 4 °C prior to further modification. A schematic of the final cross-sectional structures of the WE, RE, and CE sites is provided as Fig. 5.3.

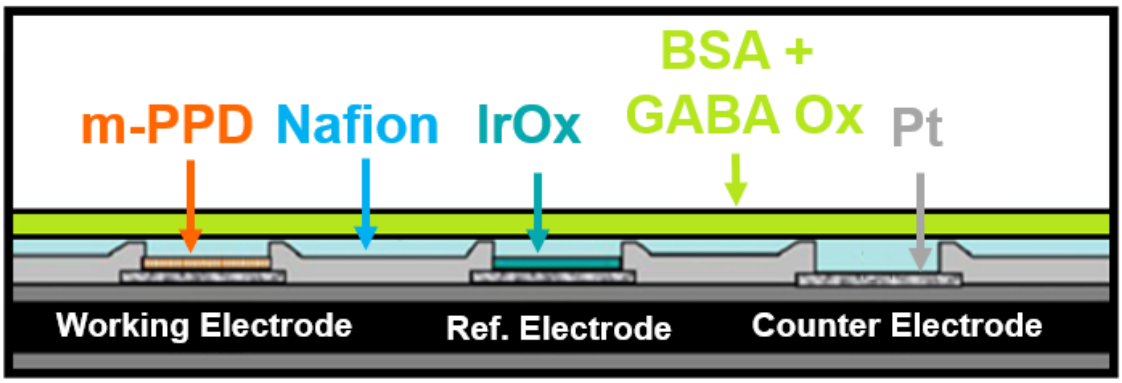

Figure 5.3 Representative cross-section of a multielectrode device (not to scale) for GABA biosensing showing the Pt microelectrode modifications to differentiate the WE, RE, and CE sites.

5.2.3 Enzyme Immobilization for Selective GABA Detection

Sensors for selective detection of GABA were achieved by immobilizing GABA oxidase (GABA Ox) onto the modified WEs through a controlled glutaraldehyde (GAH) vapor-mediated crosslinking protocol (Appendix L), designed to maintain enzymatic activity and stability. A phosphate-buffered saline (PBS) solution containing GABA Ox and bovine serum albumin (BSA) was applied to each microelectrode. The MABO enzyme mass fraction (f_{MABO}) in the enzyme layer relative to BSA was varied from 0.02 to 0.95 to optimize the balance between sensitivity and layer stability. After application, the enzyme layer was exposed to 5% GAH vapor for 1 minute to covalently crosslink the enzyme's amine groups to the electrode surface. After crosslinking, sensors were stored under desiccated conditions at 4 °C for 48 hours to further enhance enzyme adhesion and to ensure long-term stability. This immobilization strategy yields a robust enzyme layer suitable for consistent, accurate, and selective GABA detection.

5.3 Sensor Calibration and Testing

The sensors were tested in three-electrode configurations with the VMP3 potentiostat. The CE consisted of an on-probe, Nafion-coated Pt site. GABA sensor calibration and testing were conducted in a magnetically stirred 30 mL beaker in a Faraday cage. A potential of 0.6 V was applied to the GABA sensors relative to the on-probe IrOx REs, which corresponds to ~0.7 V vs. Ag/AgCl. The sensors were allowed to equilibrate until they achieved a steady-state current. First, interferents (AA, L-DOPA, DOPAC, EP, NEP, UA, and DA) were injected sequentially to assess the selectivity of the probes. Next, aliquots of GABA solutions were sequentially injected into the bulk solution. The steady-state current signals were recorded and plotted as a function of the bulk

analyte concentration to generate calibration curves. Sensitivities were determined from the slopes of the linear portions of the curves.

Noise measurement, filtering, and analysis were performed once the sensors achieved a steady-state, baseline current using the built-in noise analysis tools of the BioLogic EC-lab software. Noise was analyzed by first applying a Fourier transform to the baseline current data. Ultralow noise frequency bands were removed using the frequency filter tool. The remaining noise in the filtered, steady-state, baseline current was quantified using the electrochemical corrosion tool of the software. This calculated rms noise was used subsequently in limit-of-detection (LOD) computations. The LOD was defined as the current change corresponding to 3× filtered rms noise. All sensitivity and LOD uncertainties in this work are reported as standard errors.

5.4 Results and Discussion

5.4.1 Optimization of GABA Oxidase Enzyme Mass Fraction

Initial validation of the GABA sensing platform was conducted using the native enzyme (MABO, PDB: 7RT0) immobilized on a platinum (Pt) working electrode (WE) within a three-electrode configuration on a microelectrode array (MEA). The system included an on-probe IrOx RE and a bare Pt CE, allowing assessment of the electroenzymatic response to GABA using constant potential amperometry (CPA).

The performance of GABA sensors was evaluated across a range of native MABO enzyme mass fractions (f_{MABO}) to optimize the balance between sensitivity and enzyme layer stability. By varying the proportion MABO to bovine serum albumin (BSA), the impact of enzyme

concentration on sensor performance was assessed. Figure 5.4 illustrates the relationship between f_{MABO} and GABA sensitivity, highlighting a peak in performance at $f_{MABO} \approx 0.35$.

At lower enzyme mass fractions ($f_{MABO} < 0.35$), sensitivity was limited due to insufficient enzyme coverage on the electrode surface, reducing the conversion of GABA. Conversely, higher enzyme mass fractions ($f_{MABO} > 0.35$) also resulted in diminished sensitivity and stability. This phenomenon aligns with prior studies [9], which have suggested that an optimal balance between enzyme and crosslinking agent is critical for sensor performance. Specifically, while higher enzyme mass fractions can theoretically increase catalytic capacity, insufficient BSA at elevated f_{MABO} may lead to poor crosslinking due to the relatively low number of lysine residues on the enzyme [38]. This can result in unstable enzyme layers that are prone to delamination. Additionally, excessive enzyme concentration could hinder substrate diffusion and reduce accessibility to active sites [39], negatively impacting reaction efficiency. Based on these observations, $f_{MABO} \approx 0.35$ was identified as the optimal enzyme mass fraction, balancing sufficient enzymatic activity with layer stability to achieve reliable and sensitive GABA detection. This mass fraction of enzyme was used as the target level in subsequent studies with the engineered GABA oxidase.

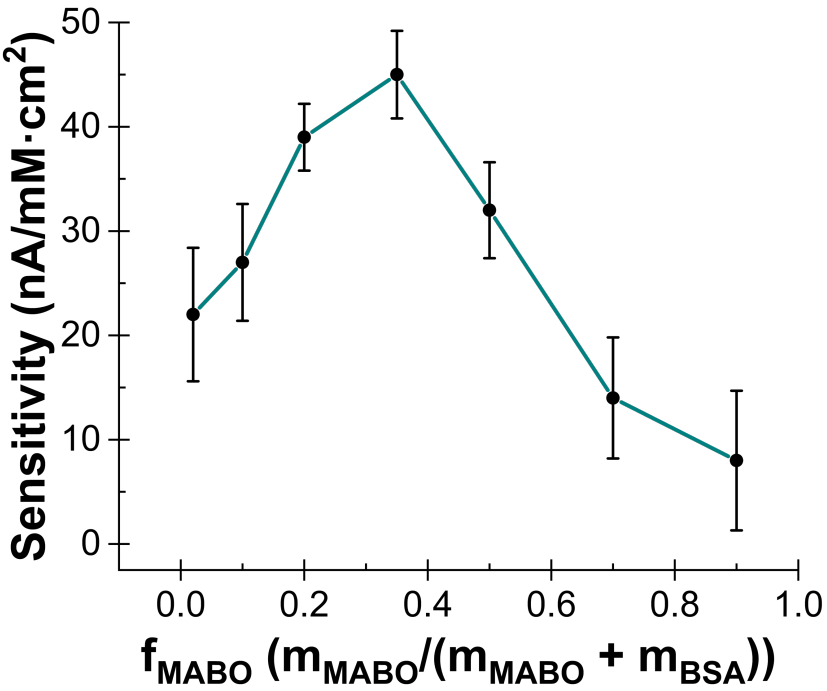

Figure 5.4 Effect of MABO surface concentration relative to BSA on GABA sensitivity, where f_{MABO} was varied from 0.02 to 0.90. Error bars correspond to standard errors for $n = 3$ at each level of enzyme mass fraction (f_{MABO}). The enzyme layer thickness was not directly measured but is inferred to be similar to that achieved in prior work with glutamate oxidase, where coatings were consistently under 5 μm, given the comparable immobilization protocol and substrate properties.

Interestingly, the optimal enzyme mass fraction ($f_{MABO} \approx 0.35$) is slightly lower than the ~0.4 value reported for glutamate oxidase-based sensors in previous work [9]. While the overall trends are comparable, the subtle difference likely reflects the unique surface chemistries and kinetic properties of MABO relative to glutamate oxidase. These properties, including differences in the density and availability of surface lysine residues for crosslinking, affect the enzyme layer's structural configuration and substrate accessibility.

This optimization demonstrates the importance of tailoring enzyme mass fractions to the specific biochemical characteristics of the immobilized enzyme, achieving significant improvements in sensitivity and layer stability while accounting for enzyme-specific factors. Sensors prepared at the optimal f_{MABO} exhibited robust performance during repeated calibrations and extended testing, underscoring the utility of these conditions for practical sensor applications.

5.4.2 Optimized GABA Sensing with Native MABO

The native enzyme-coated sensors were tested at an applied potential of 0.6 V vs. IrOx (~0.7 V vs. Ag/AgCl), where they demonstrated a linear response to GABA concentrations up to 150 mM (Fig. 5.5b), with a sensitivity of 45 ± 6 nA/(mM·cm²) and a limit of detection (LoD) of 491 ± 82 μM (n = 10 WEs). Additionally, the rms noise was calculated to be approximately 0.00048 nA, which is comparable to what was observed in non-enzymatic dopamine probes. However, this configuration was fundamentally constrained by the native enzyme's elevated K_M for GABA (3100 ± 160 mM), reflecting the enzyme's higher affinity for its native substrate, methyl-GABA, rather than GABA itself. As a result, the baseline performance, while indicative of functional detection capability, did not yet align with the lower GABA concentration ranges typical of brain extracellular fluid [40]. These preliminary metrics thus provided a crucial reference point, highlighting the need for strategic enzyme modifications to lower K_M (see chapter 4) and enhance sensor sensitivity under physiological conditions. The following section explores the protein engineering approaches undertaken to refine this sensor's performance, aiming to meet the demands of *in vivo* applications with improved affinity and detection sensitivity for GABA.

5.4.3 Enhanced GABA Sensing with Engineered GABA Oxidases

Sensors constructed with engineered GABA oxidase variants, notably the A58G/I393T double mutant, exhibited substantial improvements in sensitivity and detection limits compared to the native enzyme. The optimized sensors achieved a sensitivity of 247 ± 41 nA/(mM·cm²) and a limit of detection of 80 ± 21 μM. While this limit of detection remains above the widely accepted extracellular GABA concentration range of 0.1–10 μM, the evolved enzyme exhibits kinetic parameters that suggest potential applicability in detecting transient, localized spikes of GABA at the highest end of the physiological range [41-43], such as those occurring immediately after synaptic release and spillover. Importantly, this represents a significant advancement over the inability to detect GABA at all using chronoamperometric approaches. Additionally, the rms noise for these probes was unchanged when compared to the formulation with the native enzyme. This performance enhancement underscores the success of our protein engineering approach, which was focused on reducing the K_M for GABA, thus increasing affinity and catalytic efficiency. Notably, other variants also demonstrated improved enzyme activity and sensor performance (Fig. 5.5), further supporting the robustness of our directed evolution workflow.

Enzyme Variant	**Native**	**A58Y**	**A58G**	**A58G/I393T**
K_M (mM)	3100 ± 160	570 ± 71	160 ± 54	95 ± 43
Sensitivity (nA/mM·cm²)	45 ± 6	114 ± 20	162 ± 25	247 ± 41
Limit of Detection (μM)	491 ± 82	173 ± 91	122 ± 54	80 ± 21

Table 5.1 Summary of GABA sensor performance with different enzyme variants. The corresponding calibration plots are shown in Fig. 5.5. The reported uncertainties correspond to standard errors with $n = 8$.

These improvements in the immobilized enzyme's kinetic parameters represent a critical step toward developing a sensor capable of detecting extracellular GABA fluctuations, even though the current design remains limited to detecting concentrations at the extreme upper end of the physiological range. Thus, the optimized MABO-variant sensors provide enhanced fidelity in capturing GABA dynamics, with response times anticipated to be comparable to the ~1 s timescales demonstrated in similar electroenzymatic probes developed by our lab. However, additional rounds of mutagenesis, building upon the work described in Chapter 4, will be necessary to enhance the performance of these probes to a level suitable for detecting transient extracellular GABA concentrations.

5.4.5 Calibration Curves

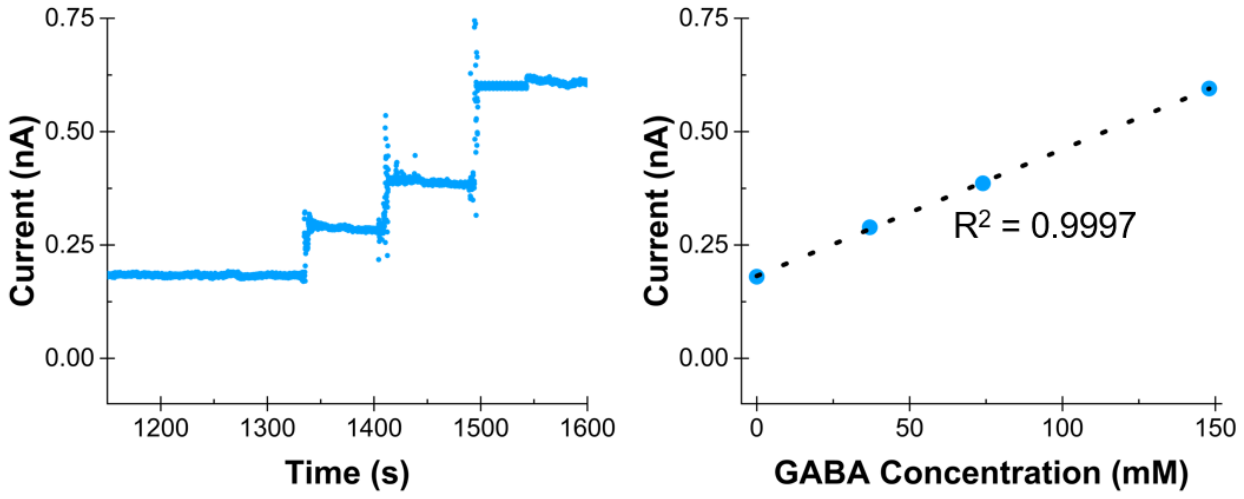

Figure 5.5 Crude GABA sensing on a representative MEA working electrode site in a three-electrode configuration using an on-probe IrOx RE and an on-probe bare Pt microelectrode as CE. Native MABO is immobilized to the electrode surface. The first two GABA injections correspond to bulk concentration increases to 37 mM, 74 mM, and 148 mM, which are well above relevant physiological concentrations.

B) Calibrations plots are made by creating linear regressions (R^2 = 0.9997) of the steady state current data (shown in A) versus the bulk GABA concentration. GABA sensing systems of this on-probe, three-electrode configuration showed an average sensitivity and limit of detection of 45 ± 6 nA/(mM·cm^2) and 491 ± 82 µM (*n* = 8 working electrodes), respectively.

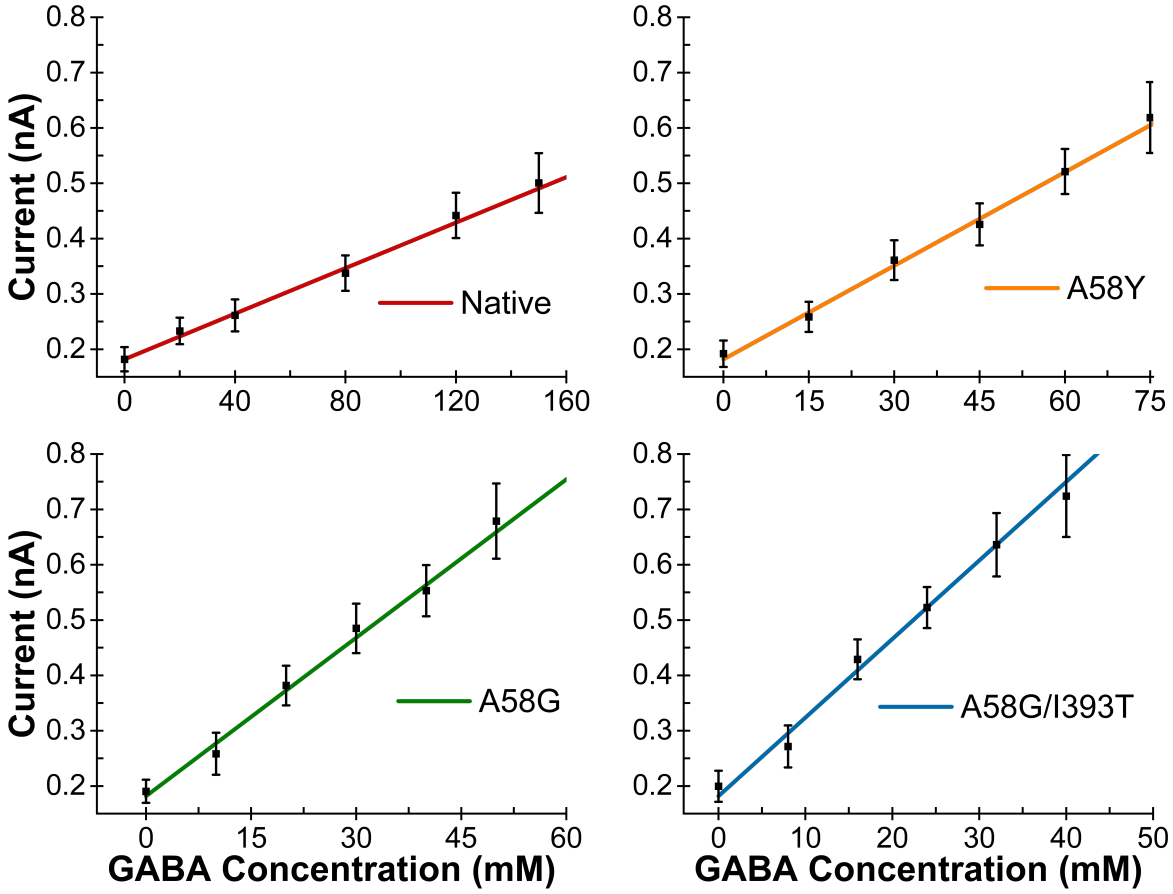

Figure 5.6 Calibration curves showing amperometric response of GABA sensors with various generations of immobilized GABA oxidase enzymes. R^2 > 0.995 for all sensors. Steeper slopes reflect enhanced sensitivity achieved through progressive, favorable enzyme mutations. Accumulating beneficial mutations was correlated with improved kinetic parameters and thus increased sensitivity (Table 5.1). The concentrations of the injected GABA solutions vary in order The superimposition of these calibrations is shown in Fig. 5.7.

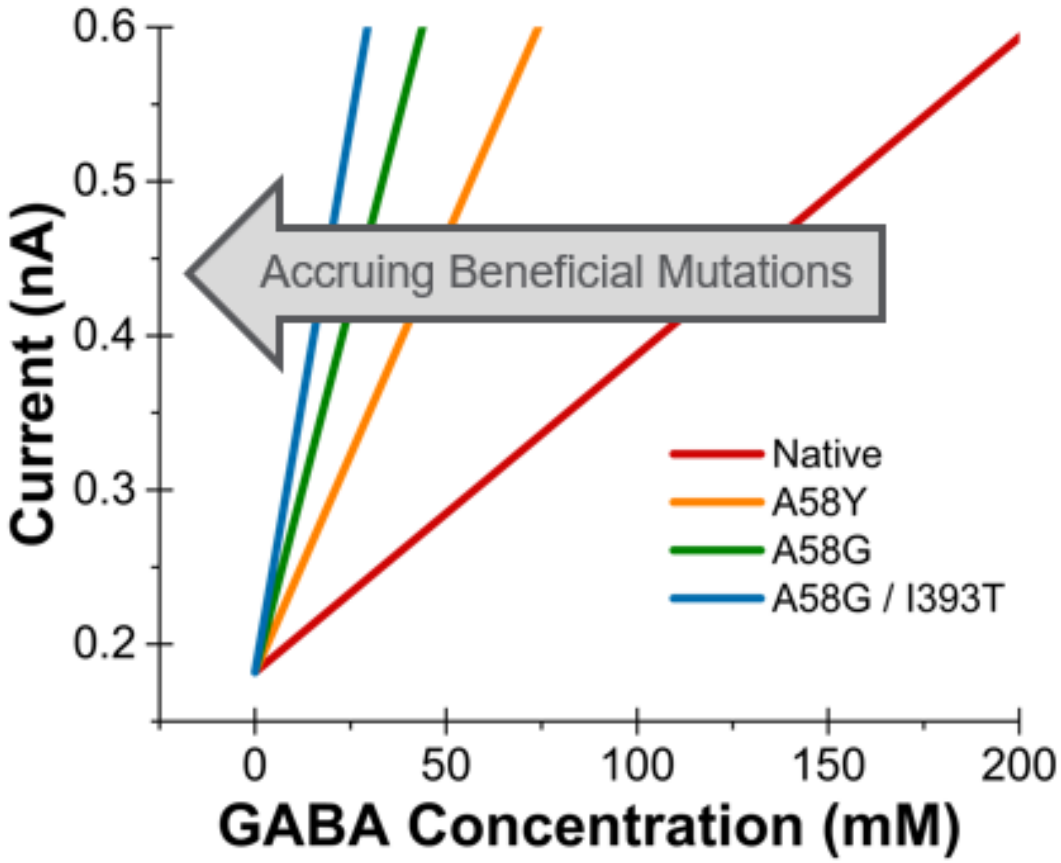

Figure 5.7 Superimposition of calibration curves (Fig. 5.6) showing amperometric response of GABA sensors. As GABA oxidase accrues favorable mutations, its kinetic parameters improve (Table 5.1). As a result, the sensitivities of MEA probes made with the immobilized enzyme also improve. Sensitivity and limit of detection are inversely related; thus, the limit of detection also improves with increased accumulation of beneficial mutations.

5.4.6 Selectivity Against Common Electroactive Interferents

Selective detection of GABA is critical for biosensors operating in the complex environment of brain extracellular fluid, where a variety of electroactive species could potentially interfere with the target signal. In this work, selectivity was quantitatively defined as the ratio of sensor sensitivity to GABA relative to its sensitivity to each interferent. The GABA microsensors,

configured in a three-electrode system, exhibited outstanding selectivity against a range of commonly encountered electroactive interferents, including ascorbic acid (AA), dopamine (DA), 3,4-dihydroxyphenylacetic acid (DOPAC), L-3,4-dihydroxyphenylalanine (L-DOPA), uric acid (UA), and glutamate, even at concentrations exceeding their physiological levels. The selectivity ratios for GABA relative to these interferents consistently surpassed 1000:1, confirming the biosensor's specificity and robustness for accurate GABA detection in brain extracellular fluid (Fig. 5.7).

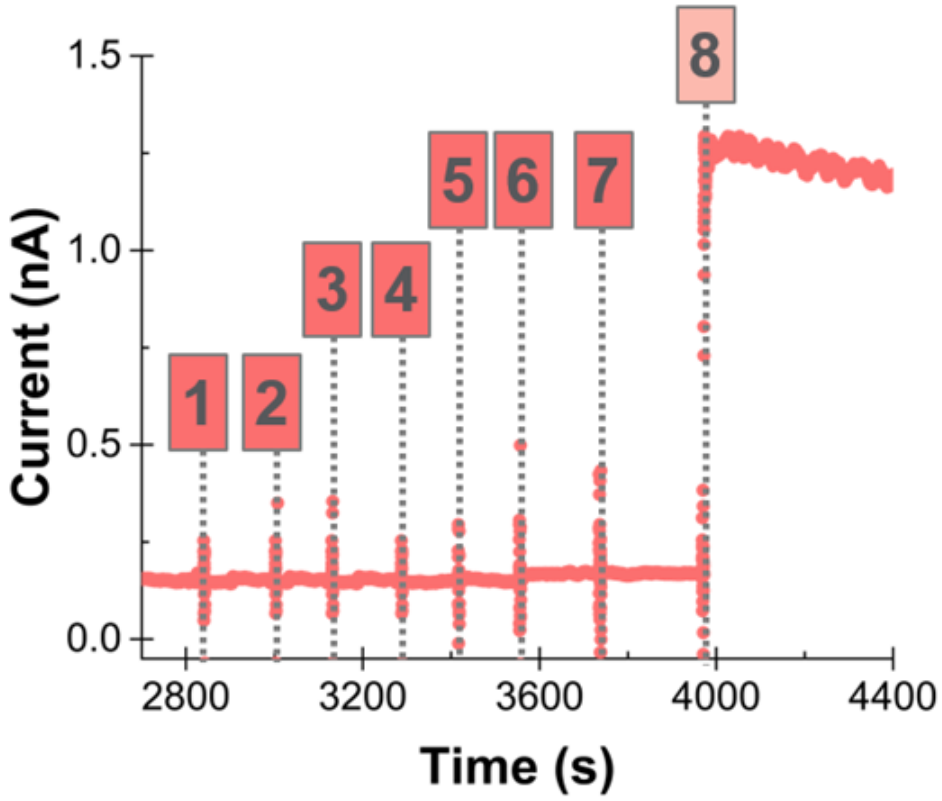

Figure 5.8 Selectivity profile of the GABA biosensor against common electroactive interferents in brain extracellular fluid: [1] 125 µM ascorbic acid (AA), [2] 50 µM L-3,4-dihydroxyphenylalanine (L-DOPA), [3] 50 µM 3,4-dihydroxyphenylacetic acid (DOPAC), [4] 12.5 µM epinephrine (EP), [5] 12.5 µM norepinephrine (NEP), [6] 50 µM uric acid (UA), and [7] 10 µM dopamine (DA), compared to [8] 400 mM GABA.

The selectivity of the engineered GABA oxidase was rigorously evaluated against all canonical amino acids using the MAK166 fluorometric hydrogen peroxide assay in a 96-well plate format. Fluorescence intensity was recorded over time with a Tecan Infinite M1000 (Tecan Group Ltd., Männedorf, Switzerland) plate reader. The enzyme exhibited robust activity only for GABA and methyl-GABA, while all other amino acids, including glutamate, showed fluorescence signals below that of the negative control (a PBS-only solution). This lack of activity for non-target substrates underscores the enzyme's high specificity. The representative plot (Fig. 5.8) highlights the activity curves for GABA and methyl-GABA, showing steep, time-dependent increases in fluorescence, while all other amino acids remained below the control threshold. These findings validate the enzyme's suitability for selective GABA detection in complex environments.

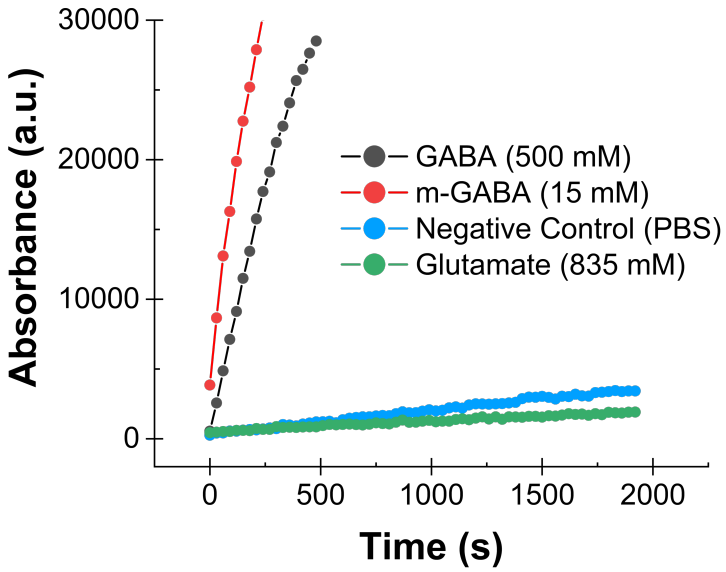

Figure 5.9 Representative fluorescence-based assay results for GABA oxidase activity. Activity curves for GABA and methyl-GABA show strong, time-dependent increases in fluorescence intensity. All other canonical amino acids exhibited fluorescence signals below the negative control. For clarity, only glutamate is shown.

5.5 Conclusions

This chapter presents the first one-step electroenzymatic sensor for the selective detection of γ-aminobutyric acid (GABA), utilizing an evolved methylaminobutyrate oxidase (MABO) enzyme to achieve high sensitivity and specificity. GABA, as the principal inhibitory neurotransmitter in the brain, plays a central role in modulating neural function and is implicated in numerous neurological and psychiatric disorders, including epilepsy, anxiety, and mood dysregulation. A sensor capable of monitoring extracellular GABA dynamics provides a powerful tool for advancing both fundamental neuroscience and clinical diagnostics.

The one-step enzymatic approach introduced here directly catalyzes GABA oxidation, producing a hydrogen peroxide byproduct that can be quantified electrochemically. This direct detection mechanism eliminates confounding background signals from secondary metabolites, providing a robust and precise platform for real-time GABA monitoring.

Previous work successfully improved MABO's catalytic properties through directed evolution, enhancing both its substrate affinity and catalytic efficiency for GABA oxidation. In this chapter, both the native and evolved MABO enzymes were employed in the fabrication of electroenzymatic GABA sensors to evaluate their functionality. The evolved MABO variant demonstrated significantly improved performance, including a lower apparent K_M, enabling detection of GABA closer to the extracellular concentration range. These findings underscore the value of protein engineering in adapting enzymes for biosensor applications.

The sensor platform was further enhanced by integrating an on-probe iridium oxide (IrOx) reference electrode, which replaces the conventional external Ag/AgCl reference electrode. The IrOx reference electrode provides superior stability and biocompatibility, addressing key challenges associated with external references, such as excessive noise and inflammatory tissue

responses. This advancement improves signal fidelity and LOD, supporting reliable operation in complex neurochemical environments. While the sensor's response time was not explicitly measured in this work, it is expected to be comparable to other enzymatic biosensors developed in our lab, which typically achieve subsecond response times.

Furthermore, these sensor configurations offer significant versatility for both *in vivo* brain monitoring and microfluidic platforms. This adaptability broadens their potential utility across diverse experimental setups, from lab-on-a-chip systems to implanted probes, enabling comprehensive neurochemical analysis in both clinical and research settings. By combining cutting-edge enzyme engineering with advanced microelectrode array design, this work establishes a transformative approach to neurotransmitter sensing based on engineered enzymes, setting a new standard for GABA detection and demonstrating the far-reaching potential of directed evolution in biosensor development.

5.6 References

[1] O. A. Petroff, "GABA and glutamate in the human brain," (in eng), *Neuroscientist,* vol. 8, no. 6, pp. 562-73, Dec 2002, doi: 10.1177/1073858402238515.

[2] E. Cherubini and F. Conti, "Generating diversity at GABAergic synapses," (in eng), *Trends Neurosci,* vol. 24, no. 3, pp. 155-62, Mar 2001, doi: 10.1016/s0166-2236(00)01724-0.

[3] M. Watanabe, K. Maemura, K. Kanbara, T. Tamayama, and H. Hayasaki, "GABA and GABA receptors in the central nervous system and other organs," (in eng), *Int Rev Cytol,* vol. 213, pp. 1-47, 2002, doi: 10.1016/s0074-7696(02)13011-7.

[4] A. Schousboe and H. S. Waagepetersen, "GABA: homeostatic and pharmacological aspects," (in eng), *Prog Brain Res,* vol. 160, pp. 9-19, 2007, doi: 10.1016/s0079-6123(06)60002-2.

[5] C. D. Rae, "A guide to the metabolic pathways and function of metabolites observed in human brain 1H magnetic resonance spectra," (in eng), *Neurochem Res,* vol. 39, no. 1, pp. 1-36, Jan 2014, doi: 10.1007/s11064-013-1199-5.

[6] J. J. Burmeister and G. A. Gerhardt, "Self-referencing ceramic-based multisite microelectrodes for the detection and elimination of interferences from the measurement of L-glutamate and other analytes," (in eng), *Anal Chem,* vol. 73, no. 5, pp. 1037-42, Mar 1 2001, doi: 10.1021/ac0010429.

[7] B. J. Venton and Q. Cao, "Fundamentals of fast-scan cyclic voltammetry for dopamine detection," *Analyst,* 10.1039/C9AN01586H vol. 145, no. 4, pp. 1158-1168, 2020, doi: 10.1039/C9AN01586H.

[8] K. N. Han, C. A. Li, and G. H. Seong, "Microfluidic Chips for Immunoassays," *Annual Review of Analytical Chemistry,* vol. 6, no. Volume 6, 2013, pp. 119-141, 2013, doi: https://doi.org/10.1146/annurev-anchem-062012-092616.

[9] I. w. Huang, M. Clay, S. Wang, Y. Guo, J. Nie, and H. G. Monbouquette, "Electroenzymatic glutamate sensing at near the theoretical performance limit," *Analyst,* 10.1039/C9AN01969C vol. 145, no. 7, pp. 2602-2611, 2020, doi: 10.1039/C9AN01969C.

[10] I. w. Huang, M. Clay, Y. Cao, J. Nie, Y. Guo, and H. G. Monbouquette, "Electroenzymatic choline sensing at near the theoretical performance limit," *Analyst,* 10.1039/D0AN01939A vol. 146, no. 3, pp. 1040-1047, 2021, doi: 10.1039/D0AN01939A.

[11] T. T. Tseng and H. G. Monbouquette, "Implantable Microprobe with Arrayed Microsensors for Combined Amperometric Monitoring of the Neurotransmitters, Glutamate and Dopamine," (in eng), *J Electroanal Chem (Lausanne),* vol. 682, pp. 141-146, Aug 15 2012, doi: 10.1016/j.jelechem.2012.07.014.

[12] M. Malvaez *et al.*, "Basolateral amygdala rapid glutamate release encodes an outcome-specific representation vital for reward-predictive cues to selectively invigorate reward-seeking actions," *Scientific Reports,* vol. 5, no. 1, p. 12511, 2015/07/27 2015, doi: 10.1038/srep12511.

[13] G. S. Wilson and R. Gifford, "Biosensors for real-time in vivo measurements," (in eng), *Biosens Bioelectron,* vol. 20, no. 12, pp. 2388-403, Jun 15 2005, doi: 10.1016/j.bios.2004.12.003.

[14] B. E. Nielsen, S. Stabile, C. Vitale, and C. Bouzat, "Design, Synthesis, and Functional Evaluation of a Novel Series of Phosphonate-Functionalized 1,2,3-Triazoles as Positive Allosteric Modulators of α7 Nicotinic Acetylcholine Receptors," *ACS Chemical Neuroscience,* vol. 11, no. 17, pp. 2688-2704, 2020/09/02 2020, doi: 10.1021/acschemneuro.0c00348.

[15] E. Castagnola *et al.*, "Implantable flexible multielectrode arrays for multi-site sensing of serotonin tonic levels," (in eng), *bioRxiv,* Jan 20 2023, doi: 10.1101/2023.01.17.524488.

[16] C. B. Chiribau, C. Sandu, M. Fraaije, E. Schiltz, and R. Brandsch, "A novel γ-N-methylaminobutyrate demethylating oxidase involved in catabolism of the tobacco alkaloid nicotine by Arthrobacter nicotinovorans pAO1," *European Journal of Biochemistry,* vol. 271, no. 23-24, pp. 4677-4684, 2004, doi: https://doi.org/10.1111/j.1432-1033.2004.04432.x.

[17] F. H. Arnold, "Directed Evolution: Bringing New Chemistry to Life," *Angewandte Chemie International Edition,* vol. 57, no. 16, pp. 4143-4148, 2018, doi: https://doi.org/10.1002/anie.201708408.

[18] D. L. Robinson, B. J. Venton, M. L. Heien, and R. M. Wightman, "Detecting subsecond dopamine release with fast-scan cyclic voltammetry in vivo," (in eng), *Clin Chem,* vol. 49, no. 10, pp. 1763-73, Oct 2003, doi: 10.1373/49.10.1763.

[19] M. P. Martres, P. Sokoloff, B. Giros, and J. C. Schwartz, "Effects of Dopaminergic Transmission Interruption on the D2 Receptor Isoforms in Various Cerebral Tissues," *Journal of Neurochemistry,* vol. 58, no. 2, pp. 673-679, 1992, doi: https://doi.org/10.1111/j.1471-4159.1992.tb09770.x.

[20] K. M. Wassum, V. M. Tolosa, J. Wang, E. Walker, H. G. Monbouquette, and N. T. Maidment, "Silicon Wafer-Based Platinum Microelectrode Array Biosensor for Near Real-Time Measurement of Glutamate in Vivo," *Sensors,* vol. 8, no. 8, pp. 5023-5036, 2008. [Online]. Available: https://www.mdpi.com/1424-8220/8/8/5023.

[21] A. Heller and B. Feldman, "Electrochemical Glucose Sensors and Their Applications in Diabetes Management," *Chemical Reviews,* vol. 108, no. 7, pp. 2482-2505, 2008/07/01 2008, doi: 10.1021/cr068069y.

[22] C. S. Pundir, V. Narwal, and B. Batra, "Determination of lactic acid with special emphasis on biosensing methods: A review," *Biosensors and Bioelectronics,* vol. 86, pp. 777-790, 2016/12/15/ 2016, doi: https://doi.org/10.1016/j.bios.2016.07.076.

[23] N. Wester *et al.*, "Simultaneous Detection of Morphine and Codeine in the Presence of Ascorbic Acid and Uric Acid and in Human Plasma at Nafion Single-Walled Carbon Nanotube Thin-Film Electrode," *ACS Omega,* vol. 4, no. 18, pp. 17726-17734, 2019/10/29 2019, doi: 10.1021/acsomega.9b02147.

[24] M. Zhang, A. Smith, and W. Gorski, "Carbon nanotube-chitosan system for electrochemical sensing based on dehydrogenase enzymes," (in eng), *Anal Chem,* vol. 76, no. 17, pp. 5045-50, Sep 1 2004, doi: 10.1021/ac049519u.

[25] M. Shen and M. L. Colombo, "Electrochemical nanoprobes for the chemical detection of neurotransmitters," *Analytical Methods,* 10.1039/C5AY00512D vol. 7, no. 17, pp. 7095-7105, 2015, doi: 10.1039/C5AY00512D.

[26] S. M. Kirwan *et al.*, "Modifications of Poly(o-phenylenediamine) Permselective Layer on Pt-Ir for Biosensor Application in Neurochemical Monitoring," *Sensors,* vol. 7, no. 4, pp. 420-437, 2007. [Online]. Available: https://www.mdpi.com/1424-8220/7/4/420.

[27] J. P. Bruno *et al.*, "Second-by-second measurement of acetylcholine release in prefrontal cortex," (in eng), *Eur J Neurosci,* vol. 24, no. 10, pp. 2749-57, Nov 2006, doi: 10.1111/j.1460-9568.2006.05176.x.

[28] K. M. Mitchell, "Acetylcholine and choline amperometric enzyme sensors characterized in vitro and in vivo," (in eng), *Anal Chem,* vol. 76, no. 4, pp. 1098-106, Feb 15 2004, doi: 10.1021/ac034757v.

[29] B. Wang, B. Koo, L.-w. Huang, and H. G. Monbouquette, "Microbiosensor fabrication by polydimethylsiloxane stamping for combined sensing of glucose and choline," *Analyst,* 10.1039/C8AN01343H vol. 143, no. 20, pp. 5008-5013, 2018, doi: 10.1039/C8AN01343H.

[30] R. Meng *et al.*, "Overoxidized polypyrrole/overoxidized poly(3,4-ethylenedioxythiophene)/graphene quantum dots-chitosan as enhanced electrochemical sensing platform for luteolin determination in peanut shells," *New Journal of Chemistry,* 10.1039/D2NJ03738F vol. 46, no. 43, pp. 20610-20622, 2022, doi: 10.1039/D2NJ03738F.

[31] H. Yang *et al.*, "An iridium oxide reference electrode for use in microfabricated biosensors and biochips," *Lab on a Chip,* 10.1039/B309899K vol. 4, no. 1, pp. 42-46, 2004, doi: 10.1039/B309899K.

[32] B. T. Seaton and M. L. Heien, "Biocompatible reference electrodes to enhance chronic electrochemical signal fidelity in vivo," *Analytical and Bioanalytical Chemistry,* vol. 413, no. 27, pp. 6689-6701, 2021/11/01 2021, doi: 10.1007/s00216-021-03640-w.

[33] I. A. Ges, I. A. Dzhura, and F. J. Baudenbacher, "On-chip acidification rate measurements from single cardiac cells confined in sub-nanoliter volumes," (in eng), *Biomed Microdevices,* vol. 10, no. 3, pp. 347-54, Jun 2008, doi: 10.1007/s10544-007-9142-7.

[34] J. Li, Y. Du, and C. Fang, "Developing an Iridium Oxide Film Modified Microelectrode for Microscale Measurement of pH," *Electroanalysis,* vol. 19, no. 5, pp. 608-611, 2007, doi: https://doi.org/10.1002/elan.200603753.

[35] R. D. Meyer, S. F. Cogan, T. H. Nguyen, and R. D. Rauh, "Electrodeposited iridium oxide for neural stimulation and recording electrodes," (in eng), *IEEE Trans Neural Syst Rehabil Eng,* vol. 9, no. 1, pp. 2-11, Mar 2001, doi: 10.1109/7333.918271.

[36] R. K. Franklin *et al.*, "Iridium Oxide Reference Electrodes for Neurochemical Sensing with MEMS Microelectrode Arrays," *IEEE Sensors,* pp. 1400-1403, 2005, doi: 10.1109/ICSENS.2005.1597971.

[37] K. Yamanaka, "Anodically Electrodeposited Iridium Oxide Films (AEIROF) from Alkaline Solutions for Electrochromic Display Devices," *Japanese Journal of Applied Physics,* vol. 28, no. 4R, p. 632, 1989/04/01 1989, doi: 10.1143/JJAP.28.632.

[38] T. Akkas, A. Zakharyuta, A. Taralp, and C. W. Ow-Yang, "Cross-linked enzyme lyophilisates (CLELs) of urease: A new method to immobilize ureases," *Enzyme and Microbial Technology,* vol. 132, p. 109390, 2020/01/01/ 2020, doi: https://doi.org/10.1016/j.enzmictec.2019.109390.

[39] A. Dwevedi, "Basics of Enzyme Immobilization," in *Enzyme Immobilization: Advances in Industry, Agriculture, Medicine, and the Environment*. Cham: Springer International Publishing, 2016, pp. 21-44.

[40] R. K. Christensen, A. V. Petersen, N. Schmitt, and J.-F. Perrier, "Fast detection of extrasynaptic GABA with a whole-cell sniffer," (in English), *Frontiers in Cellular Neuroscience,* Methods vol. 8, 2014-May-15 2014, doi: 10.3389/fncel.2014.00133.

[41] J. S. Isaacson, J. M. Solís, and R. A. Nicoll, "Local and diffuse synaptic actions of GABA in the hippocampus," (in eng), *Neuron,* vol. 10, no. 2, pp. 165-75, Feb 1993, doi: 10.1016/0896-6273(93)90308-e.

[42] M. V. Jones and G. L. Westbrook, "The impact of receptor desensitization on fast synaptic transmission," (in eng), *Trends Neurosci,* vol. 19, no. 3, pp. 96-101, Mar 1996, doi: 10.1016/s0166-2236(96)80037-3.

[43] B. Barbour and M. Häusser, "Intersynaptic diffusion of neurotransmitter," (in eng), *Trends Neurosci,* vol. 20, no. 9, pp. 377-84, Sep 1997, doi: 10.1016/s0166-2236(96)20050-5.

Chapter 6: Recommendations for Future Work

The advancements presented in this dissertation lay a strong foundation for continued research into neurochemical sensing technologies. By integrating novel enzyme engineering with state-of-the-art microelectrode designs, this work contributes meaningfully to the field of biosensing. However, several avenues for future exploration could further enhance the functionality, applicability, and impact of the technologies developed here. These recommendations address integration of sensors with microfluidic platforms, optimization of sensor performance, extended enzyme engineering campaigns, and the development of multiplexed sensing devices for simultaneous neurotransmitter monitoring.

6.1 Integration of Dopamine Sensors with Microfluidic Platforms

While the integration of dopamine sensors into a blood-brain barrier (BBB) lab-on-a-chip microfluidic platform was a key objective, this work remains incomplete. The successful implementation of such a system would provide an invaluable tool for modeling neurochemical dynamics under controlled conditions [1]. To advance this effort, future studies should focus on optimizing the microfluidic chip design to accommodate the dopamine sensor while maintaining the physiological relevance of the BBB model [2]. Particular attention should be paid to stabilizing sensor performance under fluidic conditions, as flow and shear forces can significantly impact signal stability and sensitivity [3]. Additionally, validating the platform with biologically relevant experiments—such as dopaminergic neuron depolarization studies—would demonstrate its utility

for translational research [4]. These efforts could greatly enhance the capacity to study drug delivery, neurotoxicity, and disease-related neurochemical imbalances *in vitro*.

6.2 Optimization of GABA Oxidase Crosslinking

Although the GABA sensor developed in this dissertation represents a pioneering achievement, further improvements in its functionality could be achieved through targeted optimization. One particularly promising avenue involves revisiting the crosslinking method used for enzyme immobilization. Glutaraldehyde (GAH) vapor was chosen for this work due to its simplicity and established efficacy. However, alternative crosslinkers, such as bis(sulfosuccinimidyl) suberate (BS3), may offer distinct advantages. BS3 is a homobifunctional amine-reactive crosslinker that operates via N-hydroxysuccinimide (NHS) ester chemistry [5], enabling the formation of covalent bonds between primary amine groups on adjacent proteins. Its longer spacer arm (11.4 Å compared to the 5 Å of GAH) reduces enzyme crowding [6], potentially allowing greater access to active sites and enhancing the stability of immobilized enzyme layers [7-9].

BS3 has been used successfully in related electroenzymatic sensors [10], where it was shown to improve substrate access and reduce diffusion barriers, ultimately enhancing sensitivity [11] and response time. Implementing BS3 in the immobilization process for the GABA sensor would involve systematically optimizing conditions such as BS3 concentration, enzyme-to-BSA ratio, and layer thickness. These experiments could provide valuable insights into the interplay between crosslinker chemistry and sensor performance, potentially yielding significant

improvements in the sensitivities and limits of detection in GABA detection. BS3 is commercially available and can be obtained from Thermo Fisher Scientific (Waltham, MA, USA).

6.3 Extending GABA Oxidase Enzyme Engineering

While the evolved GABA oxidase variants described in this dissertation represent significant progress, further directed evolution campaigns are likely to yield even greater improvements. The final limit of detection (LOD) achieved with this sensor was approximately 63 μM, which, while sufficient for many applications, falls short of the ~1 μM LOD achieved with our lab's glutamate sensors. Achieving similar sensitivity for GABA would greatly enhance the sensor's utility for *in vivo* applications.

Given the success of mutagenesis in improving GABA affinity at alanine-58, additional rounds of combinatorial active site saturation mutagenesis at amino acid residues surrounding this locus offers a logical path forward [12-14]. While residues 57 and 59 showed minimal individual improvements, it is possible that permutations of residues 56 and 60 unlock higher order of magnitude improvements in catalytic efficiency. Moreover, expanding random mutagenesis campaigns could help identify unexpected beneficial mutations elsewhere in the enzyme fitness landscape. Adjustments to the random mutagenesis protocol itself, such as altering the ratios of dNTPs [15] or using polymerases with distinct error biases [16], could diversify the mutation landscape, potentially uncovering novel variants with superior activity.

6.4 Development of Multiplexed Neurotransmitter Sensors

The capacity to monitor multiple neurotransmitters simultaneously would represent a transformative advancement in neurochemical sensing. By applying microcontact printing techniques [17-19], previously used in our lab [20], GABA oxidase could be selectively immobilized onto specific microelectrode sites alongside other enzymes, such as glutamate oxidase. This would enable the construction of multiplexed probes capable of simultaneously monitoring GABA and glutamate dynamics. Such a capability would be particularly valuable for investigating the excitation/inhibition (E/I) balance in the central nervous system, where GABA and glutamate play pivotal and opposing roles [21]. Simultaneous, real-time monitoring of these neurotransmitters would provide a high level of precision into pathways implicated in epilepsy, schizophrenia, and neurodegenerative diseases.

6.5 In Vivo Applications and Broader Utility

Finally, transitioning the GABA sensor from *in vitro* characterization to *in vivo* applications represents a critical direction for future work. Validation in animal models would provide important insights into sensor performance in complex biological environments [22], including issues related to biocompatibility [23], fouling [24], and long-term stability [25]. Moreover, adapting the sensor for integration with non-invasive diagnostic platforms, such as microdialysis systems [26], could expand its clinical utility for monitoring neurochemical imbalances associated with conditions like epilepsy and anxiety disorders. These applications would not only enhance the translational relevance of the work but also broaden its impact beyond basic neuroscience research.

6.6 Conclusion

The recommendations outlined here build on the successes achieved in this dissertation while addressing areas for further refinement and exploration. From improving enzyme immobilization strategies and advancing protein engineering to developing multiplexed sensing platforms and *in vivo* applications, these future directions hold significant potential for advancing the field of neurochemical biosensing. By pursuing these opportunities, researchers can continue to push the boundaries of what is achievable with electroenzymatic sensors, fostering new discoveries in neuroscience and clinical diagnostics.

6.7 References

[1] J. Fuessl, "Development of an electrochemical dopamine sensor for monitoring the neurotransmitter release of human midbrain organoids on-chip," Biomedical Engineering, Technische Universitat Wien, 2023.

[2] A. Marino, M. Battaglini, M. C. Lefevre, M. C. Ceccarelli, K. Ziaja, and G. Ciofani, "Sensorization of microfluidic brain-on-a-chip devices: Towards a new generation of integrated drug screening systems," *TrAC Trends in Analytical Chemistry,* vol. 168, p. 117319, 2023/11/01/ 2023, doi: https://doi.org/10.1016/j.trac.2023.117319.

[3] M. Li *et al.*, "Blood–brain barrier microfluidic chips and their applications," *Organs-on-a-Chip,* vol. 5, p. 100027, 2023/12/01/ 2023, doi: https://doi.org/10.1016/j.ooc.2023.100027.

[4] Y. Zhao, U. Demirci, Y. Chen, and P. Chen, "Multiscale brain research on a microfluidic chip," *Lab on a Chip,* 10.1039/C9LC01010F vol. 20, no. 9, pp. 1531-1543, 2020, doi: 10.1039/C9LC01010F.

[5] S. Gao, J. M. Guisán, and J. Rocha-Martin, "Oriented immobilization of antibodies onto sensing platforms - A critical review," *Analytica Chimica Acta,* vol. 1189, p. 338907, 2022/01/02/ 2022, doi: https://doi.org/10.1016/j.aca.2021.338907.

[6] Y. D. Han, S. Y. Song, J. H. Lee, D. S. Lee, and H. C. Yoon, "Multienzyme-modified biosensing surface for the electrochemical analysis of aspartate transaminase and alanine transaminase in human plasma," *Analytical and Bioanalytical Chemistry,* vol. 400, no. 3, pp. 797-805, 2011/05/01 2011, doi: 10.1007/s00216-011-4797-6.

[7] J. M. Alonso, A. A. M. Bielen, W. Olthuis, S. W. M. Kengen, H. Zuilhof, and M. C. R. Franssen, "Self-assembled monolayers of 1-alkenes on oxidized platinum surfaces as platforms for immobilized enzymes for biosensing," *Applied Surface Science,* vol. 383, pp. 283-293, 2016/10/15/ 2016, doi: https://doi.org/10.1016/j.apsusc.2016.05.006.

[8] M. Shen, J. F. Rusling, and C. K. Dixit, "Site-selective orientated immobilization of antibodies and conjugates for immunodiagnostics development," *Methods,* vol. 116, pp. 95-111, 2017/03/01/ 2017, doi: https://doi.org/10.1016/j.ymeth.2016.11.010.

[9] G. T. Hermanson, "Chapter 5 - Homobifunctional Crosslinkers," in *Bioconjugate Techniques (Third Edition)*, G. T. Hermanson Ed. Boston: Academic Press, 2013, pp. 275-298.

[10] I. w. Huang, M. Clay, S. Wang, Y. Guo, J. Nie, and H. G. Monbouquette, "Electroenzymatic glutamate sensing at near the theoretical performance limit," *Analyst,* 10.1039/C9AN01969C vol. 145, no. 7, pp. 2602-2611, 2020, doi: 10.1039/C9AN01969C.

[11] S. Milan and V. Karel, "Tyrosinase Electrochemical Biosensors Monitoring Medicinally Significant Substances," *Current Medicinal Chemistry,* vol. 25, no. 33, pp. 3988-4006, 2018, doi: http://dx.doi.org/10.2174/0929867324666170727121327.

[12] M. T. Reetz, G. Qu, and Z. Sun, "Engineered enzymes for the synthesis of pharmaceuticals and other high-value products," *Nature Synthesis,* vol. 3, no. 1, pp. 19-32, 2024/01/01 2024, doi: 10.1038/s44160-023-00417-0.

[13] K. E. Johnston *et al.*, "A combinatorially complete epistatic fitness landscape in an enzyme active site," *Proceedings of the National Academy of Sciences,* vol. 121, no. 32, p. e2400439121, 2024/08/06 2024, doi: 10.1073/pnas.2400439121.

[14] M. Reetz, "Making Enzymes Suitable for Organic Chemistry by Rational Protein Design," *ChemBioChem,* vol. 23, no. 14, p. e202200049, 2022, doi: https://doi.org/10.1002/cbic.202200049.

[15] R. C. Cadwell and G. F. Joyce, "Randomization of genes by PCR mutagenesis," (in eng), *PCR Methods Appl,* vol. 2, no. 1, pp. 28-33, Aug 1992, doi: 10.1101/gr.2.1.28.

[16] P. C. Cirino, K. M. Mayer, and D. Umeno, "Generating Mutant Libraries Using Error-Prone PCR," in *Directed Evolution Library Creation: Methods and Protocols*, F. H. Arnold and G. Georgiou Eds. Totowa, NJ: Humana Press, 2003, pp. 3-9.

[17] W. R. Leifert *et al.*, "NANOSCALE BIOSENSORS AND BIOCHIPS," in *Annual Review of Nano Research*, pp. 1-82.

[18] M. Thompson, L.-E. Cheran, and S. Sadeghi, *Sensor Technology in Neuroscience*. The Royal Society of Chemistry, 2013.

[19] C. Forro *et al.*, "Electrophysiology Read-Out Tools for Brain-on-Chip Biotechnology," (in eng), *Micromachines (Basel),* vol. 12, no. 2, Jan 24 2021, doi: 10.3390/mi12020124.

[20] T. T. C. Tseng and H. G. Monbouquette, "Implantable microprobe with arrayed microsensors for combined amperometric monitoring of the neurotransmitters, glutamate and dopamine," *Journal of Electroanalytical Chemistry,* vol. 682, pp. 141-146, 2012/08/15/ 2012, doi: https://doi.org/10.1016/j.jelechem.2012.07.014.

[21] M. Charney *et al.*, "Neurometabolic alterations in children and adolescents with functional neurological disorder," *NeuroImage: Clinical,* vol. 41, p. 103557, 2024/01/01/ 2024, doi: https://doi.org/10.1016/j.nicl.2023.103557.

[22] G. Rong, S. R. Corrie, and H. A. Clark, "In Vivo Biosensing: Progress and Perspectives," *ACS Sensors,* vol. 2, no. 3, pp. 327-338, 2017/03/24 2017, doi: 10.1021/acssensors.6b00834.

[23] S. Shang *et al.*, "Biocompatible dipeptide coated on Pt/PEDOT:PSS modified silicon probes for tissues rejection alleviation," *Sensors and Actuators B: Chemical,* vol. 424, p. 136891, 2025/02/01/ 2025, doi: https://doi.org/10.1016/j.snb.2024.136891.

[24] J. Xu and H. Lee, "Anti-Biofouling Strategies for Long-Term Continuous Use of Implantable Biosensors," *Chemosensors,* vol. 8, no. 3, p. 66, 2020. [Online]. Available: https://www.mdpi.com/2227-9040/8/3/66.

[25] Y. Li, N. Li, N. De Oliveira, and S. Wang, "Implantable bioelectronics toward long-term stability and sustainability," *Matter,* vol. 4, no. 4, pp. 1125-1141, 2021/04/07/ 2021, doi: https://doi.org/10.1016/j.matt.2021.02.001.

[26] X. Xu, Y. Zuo, S. Chen, A. Hatami, and H. Gu, "Advancements in Brain Research: The In Vivo/In Vitro Electrochemical Detection of Neurochemicals," *Biosensors,* vol. 14, no. 3, p. 125, 2024. [Online]. Available: https://www.mdpi.com/2079-6374/14/3/125.

Appendix A: Microprobe Fabrication

A.1 Materials

Silicon wafers were ordered from Silicon Valley Microelectronics (Santa Clara, CA) with the following parameters: 100 mm diameter, p-type boron doped, orientation <1 0 0>, 150 μm thickness. All microfabrication was conducted in the UCLA Nanofabrication Laboratory (NanoLab).

A.2 Microfabrication Process Traveler

Process	Step	Name	Description	Remarks
I. Field oxide formation process				
	1	Label	Label wafer on the back unpolished side	Use diamond pen
Cleaning Steps	2	Piranha bath	Remove organic contaminants: H_2SO_4:H_2O_2 = 17:1 T=70°C; time=10 min	Use wafer carrier Refresh solution with 250mL H2O2 if hasn't been used that day
	3	Rinse	Time = 2min	Use rinse cycle in PFC hood
	4	HF bath	Remove native oxide: 5s in HF:DI=1:10 or 1s in BOE	Caution very corrosive
	5	Rinse	Time = 2 mins, afterwards N_2 blow dry	Gentle water stream Don't use spin dryer (wafers will break)
Furnace	6	Oxide furnace	Thermally grow 1μm SiO_2 Wet recipe (WET1100.001) T=1100°C, time=2.5hr	Keep everything clean (gloves/mask on) • High temperature (use caution) • Use quartz boat. Load wafers ASAP Measure the SiO_2 thickness center/top/bottom/left/right, average it
	7	Nanospec	Measure SiO_2 thickness	Measure center/top/bottom/left/right,

			(Silicon dioxide on silicon)	average it and compare with step #6
Cleaning Steps	8	Piranha bath	Remove organic contaminants: H_2SO_4:H_2O_2 = 17:1 T=70°C; time=10min	Use wafer carrier • Refresh solution with 250mL H_2O_2 if hasn't been used that day
	9	Rinse	Time = 2 mins	Use rinse cycle in PFC Hood, need to train PFC sink
II. Electrode sites, channels, and bonding pads formation				
	10	Dehydration bake	T=150°C Time ≥ 5 min	Drive off moisture, and improve PR adhesion. Before the dehydration bake, use acetone clean the previously stored wafers and use DI water to rinse first.
Lithography I	11	HDMS coat	Improve PR adhesion Time ≥ 5 min	HMDS: hexamethyldisilazane • Toxic (operate underneath hood) • Do not place wafer in the middle of metal container. • Handle dips down and will break wafer when putting cover on. Check the HDMS inside make sure it's saturated
	12	Photoresist spin coat	PR: AZ5214-EIR Thickness: ~1.6μm 1000 RPM Ramp = 1000 Time = 20sec	Clean wafer chuck with acetone • Make sure PR covers at least 2/3 of the wafer surface prior to spin volume is about 1.5 volume of the dropper To programming the parameters: Press step button + number button (1-9) to select the step to program. Select speed/ramp to set the speed = 1000 rpm Ramp = 1000 Select step terminate button to set the time to be 20 sec

				Load the wafer and press vacuum button to turn on the vacuum. After covering wafer with PR, step on the start button on the ground using your foot. Press vacuum button to turn off vacuum and collect wafer.
	13	Soft bake	T=100°C Time = 1 min. (critical) Place at the center of hotplate	Make sure wafer is flat on hotplate
	14	Exposure	Karl Suss alignment: Soft contact Expose for 9.5 sec (when power = 8 mW/cm^2)	If power varies, use this formula to correct exposure time: t (sec) = 18 × (8 / actual power in mW/cm^2)
	15	Development	Remove exposed PR DIW:AZ400K=5:1 Developer ~19 sec.	Swishing back and forth Cover the beaker with aluminum foil
	16	Microscope	Inspection	Make sure wafer is fully developed. DO NOT hardbake after this step (for better liftoff results) If the line is very thick, that usually means overdevelop
	17	Remove ~100Å PR	Tegal (~2 mins) Or Technics	Remove 100A PR for the whole wafer to prevent metal from being washed off during lift-off. Better to inspect again.
Metal Deposition	18	Metal deposition	Old CHA (evaporated metal deposition) Cr/Pt = 200 Å/1000Å Deposition rate: 1 Å/sec	• Deposit metal within 3 days after Lithography I • Total deposition time: ~3hrs
	19	Lift-off	Sonicate in acetone (in 2L beaker)	• Use 3 beakers of acetone in series to clean each wafer. • Keep wafers wet by rinsing with acetone • Rinse with DIW and dry with N_2

	20	Microscope	Inspection	Check for broken leads, chipped sites
III. Insulation layer deposition				
Oxide/Nitride Deposition	21	PECVD oxide	STS PECVD: 7500 Å Recipe: HFSIOST Time: ~30min	• Sonicate with acetone and blow dry wafer with N_2 prior to placing in machine • Check deposition rate first (~10 min), then measure the thickness
	22	Nanospec	Measure SiO_2 thickness (Silicon dioxide on silicon) Goal: 7500 Å	Use measured value subtracts field oxide thickness to calculate deposited thickness
	23	PECVD nitride	STS PECVD: 7500 Å Recipe: HFSINST Time: ~50min	
	24	Nanospec	Nanospec Measure Si3N4 thickness (silicon nitride on silicon dioxide) Goal: 7500 Å	For previous oxide thickness, type in average from step #22
IV. Open electrodes/soldering pads				
Lithography II	25	Dehydration bake	T=150°C Time ≥ 5 min	Drive off moisture
	26	HDMS coat	Improve PR adhesion Time ≥ 5 min	
	27	Photoresist spin coat	PR: AZ5214-EIR Thickness: ~1.6μm 2500 RPM Ramp = 1000 Time = 30sec	• Clean wafer chuck with acetone • Make sure PR covers at least 2/3 of the wafer surface prior to spin To program the spin coating please see step 12.
	28	Soft bake	T=100°C, time = 1 min. (critical) Place at the center of hotplate	Make sure wafer is flat on hotplate
	29	Exposure	Karl Suss alignment: Soft contact, expose for 18 sec (when power = 8 mW/cm^2)	If power varies, use this formula to correct exposure time: t (sec) = 18× (8 / actual power in mW/cm^2) Make sure four alignment marks are all matched

	30	Development	Remove exposed PR DIW:AZ400K = 5:1 ~19 sec.	Swishing back and forth
	31	Microscope	Inspection	Make sure wafer is fully developed.
	32	Hard bake	T = 150°C, 5min. Place at center of hotplate	• Do not post bake before inspection • Let cool before storing
Nitride/Oxide Etch	33	Si wafer carrier	Apply moist cooling grease on 500μm Si wafer carrier Bake more than 3min @ 80°C on hotplate	• Use q-tips to apply grease in circles over entire surface of carrier wafer • Make sure wafer backside is clean of grease • Stick wafer onto carrier wafer tightly by placing onto wafer and rotating until flats are aligned Use Kimwipe absorbed with acetone to remove the photoresist along the edge of the wafer, otherwise the PR may get burnt and stick on the sucker.
	34	Nitride and oxide etch	AOE (recipe: OXIDAPIC) Etch time: ~4 min. (this etch time may be longer or shorter depending on the status of the AOE)	• Remove 1.5 μm of nitride and oxide insulation layer • Do not run the etching more than 2 min for each time Perform O_2 clean first with thick dummy wafer
	35	Inspection	Voltmeter or Nanospec	• Voltmeter: check if resistance between test metal electrodes is zero. • Nanospec: check if thickness of oxide ≤field oxide thickness (oxide thickness<10,000A)
Cleaning Steps	36	PR strip	Matrix stripper (Matrix Asher 105) "3 min strip" recipe	Make sure to keep wafer stuck to carrier wafer until after this step
	37	Release carrier	Slide wafer off carefully	Clean wafer backside and carrier wafer with acetone
V. Define probe outline				

Lithography III	38	Dehydration bake	T=150°C Time ≥ 5 min	Drive off moisture
	39	Photoresist spin coat	PR: AZ4620 Thickness: ~7μm 3000RPM, Ramp: 1000, Time: 30sec	• Clean chuck with acetone • Make sure PR covers at least 2/3 of wafer surface To program the spin coating please see step 12.
	40	Soft bake (prebake)	T=100°C, 1'30". (critical) Place at center of hotplate	Make sure wafer is flat on hotplate
	41	Exposure	Karl Suss alignment: Soft contact, exposure time: 18 sec (power: 8mW/cm^2). After the exposure relax the wafer in ambient temperature for 5 mins.	If power varies, use this formula to correct exposure time: t (sec) = 18× (8/actual power in mW/cm^2)
	42	Development	Remove exposed PR DIW:AZ400K = 4:1 4-10 mins. Depending on the situation higher ratio like 3:1 or 2:1 could be used	For post development, rinse with DI water for 2 min. Blow dry with N_2
	43	Microscope	Inspection	Make sure wafer is fully developed
	44	Hard bake	120°C for 5 mins	
Si Wafer Etch-Through	45	Si wafer carrier	Apply moist cooling grease on 500μm thick Si carrier wafer Bake 3 min. @ 75°C	• Use q-tips to apply grease in circles over entire surface of carrier wafer • Make sure wafer backside is clean of grease • Stick wafer onto carrier wafer tightly by placing onto wafer and rotating until flats are aligned
	46	Nitride/oxide etch	AOE (recipe: OXIDAPIC) Etch time: ~7-8 min. (This etch time may be	• Remove all nitride and oxide from exposed areas • Do not run the etching

			longer or shorter depending on the status of the AOE)	more than 2 mins for each time
	47	Si etch through	FDRIE (deep reactive ion etch): Recipe FN-DY ~20 min. total etch time (this etch time may be longer or shorter depending on the status of the FDRIE)	• Do not run DRIE for more than 5 minutes at a time (could overheat the wafer) • O_2 plasma clean for 30 min BEFORE use
	48	Inspection	Microscope	Do not release wafer from carrier until etch through of silicon is confirmed. Should be able to see cooling grease through the outlines for silicon etch through. Also use nanospec to check the gap between probes, should be less than 100 Å
Stripping PR	49	Release carrier	Slide wafer off carefully	Clean carrier with acetone
	50	PR strip	PR stripper sink (ALEG 355) T=75°C, at least 30 min.	Rinse with DI water for 2 min. Blow dry with N_2 after

Appendix B: Preparation of Dopamine Sensors

B.1 Materials

Nafion (5 wt% solution in lower aliphatic alcohols/H_2O mix), m-phenylenediamine (99%), dibasic sodium phosphate, sodium chloride, sodium hydroxide pellets, hydrochloric acid (37%), and sulfuric acid (99.999%) were purchased from Aldrich Chemical Co. (Milwaukee, WI, USA). PBS buffer consisted of 50 mM dibasic sodium phosphate with 100 mM sodium chloride adjusted to pH 7.4 with concentrated HCl. A Millipore Milli-Q Water System was used to generate ultrapure water for the preparation of all solutions used. Electrochemical preparations and calibration measurements were performed using a Versatile Multichannel Potentiostat equipped with the 'p' low current option and low current N' Stat box (VMP3, Bio- Logic USA LLC, Knoxville, TN, USA). For experiments in which an external reference electrode was necessary, Ag/AgCl glass-bodied reference electrodes with 3 M NaCl electrolyte and a 0.5 mm diameter platinum (Pt) wire auxiliary electrode were purchased from BASi (West Lafayette, IN).

B.2 Procedure

B.2.1 Probe Assembly

1. Detach each probe off of wafer (press on corner w/ fine forceps) and check for broken leads, chipped site and poor insulation layer under microscope.
2. Cut 4 insulated Pt wires per probe and strip one end ~5 mm and another end ~1 cm.
3. Solder (@ 510 °C) wires on soldering pads of the microprobe. Liberally apply rosin soldering flux to the soldering pads and position Pt wires with 5 mm stripped ends close to

the surface. Solder Pt wires to the soldering pad surface. The ideal shape should be that of a relatively uniform droplet that envelops the tip of the Pt wire.

4. Sonicate the soldered microprobe in isopropyl alcohol for approximately 5 minutes. Rinse with DI water and blow dry with gas. Repeat this step again with a fresh beaker of isopropyl alcohol.
5. Insulate the soldering pad connection with epoxy resin on the front of the microprobe. Repeat this step until no wire or solder is exposed. Wait for about 20 mins.
6. Label probe with tape

B.2.2 Acid Cleaning

A clean scan in 0.1 M H_2SO_4 (diluted with DI water; Cyclic voltammetry: -0.2 V to 1.5 V, 50 mV/s, 10 cycles) was done to remove any surface impurities.

B.2.3 Bare Sensor Testing

1. Make a 10 mM H_2O_2 (diluted with DI) dilution solution.
2. A bare sensor test in 10 mL PBS (0.7 V vs Ag/AgCl) was done to check sensor response to 20 μM H_2O_2 (inject 20 μL of 10 mM H_2O_2). Good sensors should give an increase in current of ~2 nA.

B.2.4 PPD Deposition and Nafion Coating

1. Prepare 5 mM PPD in 1× PBS (5.4 mg PPD powder + 10 mL 1× PBS) in 15 mL falcon tube. Vortex for 1 minute. Insert the MEA tips into the bulk solution and connect to the potentiostat.

2. Electrodeposit PPD: Apply 0.85 V vs Ag/AgCl until charge, Q (nA*h) reaches 0.2. Remove the probe tips from the solution.
3. Prepare 0.2 M NaOH. Insert the MEA tips into the bulk solution and connect to the potentiostat.
4. Overoxidize PPD: Apply 1.042 V vs Ag/AgCl for 20 minutes.
5. Dip-coat in 2% Nafion and bake the sensor at 115 °C for 20 minutes.

Appendix C: Iridium Oxide Reference Electrode Fabrication

If it is desired to incorporate an integrated iridium oxide reference electrode, then the following protocol should be inserted between B.2.3 and B.2.4.

C.1 Materials

Iridium tetrachloride hydrate, anhydrous oxalic acid (99%), hydrogen peroxide (30 wt% solution in water), chloroplatinic acid hydrate, and anhydrous potassium carbonate were purchased from Aldrich Chemical Co. (Milwaukee, WI, USA). Electrochemical preparations and calibration measurements were performed using a Versatile Multichannel Potentiostat equipped with the 'p' low current option and low current N' Stat box (VMP3, Bio- Logic USA LLC, Knoxville, TN, USA). For experiments in which an external reference electrode was necessary, Ag/AgCl glass-bodied reference electrodes with 3 M NaCl electrolyte and a 0.5 mm diameter platinum (Pt) wire auxiliary electrode were purchased from BASi (West Lafayette, IN).

C.2 Procedure

C.2.1 Pt Grass Electrodeposition

1. Prepare Pt Grass solution with 25 mM H_2PtCl_6 and 15 mM formic acid.
2. Electrodeposit Pt Grass at constant potential (-0.1 V vs Ag/AgCl) for 600 s.

C.2.2 Iridium Oxide Electrodeposition

1. Dissolve 15 mg of iridium tetrachloride in 10 mL of water then stir solution for 30 min. Purge the IrCl4 bottle then store in container with desiccant in 4°C.
2. Add 0.1 mL of aqueous 30% hydrogen peroxide solution then stir for 10 min.

3. Add 50 mg of oxalic acid dihydrate to solution and stir for 10 min.
4. Adjust pH of solution to 10.5 by adding small portions of anhydrous potassium carbonate.
5. Allow the resulting solution to sit quiescently for 48 h before electrodeposition. After this process, the solution should change to a deep purple color.
6. Cycle 100 times between 0.0 V and 0.6 V at 50 mV/s. Do not use a stir bar. Film should be a purple or blue color when inspected under the microscope.
7. Place ~200 uL of PBS in microcentrifuge tube. Insert probe such that only shaft is submerged in PBS. Do not let head touch PBS. Hold probe in place and seal top with putty. *Sensor should be stored in this manner ~2 days prior to further sensor modifications (*i.e.* for electroenzymatic sensors).

Appendix D: Cloning of Wild Type MABO Plasmid

D.1 Materials

Purchase MABO gene fragment (sequence below). Optimize for expression in *E. coli* by adding 6-7 histidine residues (CAT) and a TAA stop codon at the C terminus of the sequence prior to purchasing.

```
        10         20         30         40         50
MGRIGILGAG LAGLAAATKL AEAGENVTVF EARNRPGGRV WSETLDTPKG
        60         70         80         90        100
SYVIERGAEF VLDGYTSMRR LLSQFGLSLV DTGMSYYVRE PGDTTGITCD
       110        120        130        140        150
DIIRTGREAL ELASGSGLQG TAEELLAKLP DEPELVDALR ARIEISTAVS
       160        170        180        190        200
ASEVTARSLQ HIASFEPKPS WRVAGGNQRL PDAMAAALGS AVRYGETVRA
       210        220        230        240        250
VENISDGGVL VTTDTDTSVF DTVVVALPLA VIRDSQLNLP TTEARDAALK
       260        270        280        290        300
HVLQGHAAKL HLPLETQPAT SAVMSVEGRY WTWTATDESG AVAPVLNAFM
       310        320        330        340        350
GSPSAITRAN LKQRPAEWVA KARALRTDLA IPQDAAALTT VWSEDQLAGG
       360        370        380        390        400
AYAAHAPGVT AAGTALLEKP VGDVFWAGEY SEPEFVGLME GAIRSGERAA
       410        420
GRVMQRLETK SGNSDSERSK A
```

The pET28a vector was generously provided by the lab of Professor Yi Tang. Plasmid DNA was recovered using the ZymoClean DNA Recovery Kit. A NEBuilder HiFi DNA Assembly Kit was used for all cloning and assembly workflows. Cloning product plasmids were transformed into chemically competent NEB SoluBL21 *E. coli* cells. LB agar plates treated with 50 µg/mL kanamycin were used for selecting colonies, and SOC medium was utilized for recovery of transformed cells.

D.2 Procedure

D.2.1 PCR Amplification of the Native MABO Gene Fragment

1. Design and purchase primers (MABO-F & MABO-R) to anchor both ends of the MABO gene sequence
2. PCR amplify MABO gene fragment and vector backbone separately.
    A. 50 µL Q5 PCR amplification of the MABO gene fragment
        i. 38 µL water, 10 µL Q5 buffer, 1 µL dNTP, 0.5 µL Q5 polymerase, 0.25 µL of MABO-F primer, 0.25 µL of MABO-R primer, 1 µL of working stock DNA fragment
        ii. Choice of PCR Recipe:
            a. Q5 PCR

Step	Temperature	Time
Initial Denaturation	98°C	1 minute
32 Cycles	98°C	15 seconds
	60°C	30 seconds
	72°C	45 seconds
Final Extension	72°C	5 minutes
Hold	12°C	∞

            b. Q5 Touchdown PCR: Same recipe as Q5 PCR except the annealing temperature starts at 68°C and drops by 1°C every cycle for 10 cycles, [98°C for 15s, 60°C for 30s, 72°C for 45s] × 24, 72°C for 5 mins, 12°C for stability until sample is removed
3. 50 µL Q5 PCR Amplification of the backbone

A. 37 µL H_2O, 10 µL Q5 reaction buffer, 1 µL 50× dNTP mix, 0.25 µL MABO-BB F primer, 0.25 µL of MABO-BB R primer, 0.5 µL Q5 polymerase, 1 µL template DNA

B. Vector backbone (unmutated) Amplification with Q5 Touchdown PCR

Step	Temperature	Time
Initial Denaturation	95°C	3 minutes
14 Cycles	95°C	20 seconds
	65°C - 1 °C/cycle	30 seconds
	68°C	90 seconds
25 Cycles	95°C	20 seconds
	64°C	30 seconds
	68°C	90 seconds
Final Extension	68°C	5 minutes
Hold	4-10°C	∞

D.2.2 Gel Electrophoresis to Verify PCR Efficiency

This step is optional because the resolution is low.

1. Add 8 µL DNA dye to the PCR product tube.
2. Load into agarose gel.
3. Run the gel at 150 V and 400 mA for 8 minutes.
4. Use Image Lab software to validate that the gel has run sufficiently long.
5. Place gel block on the transilluminator. Excise the DNA fragment corresponding to approximately 1.5 kbp from the agarose gel using a razor blade, scalpel or other device and transfer it into a 1.5 mL microcentrifuge tube

D.2.3 ZymoClean DNA Recovery

1. Add 3 volumes of Agarose Dissolving Buffer (ADB) to each volume of agarose excised from the gel (e.g. for 100 µL of agarose gel slice add 300 µL of ADB)
2. Incubate at 37-55°C for 5-10 minutes until the gel slice is completely dissolved
3. Transfer the melted agarose solution to a Zymo-Spin Column in a Collection Tube. Centrifuge for 30-60 seconds. Discard the flow-through.
4. Add 200 µL of DNA Wash Buffer to the column and centrifuge for 30 seconds. Discard the flow-through. Repeat the wash step.
5. Add ≥ 6 µL (10-20 µL is typically good) DNA Elution Buffer or water directly to the column matrix. Place column into a 1.5 mL tube and centrifuge for 30-60 seconds to elute DNA

D.2.4 NEBuilder HiFi DNA Assembly Protocol for Cloning into pET28a Vector

1. Prepare DNA Fragment
    A. Ensure that all DNA fragments, including the pET28a vector backbone and the insert(s), have overlapping regions of 15–20 base pairs at their ends.
    B. Use PCR or restriction enzyme digestion to prepare the fragments. Confirm fragment integrity via gel electrophoresis.
2. Quantify DNA concentrations of the vector and insert fragments using a NanoDrop or plate reader (spectrophotometry). Aim for a molar ratio of 1:2 (vector:insert) to achieve optimal assembly.
3. Prepare the reaction mixture: 0.03-0.2 pmol pET28a vector backbone, 2× as many moles of the insert as compared with the vector backbone, 10 µL of 2× NEBuilder HiFi DNA Assembly Master Mix, and 20 µL of nuclease-free water.

Appendix E: Transformation of Wild Type MABO Plasmid

1. Add 2–5 µL of the assembled product to 50–100 µL of chemically competent SoluBL21 cells.
2. Perform a heat shock at 42°C for 30 seconds.
3. Recover cells in SOC medium for 1 hour at 37°C with agitation.
4. Plate 100–200 µL of the transformed cells on LB agar plates containing 50 µg/mL kanamycin to select for MABO-pET28a transformants.
5. Incubate the plates at 37°C overnight.
6. Pick colonies and inoculate in 3 mL LB Kan overnight. Extract the plasmids using a Zyppy Plasmid Miniprep Kit.
7. Send in plasmids for Sanger sequencing via Laragen Inc. (Culver City, CA) to verify genetic fidelity in comparison with the intended MABO gene sequence.
8. Prepare frozen stock of ideal transformants by mixing equal parts of overnight cell culture and 40% glycerol (v/v). Store in cryovial at -80ºC.

Appendix F: Site Directed Mutagenesis Library Generation

F.1 Materials

Site-directed mutagenesis was performed using the NEB Q5 Site-Directed Mutagenesis Kit, following the manufacturer's protocol. This kit provides all necessary reagents for high-fidelity PCR amplification and efficient mutagenesis, ensuring precise introduction of targeted mutations into the MABO construct. Forward and reverse primers were designed surrounding the locus of alanine-58.

F.2 Procedure

F.2.1 Site Directed Library Exponential Amplification (PCR)

1. Assemble 12.5 µL Q5 Hot Start High-Fidelity 2× Master Mix, 0.25 µL forward primer (10 µM), 0.25 µL reverse primer (10 µM), 1 µL template DNA (1-25 ng/µL), 11 µL nuclease-free water
2. Mix reagents completely and transfer to a thermocycler

Step	Temperature	Time
Initial Denaturation	98°C	30 seconds
25 Cycles	98°C	10 seconds
	50-72°C	10-30 seconds
	72°C	20-30 seconds
Final Extension	72°C	2 minutes
Hold	4-10°C	

3. Kinase, Ligase, and Dpn I (KLD) Treatment
    A. Assemble 1 μL PCR product, 5 μL 2× KLD reaction buffer, 1 μL 10× KLD enzyme mix, 3 μL nuclease-free water
    B. Mix well by pipetting. Incubate at room temperature for 5 minutes.

F.2.2 Transformation into NEB 5α Cloning Cells

1. Thaw a tube of NEB 5-alpha competent *E. coli* cells on ice
2. Add 5 μL of the KLD mix to the tube of thawed cells. Carefully flick the tube 4-5 times to mix. Do not vortex
3. Place the mixture on ice for 30 minutes
4. Heat shock at 42°C for 30 seconds
5. Place on ice for 5 minutes
6. Pipette 950 μL of room temperature SOC into the mixture
7. Incubate at 37°C for 60 minutes with shaking (250 rpm)
8. Mix the cells thoroughly by flicking the tube and inverting, then spread 50-100 μL onto a selection plate and incubate overnight at 37°C. It may be necessary (particularly for simple substitution experiments) to make a 10- to 40-fold dilution of the transformation mix in SOC prior to plating, to avoid a lawn of colonies
9. Inoculate a single transformant colony into 3 mL of LB liquid media supplemented with 50 mg/L kanamycin. Incubate at 37° C (250 rpm) for 12-14 hours.
10. Miniprep the plasmids. Send 8-10 μL for sequencing and store the remainder at -20°C.

F.2.3 Transformation of Mutants into NEB SoluBL21 Expression Cells

1. Inoculate 3 mL LB Kan with frozen stock from F.2.2. Culture overnight. Miniprep using the Zyppy Plasmid Miniprep Kit.
2. Thaw one vial of chemically competent SoluBL21 cells on ice for a few minutes.
3. Transfer 25 μL of cells into two sterile microcentrifuge tubes.
4. Add 1-10 ng (approx. 1-2 μL) of plasmid DNA to the SoluBL21 cells.
5. Mix cells and DNA well, and incubate on ice for 15 minutes.
6. Heat shock the transformation mix at 42°C for 45 seconds.
7. Add 0.25 μL room temperature SOC medium and incubate at 37°C for 1 hour in a shaking air incubator.
8. Plate the entire contents of the transformation reaction on an LB plate with appropriate antibiotic selection. Incubate overnight at 37°C.
9. Inoculate mutant *E. coli* transformants. Use a red pipette tip to place a single colony from the LB plate into 1 mL of LB Kan. Incubate at 37°C (250 rpm) for 12-14 hours.
10. Prepare of Frozen Stocks by mixing equal parts of overnight LB Kan culture with 40% (v/v) glycerol solution in a cryovial. Store at -80°C.

Appendix G: Random Mutagenesis Library Generation

G.1 Materials

Random mutagenesis was conducted using NEB Taq DNA Polymerase with Standard Taq Buffer, the Deoxynucleotide (dNTP) Solution Set, and the NEBuilder HiFi DNA Assembly Kit. These reagents enabled error-prone PCR to introduce random mutations into the MABO gene, followed by efficient cloning of the mutated fragments into the pET28a vector.

G.2 Procedure

G.2.1 Taq PCR Amplification of Random MABO Mutants

1. Design and purchase primers (MABO-Gib F & MABO-Gib R) to anchor both ends of the MABO gene sequence. These primers will need to be different than those used in Appendix D due to the lower annealing temperature of the *Taq* polymerase.
2. Prepare mutagenic dNTP mixture: 10 µL 50× dNTP mix, 4 µL 100 mM dCTP, and 4 µL 100 mM dTTP.
3. Prepare the PCR reaction mixture: 33.7 µL H_2O, 5 µL 10× *Taq* polymerase reaction buffer, 1.8 µL mutagenic dNTP mix, 1.5 µL MABO-Gib F primer, 1.5 µL of MABO-Gib R primer, 0.5 µL *Taq* polymerase, 5 µL 55 mM $MgCl_2$, 0.5 µL 10 ng template plasmid, 0.5 µL 10 mM $MnCl_2$ (added last, immediately before thermocycling).

Step	Temperature	Time
Initial Denaturation	95°C	3 minutes
14 Cycles	95°C	20 seconds
	65°C - 1 °C/cycle	30 seconds
	68°C	90 seconds
25 Cycles	95°C	20 seconds
	64°C	30 seconds
	68°C	90 seconds
Final Extension	68°C	5 minutes
Hold	4-10°C	∞

G.2.2 Q5 PCR Amplification of the Backbone

1. Prepare the PCR reaction mixture: 37 µL H_2O, 10 µL Q5 reaction buffer, 1 µL 50× dNTP mix, 0.25 µL MABO-BB F primer, 0.25 µL of MABO-BB R primer, 0.5 µL Q5 polymerase, 1 µL template DNA

Step	Temperature	Time
Initial Denaturation	95°C	3 minutes
14 Cycles	95°C	20 seconds
	65°C - 1 °C/cycle	30 seconds
	68°C	90 seconds
25 Cycles	95°C	20 seconds
	64°C	30 seconds
	68°C	90 seconds
Final Extension	68°C	5 minutes
Hold	4-10°C	∞

G.2.3 Gibson Assembly and Transformation of Random Mutagenesis Products

1. Quantify DNA concentrations of the vector and insert fragments using a NanoDrop or plate reader (spectrophotometry). Aim for a molar ratio of 1:2 (vector:insert) to achieve optimal assembly.
2. Prepare the reaction mixture. In a PCR tube, combine the following components:
    A. pET28a Vector Backbone: Add ~0.03–0.2 pmol
    B. Insert random MABO mutant fragments: Add twice as many moles of the insert as compared with the vector backbone.
    C. 2× NEBuilder HiFi DNA Assembly Master Mix: Add 10 µL.
    D. Nuclease-Free Water: Adjust the reaction volume to a total of 20 µL.
3. Mix the reaction mixture by gently pipetting up and down to ensure thorough mixing. Avoid introducing bubbles.
4. Incubate the reaction mixture in a thermocycler or heating block. Incubate at 50°C for 15–60 minutes.
5. Transform according to the same protocol as in Appendix E.

Appendix H: Preparation of Flow Cytometry Assay Stocks

1. Start an overnight culture (using previously made frozen stocks as seed culture) of a library that is to be screened with flow cytometry.
2. Inoculate 3 mL of fresh LB Kan culture with 100 µL of an overnight LB Kan culture. Prepare several extra culture tubes under the same conditions to a create controls for OD measurements.
3. Take periodic measurements until the controls hit an OD of 0.6. Place 900 µL of fresh LB Kan into a cuvette, mix with 100 µL of an OD control, and the resulting OD reading will be a 10× dilution of the actual samples.
4. Add 3 µL of 0.1M IPTG to each culture. Incubate at 37°C for 2.5-4 hours.
5. Split cultures into 1.5 mL samples, spin down at maximum speed (30 seconds to 1 minute) and 4°C, remove supernatant, store at -80°C overnight.
6. Thaw cell pellets of transformant libraries and resuspend in 1 mL of 100 mM pH 6.2 potassium phosphate buffer containing 100 mM KCl, 3 mM $MgCl_2$, and 1% (v/v) 1-butanol to an OD_{600} of 1.
7. Add 25 µL 2',7'-dichlorodihydrofluorescein diacetate C-H_2DCFDA (as a 10 mM solution in DMSO) to a final concentration of 250 µM and incubate the cells at 37°C & 180 rpm (5.1 cm orbit diameter) for 1 hour.
8. Harvest the cells by centrifugation (9500 × g, 5 minutes, 4°C) and discard the supernatant
9. Resuspend the cell pellets in 50 mM potassium phosphate buffer containing 100 mM KCl and 3 mM $MgCl_2$ at pH 7.5.
10. Add the target amine substrate (100 µL of 1M m-GABA ***or*** 200 µL of 5M GABA) to initiate the reaction. Catalase from bovine liver can be added during substrate addition (to

a final concentration of 0.01 mg/mL) to scavenge H_2O_2 in the extracellular media (minimizing crosstalk between cells).

11. After 30 minutes, the reaction quenched with the addition of 100 μL ascorbic acid (as a 100 mM solution in Milli-Q water) to a final concentration of 10 mM.
12. Run the samples on the cytometer.

Appendix I: Purification via Immobilized Metal Ion Affinity Chromatography

I.1 Materials

Protein purification was performed using Bio-Rad Bio-Scale Mini Profinity IMAC Cartridges. These cartridges facilitated the efficient purification of His-tagged MABO, which enabled downstream kinetic and analyses. An FPLC system was not used. The cartridge was connected to a 50 mL syringe with a Luer lock fitting.

I.2 Procedure

1. For *E. coli* cultures expressing medium to high levels of histidine-tagged proteins, 200 mL of culture will yield sufficient material for a 1 mL cartridge purification, and 1000 mL of culture will yield sufficient material for a 5 mL cartridge purification run
2. Preparation of *E. coli* Lysates
    A. Harvest cell pellet by centrifugation at 8000 × g for 10 minutes at 4°C
    B. Determine weight of pellet and resuspend in 10 volumes native lysis/wash buffer 1 (200 mL of culture typically yields 0.8 g of paste, and results in 8 mL of lysate)
    C. Sonicate the lysate (on ice) 4 times at 1 min intervals
    D. Centrifugate the lysate at 12000 × g for 20 minutes at 4°C
    E. Remove the supernatant, and filter through a 0.2 μM filter immediately before applying to the cartridge
3. Preparing a Cartridge, and Subsequent Purification
    A. Equilibrate the cartridge with 5 column volumes (CV) of equilibration/wash buffer 1 at 10 mL/min

B. Load the sample lysate at 10 mL/min

C. Wash the cartridge with 6 CV of wash buffer 1 at 10 mL/min

D. Wash the cartridge with 6 CV of wash buffer 2 at 10 mL/min

E. Elute the purified protein with 10 CV of elution buffer at 10 mL/min

F. Prior to quantitation of the protein concentration, the purified protein should be exchanged into a non-imidazole buffer (imidazole can absorb at 280 nm)

4. Regeneration, Cleaning, Sanitation, and Storage

A. Rinse the cartridge with 2 CV water at 5 mL/min

B. Wash the cartridge with 5 CV 500 mM NaCl, 50 mM Tris, pH 8.0 at 5 mL/min

C. Wash the cartridge with 5 CV 500 mM NaCl, 100 mM NaOAc, pH 4.5 at 5mL/min

D. Rinse the cartridge with 2 CV water at 5 mL/min

E. Store the cartridge in 20% EtOH at 4^{o}C

5. Stripping and Recharging

A. In situations where it is desired to run different proteins over the same cartridge, a complete sanitation, stripping, and recharging is recommended between sample runs.

B. Clean the cartridge with 10 CV 1M NaOH

C. Rinse the cartridge with 10 CV water

D. Strip metal ions with 5 CV of 0.1M EDTA

E. Recharge the cartridge with 5 CV of 0.1M $NiSO_4$, pH 4.5

F. Rinse the cartridge with 10 CV water

G. Store the cartridge in 20% ethanol

Appendix J: Bradford Protein Assay for Concentration Quantitation

J.1 Materials

Protein concentration quantification was performed using the Coomassie (Bradford) Protein Assay Reagent, which contains Coomassie G-250 dye, methanol, phosphoric acid, and solubilizing agents in water. The assay was calibrated using a BSA standard at a concentration of 2 mg/mL.

J.2 Procedure

1. Preparation of BSA Dilution Standards

Vial	Volume of Diluent	Volume and Source of BSA	Final BSA Concentration
A	0 µL	300 µL of stock	2000 µg/mL
B	125 µL	375 µL of stock	1500 µg/mL
C	325 µL	325 µL of stock	1000 µg/mL
D	175 µL	175 µL of vial B	750 µg/mL
E	325 µL	325 µL of vial C	500 µg/mL
F	325 µL	325 µL of vial E	250 µg/mL
G	325 µL	325 µL of vial F	125 µg/mL
H	400 µL	100 µL of vial G	25 µg/mL
I	400 µL	0 µL	0 µg/mL

2. Pipette 5 µL of each standard or unknown sample into the appropriate wells of a 96 well plate. A black plate with a clear bottom should be used.
3. Add 250 µL of the Coomassie Reagent to each well and mix with plate shaker for 30 seconds.
4. Remove plate from shaker. For the most consistent results, incubate plate for 10 minutes at room temperature.
5. Measure the absorbance at or near 595 nm with a plate reader

6. Subtract the average 595 nm measurement for the blank replicates from the 595 nm measurements of all other individual standard and unknown sample replicates
7. Prepare a standard curve by plotting the average blank-corrected 595 nm measurement for each BSA standard vs. its concentration in µg/mL. Use the standard curve to determine the protein concentration of each unknown sample.
8. **Note:** If using curve-fitting algorithms associated with a microplate reader, a four-parameter (quadratic) or best-fit curve will provide more accurate results than a purely linear fit. If plotting results by hand, a point-to-point curve is preferable to a linear fit to the standard points.

Appendix K: Fluorometric Kinetic Parameter Characterization

K.1 Materials

Kinetic parameter characterization was performed using the Fluorometric Hydrogen Peroxide Assay Kit (Sigma-Aldrich, Catalog Number MAK166). This kit provided all necessary reagents, including the Infra-red Peroxidase Substrate (Catalog Number MAK166A), Hydrogen Peroxide, 3% (0.88 M) solution (Catalog Number MAK166B), Assay Buffer (Catalog Number MAK166C), Horseradish Peroxidase (Catalog Number MAK166D), and DMSO (Catalog Number MAK166E).

K.2 Procedure

1. Allow all reagents to come to room temperature before use.
2. Infra-red Peroxidase Substrate: Reconstitute vial with 250 mL of DMSO to prepare the Infra-red Peroxidase Substrate stock solution. Mix well by pipetting. Aliquot and store at –20 °C, protected from light. Stock solution should be used promptly upon preparation or thawing. Remaining stock solution should be immediately frozen.
3. Horseradish Peroxidase: Reconstitute with 1 mL of Assay Buffer to prepare a 20 units/mL stock solution. Mix well by pipetting. Divide into single-use aliquots and store at –20 °C, protected from light. Stock solution should be used promptly upon preparation or thawing. Remaining stock solution should be immediately frozen.
4. Hydrogen Peroxidase Assay for Calibration Curve

A. Add 22.7 µL of 3% H_2O_2 solution to 977 µL of Assay Buffer to prepare a 20 mM H_2O_2 stock solution. Add 1 µL of the 20 mM stock solution to 1,999 µL of Assay Buffer to get a 10 µM working solution.

B. Further dilute the 10 µM working solution to prepare 10, 3, 1, 0.3, 0.1, 0.03, 0.01, and 0 µM standards. Add 50 µL of the prepared standards to the appropriate wells in a 96 well plate. Add up to 50 µL of sample to wells. Bring samples to a final volume of 50 µL with Assay Buffer

C. Prepare the Master Mix according to the scheme in the MAK166 technical bulletin: 50 µL Infra-red Peroxidase Substrate Stock, 200 µL of 20 units/mL Peroxidase Stock, 4.75 mL Assay Buffer.

D. Add 50 µL of the Master Mix to each of the wells (samples, standards, and controls). Mix well and incubate the plate at room temperature for 1–30 minutes. Protect the plate from light during the incubation.

E. Measure the fluorescence intensity at (λ_{ex} = 640/ λ_{em} = 680 nm) using a Tecan Infinite M1000 plate reader. The background blank for the assay is the value obtained for the 0 (blank) Hydrogen Peroxide standard. Correct for the background by subtracting the blank value from all readings. The hydrogen peroxide concentrations for the samples in the following assay can be determined from this standard curve.

5. MABO *in vitro* Kinetic Assay

A. Prepare the Master Mix according to the scheme in the MAK166 technical bulletin: 50 µL Infra-red Peroxidase Substrate Stock, 200 µL Peroxidase Stock 20 units/mL, 4.75 mL Assay Buffer. Add 50 µL of the Master Mix to each of the wells. Add

MABO enzyme. Calculate the final enzyme concentration based upon the dilution factor.

B. Prepare MABO substrate stock solutions.

C. Pipette 50 μL of the substrate stock solutions into the wells containing the Master Mix. It is recommended to use a multichannel pipette for this time sensitive process to guarantee that the plate reader simultaneously captures the initial rate data for all the wells.

D. Measure the fluorescence intensity at (λ_{ex} = 640/ λ_{em} = 680 nm) using a Tecan Infinite M1000 plate reader.

E. Convert the data in obtained into enzymatic H_2O_2 product concentrations using the previously obtained calibration curve.

Appendix L: Preparation of GABA Sensors

L.1. Materials

The materials required for the fabrication of GABA sensors are identical to those listed in Appendix B for dopamine sensors. However, in addition to those materials, this procedure requires GABA oxidase as well as a crosslinker, specifically 5% glutaraldehyde vapor. The enzyme, isolated and quantified as described in Appendices I and J, is essential for the selective electroenzymatic detection of GABA. The crosslinker was purchased from Aldrich Chemical Co. (Milwaukee, WI, USA).

L.2 Procedure

1. Preliminary sensor preparation: follow all electrode processing steps as detailed for dopamine sensors in Appendix B.
2. Prepare the enzyme solution: Mix MABO enzyme (targeting a mass fraction of approximately 0.35 relative to BSA) with a BSA solution (10 mg/mL in PBS) to achieve the desired proportion.
3. Apply enzyme layer using a microsyringe to manually spread the enzyme solution evenly over the surface of the platinum working electrode (WE). 20-30 passes may be necessary for sufficient coverage.
4. Monitor the process under a microscope.
5. Crosslink the enzyme layer by expose the enzyme-coated electrode to 5% saturated glutaraldehyde vapor for 1 minute to facilitate covalent crosslinking of the enzyme to the electrode surface.

6. Store the sensor in a desiccated container at 4 °C for at least 48 hours to ensure full adhesion and stability of the enzyme layer.